Stochastic Information in the Assessment of Climate Change

Dissertation

zur Erlangung des akademischen Grades
Doktor der Naturwissenschaften (Dr. rer. nat.)
in der Wissenschaftsdisziplin Theoretische Physik

eingereicht an der
Mathematisch-Naturwissenschaftlichen Fakultät
der Universität Potsdam

von
Thomas Christopher Kleinen
geboren am 16.1.1973 in Braunschweig
Potsdam, im Februar 2005

b

Abstract

Stochastic information, to be understood as "information gained by the application of stochastic methods", is proposed as a tool in the assessment of changes in climate.

This thesis aims at demonstrating that stochastic information can improve the consideration and reduction of uncertainty in the assessment of changes in climate. The thesis consists of three parts. In part one, an indicator is developed that allows the determination of the proximity to a critical threshold. In part two, the tolerable windows approach (TWA) is extended to a probabilistic TWA. In part three, an integrated assessment of changes in flooding probability due to climate change is conducted within the TWA.

The thermohaline circulation (THC) is a circulation system in the North Atlantic, where the circulation may break down in a saddle-node bifurcation under the influence of climate change. Due to uncertainty in ocean models, it is currently very difficult to determine the distance of the THC to the bifurcation point. We propose a new indicator to determine the system's proximity to the bifurcation point by considering the THC as a stochastic system and using the information contained in the fluctuations of the circulation around the mean state. As the system is moved closer to the bifurcation point, the power spectrum of the overturning becomes "redder", i. e. more energy is contained in the low frequencies. Since the spectral changes are a generic property of the saddle-node bifurcation, the method is not limited to the THC, but it could also be applicable to other systems, e. g. transitions in ecosystems.

In part two, a probabilistic extension to the tolerable windows approach (TWA) is developed. In the TWA, the aim is to determine the complete set of emission strategies that are compatible with so-called guardrails. Guardrails are limits to impacts of climate change or to climate change itself. Therefore, the TWA determines the "maneuvering space" humanity has, if certain impacts of climate change are to be avoided. Due to uncertainty it is not possible to definitely exclude the impacts of climate change considered, but there will always be a certain probability of violating a guardrail. Therefore the TWA is extended to a probabilistic TWA that is able to consider "probabilistic uncertainty", i. e. uncertainty that can be expressed as a probability distribution or uncertainty that arises through natural variability.

As a first application, temperature guardrails are imposed, and the dependence of emission reduction strategies on probability distributions for climate sensitivities is investigated. The analysis suggests that it will be difficult to observe a temperature guardrail of 2°C with high probabilities of actually meeting the target.

In part three, an integrated assessment of changes in flooding probability due to climate change is conducted. A simple hydrological model is presented, as well as a downscaling scheme that allows the reconstruction of the spatio-temporal natural variability of temperature and precipitation. These are used to determine a probabilistic climate impact response function (CIRF), a function that allows the assessment of changes in probability of certain flood events under conditions of a changed climate.

The assessment of changes in flooding probability is conducted in 83 major river basins. Not all floods can be considered: Events that either happen very fast, or affect only a very small area can not be considered, but large-scale flooding due to strong longer-lasting precipitation events can be considered. Finally, the probabilistic CIRFs obtained are used to determine emission corridors, where the guardrail is a limit to the fraction of world population that is affected by a predefined shift in probability of the 50-year flood event. This latter analysis has two main results. The uncertainty about regional changes in climate is still very high, and even small amounts of further climate change may lead to large changes in flooding probability in some river systems.

Kurzzusammenfassung

Stochastische Information, zu verstehen als “Information, die durch die Anwendung stochastischer Methoden gewonnen wird”, wird als Hilfsmittel in der Bewertung von Klimaänderungen vorgeschlagen.

Das Ziel dieser Doktorarbeit is es, zu zeigen, dass stochastische Information die Berücksichtigung und Reduktion von Unsicherheit in der Bewertung des Klimawandels verbessern kann. Die Arbeit besteht aus drei Teilen. Im ersten Teil wird ein Indikator entwickelt, der die Bestimmung des Abstandes zu einem kritischen Grenzwert ermöglicht. Im zweiten Teil wird der “tolerable windows approach” (TWA) zu einem probabilistischen TWA erweitert. Im dritten Teil wird eine integrierte Abschätung der Veränderung von Überflutungswahrscheinlichkeiten im Rahmen des TWA durchgeführt.

Die thermohaline Zirkulation (THC) ist ein Zirkulationssystem im Nordatlantik, in dem die Zirkulation unter Einfluss des Klimawandels in einer Sattel-Knoten Bifurkation abreißen kann. Durch Unsicherheit in Ozeanmodellen ist es gegenwärtig kaum möglich, den Abstand des Systems zum Bifurkationspunkt zu bestimmen. Wir schlagen einen neuen Indikator vor, der es ermöglicht, die Nähe des Systems zum Bifurkationspunkt zu bestimmen. Dabei wird die THC als stochastisches System angenommen, und die Informationen, die in den Fluktuationen der Zirkulation um den mittleren Zustand enthalten sind, ausgenutzt. Wenn das System auf den Bifurkationspunkt zubewegt wird, wird das Leistungsspektrum “roter”, d. h. die tiefen Frequenzen enthalten mehr Energie. Da diese spektralen Veränderungen eine allgemeine Eigenschaft der Sattel-Knoten Bifurkation sind, ist die Methode nicht auf die THC beschränkt, sondern weitere Anwendungen könnten möglich sein, beispielsweise zur Erkennung von Übergängen in Ökosystemen.

Im zweiten Teil wird eine probabilistische Erweiterung des “tolerable windows approach” (TWA) entwickelt. Das Ziel des TWA ist die Bestimmung der Menge der Emissionsreduktionsstrategien, die mit sogenannten Leitplanken kompatibel sind. Diese Leitplanken sind Begrenzungen der Auswirkungen des Klimawandels, oder des Klimawandels selber. Der TWA bestimmt daher den Spielraum, den die Menschheit hat, wenn bestimmte Auswirkungen des Klimawandels vermieden werden sollen. Durch den Einfluss von Unsicherheit ist es aber nicht möglich, die betrachteten Auswirkungen des Klimawandels mit Sicherheit auszuschließen, sondern es existiert eine gewisse Wahrscheinlichkeit, dass die Leitplanke verletzt wird. Der TWA wird daher zu einem probabilistischen TWA weiterentwickelt, der es ermöglicht, “probabilistische Unsicherheit”, also Unsicherheit, die durch eine Wahrscheinlichkeitsverteilung ausgedrückt werden kann, oder die durch den Einfluß von natürlicher Variabilität entsteht, zu berücksichtigen.

Als erste Anwendung werden Temperaturleitplanken betrachtet, und die Abhängigkeit der Emissionsreduktionsstrategien von Wahrscheinlichkeitsverteilungen über die Klimasensitivität wird bestimmt. Die Analyse ergibt, dass die Einhaltung einer Temperaturleitplanke von 2°C sehr schwierig wird, wenn man hohe Wahrscheinlichkeiten des Einhaltens der Leitplanke fordert.

Im dritten Teil wird eine integrierte Abschätzung der Änderungen von Überflutungswahrscheinlichkeiten unter Einfluss des Klimawandels durchgeführt. Ein einfaches hydrologisches Modell wird vorgestellt, sowie ein Skalierungsansatz, der es ermöglicht, die raum-zeitliche natürliche Variabilität von Temperatur und Niederschlag zu rekonstruieren. Diese werden zur Bestimmung einer probabilistischen Klimawirkungsfunktion genutzt, einer Funktion, die es erlaubt, die Veränderungen der Wahrscheinlichkeit bestimmter Überflutungsereignisse unter Einfluss von Klimaänderungen abzuschätzen.

Diese Untersuchung der Veränderung von Überflutungswahrscheinlichkeiten wird in 83 großen Flusseinzugsgebieten durchgeführt. Nicht alle Klassen von Überflutungen können dabei berücksichtigt werden: Ereignisse, die entweder sehr schnell vonstatten gehen, oder die nur ein kleines Gebiet betreffen, können nicht berücksichtigt werden, aber großflächige Überflutungen, die durch starke, langanhaltende Regenfälle hervorgerufen werden, können berücksichtigt werden.

Zuguterletzt werden die bestimmten Klimawirkungsfunktion dazu genutzt, Emissionskorridore zu bestimmen, bei denen die Leitplanken Begrenzungen des Bevölkerungsanteils, der von einer bestimmten Veränderung der Wahrscheinlichkeit eines 50-Jahres-Flutereignisses betroffen ist, sind. Letztere Untersuchung hat zwei Hauptergebnisse. Die Unsicherheit von regionalen Klimaänderungen ist immer noch sehr hoch, und außerdem können in einigen Flusssystemen schon kleine Klimaänderungen zu großen Änderungen der Überflutungswahrscheinlichkeit führen.

Contents

1 Stochastic Information **1**

2 Stochastic indicator for the proximity to a critical threshold **7**

2.1 Introduction 7

2.2 Model description and behavior 9

2.2.1 The Stommel model 9

2.2.2 Properties of the deterministic system 11

2.2.3 Model Reduction 13

2.2.4 Freshwater Flux Variability 14

2.3 Spectral changes at the bifurcation 16

2.4 Probability density at the bifurcation 19

2.5 Stability of the THC 21

2.6 Beyond the simplifi ed Stommel model 25

2.7 Summary and Conclusions 28

3 Probabilistic extension of the Tolerable Windows Approach **31**

3.1 Introduction 31

3.2 The TWA under probabilistic uncertainty 34

3.2.1 Two concepts 34

3.2.2 Uncertainty in the integrated assessment of climate change . . . 38

3.2.3 The ICLIPS climate model 42

3.2.4 Consequences of uncertainty for the TWA 44

3.3 The probabilistic TWA 48

3.3.1 Probabilistic guardrails 48

3.3.2 Probabilistic CIRFs 50

3.3.3 Calculation of emission corridors 52

3.4 Emission corridors in the probabilistic TWA 55

3.5 Summary and conclusions 60

4 Integrated assessment of changes in flooding probability **62**
4.1 Introduction 62
4.2 Model description 64
4.2.1 Aims and scope 64
4.2.2 Downscaling of climate change 65
4.2.3 Runoff calculation 68
4.3 Data and Methods 69
4.3.1 River basin description 69
4.3.2 Input and validation data 70
4.3.3 Population scenario 71
4.3.4 Validation of annual and monthly runoff 71
4.3.5 Validation of runoff extremes 73
4.3.6 Sensitivity analysis 74
4.4 Model validation 75
4.4.1 Verifi cation of annual and monthly runoff 75
4.4.2 Validation of runoff extremes 77
4.4.3 Sensitivity analysis 79
4.5 Changed probabilities for extreme runoff events under climate change . 81
4.5.1 A single scenario experiment 81
4.5.2 Climate Impact Response Function 85
4.6 Emission corridors limiting the change in fboding probability 89
4.7 Discussion and Conclusions 92

5 Summary and Outlook **95**
5.1 Summary 95
5.2 Outlook 97

A List of river basins considered **99**

Bibliography **101**

Acknowledgements **115**

Chapter 1

Stochastic Information

The reader may initially be surprised by the term "stochastic information" in the title, since the term does not appear in a physics textbook. In this thesis, we use "stochastic information" as a short form of "information gained by the application of stochastic methods", and we propose that stochastic information can be a valuable tool for the consideration of uncertainty in the assessment of changes in climate.

Archetypically, the assessment of changes in climate can be approached from two distinct points of view. On the one hand, there is the scientific analysis of the climate system, and on the other hand there is scientific assessment for purposes of policy advice. Now, what are distinctions between these cases? Within pure science, the problem investigated typically arises out of other scientific investigations, and results of an analysis serve scientific purposes only. In scientific assessment for purposes of policy advice, the question investigated typically arises outside of science, and results of the analysis are supposed to inform the policy-making process, which may in turn generate new scientific questions.

In pure science, one traditionally strives for the "objective truth". Starting from first principles and / or measurement data, uncertainties are successively reduced, until certainty has been achieved. Within this framework, consistency with empirical evidence is the ultimate quality criterion.

If a scientific assessment is conducted for purposes of policy advice, on the other hand, the search for the objective truth may turn out to be a luxury one cannot afford. In cases where facts are uncertain, values in dispute, stakes high, and decisions urgent, the "post-normal" approach to science (Funtowicz and Ravetz, 1993, Ravetz, 1999) may be more appropriate. Two examples, where this was the case, are the BSE (bovine spongiform encephalopathy) epidemic in the 1990s, and the admission of genetically modified crops (Marchi and Ravetz, 1999). In the case of the BSE epidemic, the way the disease is transmitted was very uncertain at first, as was the extent of the epidemic and ways of

countering it, but political decisions had to be made in spite of this. Similarly, it is still uncertain, whether genetically modified crops may turn out to be harmful, but political pressure to allow the cultivation is high. In these cases the scientific community was – and still is – not able to give an objective analysis of the matter at hand. Instead, science could present the available evidence and thereby inform the policy-making process, and thus the uncertainty is still very high, when decisions are made.

In the post-normal approach to science, the guiding principle of science, the search for truth, has to be extended, since it is highly unlikely that the truth can be determined in time. Instead, it has to follow a principle of quality assurance, where uncertainties are acknowledged and value judgments underlying an assessment are made explicit.

This change in the guiding principles of science does not mean that the traditional scientific principles become irrelevant, or that science becomes a political undertaking, but it is rather a recognition that the search for the objective truth alone may no longer be the appropriate response to societal problems, where facts are uncertain, stakes high, and decisions urgent. In addition, this change does not necessarily change the way science is conducted, but it rather changes how problems are formulated, the way that results are presented, and the criteria of what constitutes "good" science. An additional aspect to this question is that pure science is typically only concerned with problems that are considered soluble, whereas science in a post-normal setting may have to investigate problems considered insoluble (Ravetz, 1997).

Funtowicz and Ravetz (1993) have coined the term "post-normal science" for scientific policy advice in cases where facts are uncertain, values in dispute, stakes high, and decisions urgent. Is this a suitable characterization for the case of climate change? Here, the stakes are high, obviously. The mitigation of climate change may become a very expensive undertaking, but major changes in the climate system might well have a major effect on humanity. Similarly, decisions are urgent, if humanity wants to limit climate change. According to the latest report by the intergovernmental panel on climate change (IPCC), the global mean temperature has already changed by $0.6 \pm 0.2^{\circ}$C relative to preindustrial (Houghton et al., 2001), and temperatures will continue to rise until some time after emissions of substances that change the radiative balance of our planet have been reduced. These points therefore apply to the climate change issue. In addition, facts about climate change are uncertain, as we will elaborate in the next paragraphs.

In the assessment of climate change, uncertainty is a factor that has to be acknowledged in every link in the chain of cause and effect, ranging from uncertainty about the socio-economic system causing the emissions of greenhouse gases (GHG) and other substances modifying the radiative balance, over uncertainty about the current state of the climate system and climate system response to the emissions of greenhouse gases,

to uncertainty about the impacts of climate change. One very illustrative example is that the latest assessment report by the IPCC states a range from 1.4 to 5.8°C for the warming that is to be expected between 1990 and 2100 (Houghton et al., 2001). The width of this range, as well as the fact that the authors did not give a probability distribution or most likely value, clearly shows the large uncertainty.

The chain of cause and effect of future climate change starts with the anthropogeneous emissions of greenhouse gases. These future emissions depend on a number of factors, none of which can be predicted with any accuracy. Among other factors, there is the future growth in population, as well as the future economic development, and the technologies that will be used. All of these factors are the result of decisions by humans, which are unpredictable. This causes a huge uncertainty about the future emissions in GHGs. Since this uncertainty cannot be resolved, scenarios are commonly used to represent the future emissions in assessments of climate change.

The next link in the chain of cause and effect is the climate system itself. The climate system is a complex nonlinear system, composed of a large number of components. Any state of the climate system is the result of a large web of interactions between large numbers of processes on widely differing scales, both spatial and temporal. These scales range from the microscopic to continental for the spatial scales, and from sub-second to millennial for the temporal scales (e. g. Peixoto and Oort (1991)).

These observations have a number of consequences for the assessment of changes in climate. The nonlinear nature of the climate system leads to a sensitive dependence on initial conditions and to the possibility of multiple equilibria in the climate system, while the complexity of the climate system requires the representation of all relevant processes at all scales, since cross-scale interactions might have a strong influence on other processes at other scales.

Comprehensive climate models, the general circulation models (GCM), are the most comprehensive tool available for assessing the climate system. These models aim to solve the equations of the climate system on all relevant scales. Unfortunately, this is not possible because current computer technology limits the ability to resolve processes, and uncertainty about some processes prevents their consideration. As a result, there inevitably are some processes that cannot be resolved explicitly, and these must therefore be represented by some parameterized closure scheme (Palmer, 2000). Examples for this are mixing processes in the oceans, and cloud formation in the atmosphere.

Therefore there is uncertainty about the parameterizations of sub-gridscale processes. This may be uncertainty about parameter values, but it may also be uncertainty about the processes themselves. In addition, there also is uncertainty about the current state of the climate system. While some properties can be measured by satellites nowadays, this

is not possible for all relevant properties, e. g. water mass properties below the ocean surface, and the density of measurement networks is in many cases insufficient for a reliable estimation of the current state of the climate system. Finally, many processes in the climate system display some natural variability, which also adds to the uncertainty.

All of the uncertainties mentioned above then propagate into the assessment of impacts of climate change. Here, the climate change realized due to some forcing is uncertain, but in addition to that the impact of some defined climate change scenario may also be uncertain, once again due to uncertainty in parameters and processes, as well as insufficient knowledge.

It can therefore be concluded that climate change research is an area of science, where uncertainty is still very high, especially with regard to future changes in climate, and political stakes are also very high, since slowing or even reversing climate change may severely affect the way we conduct our lives. Therefore, much of the climate research conducted takes place within the paradigm of post-normal science, and the IPCC[1] process can be seen as a manifestation of this (Saloranta, 2001).

An example of what post-normal science may be like when applied to climate change research is the "Delft process" (van Daalen et al., 1998). The Delft process was a series of five workshops that took place between 1995 and 1997. In these workshops the IMAGE 2 model (Rotmans et al., 1989, Alcamo et al., 1998) was applied in support of international climate negotiations, and a dialogue between the scientists involved in the development of IMAGE 2 and policymakers took place. This series of workshops had two effects. On the one hand, it helped the workshop participants from the policy side in the preparation of policy documents. On the other hand, it also helped the scientists understand the needs of policymakers and thereby improved the scientific policy advice.

These workshops also illustrate the perils of approaching research for policy advice from a purely scientific point of view. At the first workshop, the IMAGE team presented some analyses they thought were relevant to policymakers. These consisted of an analysis of the consequences of no action, and of an evaluation of the impacts of various scenarios stabilizing the CO_2 concentration in 2100. These analyses, however, did not fulfill the needs of the policy makers involved, since these needed guidance for the upcoming negotiations, which were focused on short-term actions. They therefore requested information on short-term actions, burden sharing, impacts and costs. As a con-

[1]The intergovernmental panel on climate change (IPCC) was established by the World Meteorological Organization (WMO) and the United Nations Environmental Programme (UNEP) in 1988 to assess available information on climate change and its environmental and socio-economic impacts. It regularly publishes reports summarizing the accumulated peer-reviewed scientific literature on climate change. After compilation, these reports are reviewed by scientists, as well as governments and non-governmental organizations. The IPCC has published three reports so far, with the third assessment report appearing in 2001 (Houghton et al., 2001, McCarthy et al., 2001, Metz et al., 2001).

sequence, the IMAGE team subsequently developed the "safe landing analysis" (Swart et al., 1998), which allowed the determination of the short-term policy options that were compatible with the long-term goal of avoiding dangerous anthropogenic interference with the climate system (van Daalen et al., 1998).

Stochastic information is a tool that may improve the assessment of changes in climate. Considering the climate system as a stochastic system lends itself naturally to noisy (stochastic) timeseries and the necessarily truncated analysis of the system, since it will rarely be possible to consider all scales that affect system behavior if one starts from first principles. This way, all the information that is contained in the timeseries can be utilized, while an analysis within a deterministic framework may disregard information hidden in fluctuations about the mean state. Therefore the consideration of information gained by the application of stochastic methods may aid the scientific analysis of the climate system.

For policy advice, on the other hand, the focus is not on the development of a perfect understanding of the climate system, but rather on developing robust strategies for the future management of the climate system. Since the focus is not on the current state of the climate system, but on projections of the future development, uncertainty that is inherent in climate change assessment needs to be taken into account explicitly, and it is also necessary to communicate the uncertainty. Stochastic methods can allow the consideration of some of the uncertainty, and they can also aid in the communication of the uncertainty, since uncertainty that is quantified and considered explicitly can be communicated more effectively.

Stochastic information therefore may aid the scientific analysis of the climate system, regardless of whether one works within the "normal" or the "post-normal" paradigm of science. In the end, the difference between the two paradigms becomes very small when it comes to the actual scientific analysis, since one wants to reduce the uncertainty as far as possible in both cases.

This thesis will present two cases, where information gained by the use of stochastic methods aids in the assessment of climate change. The first example is an example taken from oceanography. The North Atlantic thermohaline circulation (THC), also called meridional overturning circulation (MOC), is a circulation system in the North Atlantic, that is driven by temperature and salinity gradients. The current state of this system is difficult to determine, and chapter2 will present a novel way of determining the system's state by considering it as a stochastic system. This provides additional information on the state of the system that cannot be gained by deterministic methods.

Chapters 3 and 4 will then present an extension of the tolerable windows approach (TWA), so far a deterministic approach to the integrated assessment of climate change, to

a probabilistic approach. The deterministic TWA already evades some of the uncertain factors since it determines the set of emission trajectories compatible with predefined criteria instead of relying on single emission trajectories, and the extension to a probabilistic TWA allows the explicit consideration of probabilistic uncertainty in the TWA, as well as the consideration of impacts of climate change, where climate change leads to a change in probability of a certain event happening. The basic framework of the probabilistic TWA will be developed in chapter 3, while chapter 4 will present an assessment of changes in flooding probabilities under climate change, a first application of the probabilistic TWA to a probabilistic impact of climate change.

The thesis will finish with a summary and an outlook in chapter 5.

Chapter 2

Stochastic indicator for the proximity to a critical threshold

2.1 Introduction

It is becoming increasingly evident that there are critical thresholds in the Earth system, where the climate may change dramatically (Smith et al., 2001, Scheffer et al., 2001). The exact positions of these thresholds in the phase space of the Earth system are, however, still unclear and it might be doubted, whether they can be determined with enough precision to give concrete information on the threat of crossing the threshold. Therefore additional independent methods for assessing the closeness of the system to these thresholds are needed. These methods could contribute to an "early warning system" for assessing the danger of crossing a threshold and possibly provide the information necessary for controlling the system.

One subsystem that displays such a threshold is the North Atlantic thermohaline circulation (THC) (Clark et al., 2002). Considering the system of the THC under a global warming scenario, the circulation may collapse if certain threshold values in northern Atlantic temperature and salinity are exceeded. This system has been thoroughly investigated using a whole range of models, ranging from conceptual models (Stommel, 1961, Cessi, 1994, Rahmstorf, 1996, Scott et al., 1999, Titz et al., 2002) over models of intermediate complexity (Stocker and Schmittner, 1997, Rahmstorf and Ganopolski, 1999a, Kleinen, 2000) to highly complex general circulation models (GCM) (Manabe and Stouffer, 1988, Rahmstorf, 1995, Schiller et al., 1997, Wood et al., 1999). While most of these investigations agree with respect to the fact that there is a threshold, where the circulation breaks down, the exact value of this threshold in the climate system has not yet been determined. Currently it seems questionable, whether the exact position

of the threshold will be determined within the near future, as the disagreement on overturning strength and sensitivity to freshwater fluxes is still quite large between different GCMs. In addition it has not been possible to accurately measure the present overturning strength of the THC in the real climate system so far.

Due to the large uncertainty it is also questionable, whether one would actually gain information on the position of the threshold in the "real" climate system, if one could accurately determine the threshold in a GCM. As Schmittner and Weaver (2001) have shown, it is possible to generate widely differing responses of the THC to freshwater forcing by varying the diffusivities in ocean models. As a result, the model gives different distances to the threshold for the same mean overturning. Since these uncertain parameterizations cannot be well constrained by measurements, uncertainty about the distance to the threshold remains large.

Simple box models have shown a remarkable ability to capture important aspects of the behavior of the THC manifested in GCM experiments. So far most investigations have concentrated either on the deterministic behavior of the THC or on the stochastic properties. Deterministic models have mainly been used to investigate the bifurcations and attractors of the models (Stommel, 1961, Rahmstorf, 1996, Scott et al., 1999, Titz et al., 2002), whereas the work with stochastic models has concentrated on the spectrum and on the stationary distribution (Stommel and Young, 1993, Cessi, 1994, Bryan and Hansen, 1995). Combining the two points of view, Timmermann, Lohmann and Monahan have investigated how the stationary distribution changes as a function of the bifurcation parameter (Timmermann and Lohmann, 2000, Monahan et al., 2002, Monahan, 2002). What has not been investigated so far is the dependence of the power spectrum on the bifurcation parameter.

The concept of stochastic climate models goes back to a paper by Hasselmann (1976). He observed that there are many fast processes (e.g. weather) within the climate system. These processes may affect the long term development of the system, so that they cannot be omitted from an assessment. On the other hand, these processes can not be incorporated into comprehensive models due to resolution, computation and conceptual restraints. Therefore Hasselmann proposed that the influence of the fast processes on climate could be modeled as a stochastic forcing to the system.

With respect to bifurcations, the influence of fluctuations becomes even more important, as fluctuations may increase in the vicinity of bifurcation points, eventually leading to critical fluctuations (Haken, 1980, Sornette, 2000). This might induce a switch in the system even before reaching the bifurcation itself (Monahan, 2002).

The freshwater flux is the bifurcation parameter within the THC-system. It is composed of a multitude of components, including precipitation and wind-driven transports

among others. These processes are subject to short term processes and fluctuations. Therefore critical fluctuations might occur.

The aim of this chapter is to investigate, whether the system's response to fluctuations can be used as an indicator for the proximity of the system to the bifurcation point, and to determine whether this might yield additional information compared to purely deterministic methods. Potential applications of this method could span a large range, ranging from the THC itself over other climatic processes to ecosystem dynamics (Scheffer and Carpenter, 2003).

The structure of the chapter is as follows: In section 2.2 the model used in this investigation will be described, and the variability of North Atlantic freshwater fluxes will be estimated. In section 2.3 the dependence of the power spectral density on the bifurcation parameter will be investigated, while section 2.4 will concentrate on the dependence of the probability density on the bifurcation parameter. In section 2.5 the stability of the present day THC and its dependence on bifurcation parameter and noise strength will be analyzed, while we will extend our findings to more comprehensive models in section 2.6. The chapter will finish with summary and conclusions in section 2.7.

Parts of this chapter have already been published in Ocean Dynamics as Kleinen et al. (2003).

2.2 Model description and behavior

2.2.1 The Stommel model

The Stommel model (Stommel, 1961) is a well-known nonlinear conceptual model of the thermohaline circulation. It is a hemispheric two-box model consisting of interconnected boxes of temperature T_i and salinity S_i representing the North Atlantic at low and high latitudes. The model calculates the circulation strength in a channel connecting the two boxes, as well as the changes in salinity and temperature resulting from advective transport between the boxes. The circulation is proportional to the density difference between the boxes.

In the model version used here, the temperatures T_i and salinities S_i of the boxes are not considered explicitly, but only their differences, ΔT and ΔS respectively, appear in the model equations. With regard to the model formulation we follow Monahan (2002), without using the additional noise term affecting the advective transport he used.

The model equations are

$$\frac{d}{dt}\Delta T = -\frac{|q|}{V}\Delta T + \Gamma(\Delta T_0 - \Delta T) \tag{2.1}$$

$$\frac{d}{dt}\Delta S = -\frac{|q|}{V}\Delta S + \frac{S_0}{h}\Delta F. \tag{2.2}$$

The change in temperature difference ΔT is determined by the advective temperature flux $-(|q|/V)\Delta T$ with box volume V (both boxes are of equal volume), and by the Newtonian temperature restoring $\Gamma(\Delta T_0 - \Delta T)$ with the relaxation timescale Γ^{-1} and the reference temperature difference ΔT_0. The change in salinity difference ΔS is again determined by the advective transport of salinity and by the difference in the freshwater fluxes ΔF. The freshwater flux is converted to a haline flux by multiplication with the reference salinity S_0. The depth of both boxes is equal and denoted by h. The overturning q is proportional to the pressure difference between the boxes. It is obtained from the density difference with the thermal and haline expansion coeffi cients α and β, while c is a hydraulic constant relating overturning strength to density difference. The volume-mean-fbw q is determined by

$$q = c\,(\alpha\Delta T - \beta\Delta S)\,. \tag{2.3}$$

In order to introduce fluctuations of the moisture flux, the following substitution has to be applied: $(S_0/h)\,\Delta F \rightarrow (S_0/h)\,\Delta F + \Sigma\dot{W}$, with W a Wiener process (Gardiner, 1994). $\Sigma\dot{W}$ is white noise with standard deviation Σ.

In order to facilitate the analytical treatment, the system is transformed to a nondimensional formulation. By introducing the quantities

$$\tilde{t} = \frac{c\alpha\Delta T_0}{V}t \tag{2.4}$$

$$x = \frac{1}{\Delta T_0}\Delta T \tag{2.5}$$

$$y = \frac{\beta}{\alpha\Delta T_0}\Delta S \tag{2.6}$$

and by substituting them into the model equations, the formulation

$$\dot{x} = -|x-y|\,x + \gamma(1-x) \tag{2.7}$$

$$\dot{y} = -|x-y|\,y + \mu + \sigma\dot{W} \tag{2.8}$$

is derived (Monahan, 2002). Here, all time derivatives are with respect to rescaled time. Here, the transport q is transformed to $q = x - y$. The parameters in Eq. 2.7-2.8 are

$$\begin{aligned}
\gamma &= \frac{V}{c\alpha\Delta T_0}\Gamma \\
\mu &= \frac{\beta V S_0}{ch\left(\alpha\Delta T_0\right)^2}\Delta F \\
\sigma &= \left(\frac{\beta^2 V}{c\left(\alpha\Delta T_0\right)^3}\right)^{\frac{1}{2}}\Sigma.
\end{aligned}$$

In principle, values for these parameters would have to be obtained by fitting the box model to GCM output or measurement data. Instead we obtained the values for all parameters but h and Γ from Monahan (2002), and Timmermann and Lohmann (2000). h is the maximum depth of North Atlantic Deep Water (Warren, 1981), whereas Γ has been used by Rahmstorf and Ganopolski (1999b) for a 4-box model of the thermohaline circulation. Performing their calculations for the 2-box model, we arrive at a similar result. The values for the model parameters are listed in Table 2.1, but the argument

Parameter	Value
α	$0.15\,\mathrm{K}^{-1}$
β	$0.8\,\mathrm{psu}^{-1}$
c	$17\cdot10^6\,\mathrm{m}^3\mathrm{s}^{-1} = 5.36\cdot10^{14}\,\mathrm{m}^3\mathrm{a}^{-1}$
V	$2\cdot10^{15}\,\mathrm{m}^3$
ΔT_0	$15\,\mathrm{K}$
h	$4000\,\mathrm{m}$
Γ	$25^{-1}\,\mathrm{a}^{-1}$

Table 2.1: Possible values for model parameters.

presented in this chapter does not depend on the exact values of these parameters. Using these parameter values, a model year corresponds to 1.66 real years.

2.2.2 Properties of the deterministic system

Before tackling the stochastic problem, we want to familiarize us with the properties of the deterministic system. The steady state solution to the system is obtained by setting $\dot{x} = \dot{y} = \sigma = 0$. The solution to this problem is the solution of a 3rd order polynomial. As we don't want to bore the reader, we don't show it here.

In the case of positive overturning and positive μ, corresponding to an excess of precipitation over evaporation, the system is driven by thermal gradients and braked by

haline gradients (see Eq. 2.3). For positive overturning there is one stable solution, a stable node (Stommel, 1961), for all $\mu < 0.03$. For $\mu > \mu_c = 0.03$ the stable solution breaks down in a saddle-node bifurcation, and the circulation changes to the haline-driven equilibrium solution with negative overturning. A change in the relaxation timescale γ^{-1} shifts the bifurcation point: An increase in γ results in an increase in μ_c.

For negative overturning the system is driven by haline gradients. There is one stable solution, a stable focus (Stommel, 1961), for all $\mu > 0$. It breaks down at $\mu = 0$, where the overturning changes sign. For $\mu < 0$ only one stable solution exists – both thermal and haline driving force the system in the same direction. Therefore only one solution with strong positive overturning is possible.

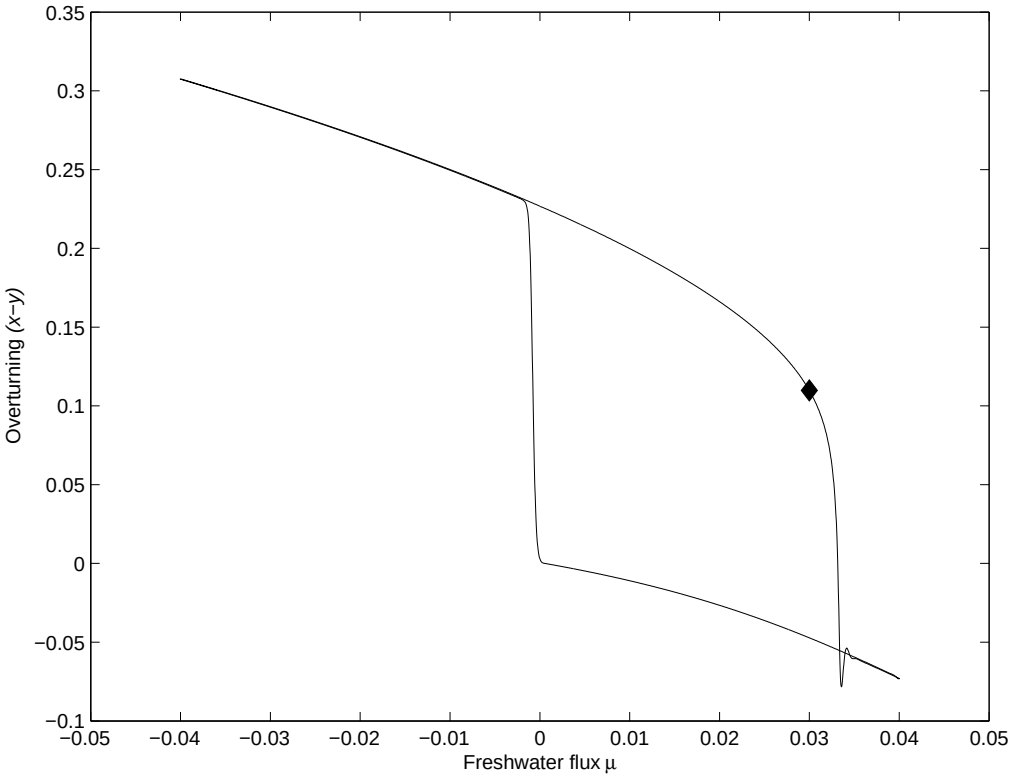

Figure 2.1: Hysteresis loop of overturning strength with varying freshwater flux μ at noise amplitude 0. The bifurcation point at the critical freshwater flux μ_c is marked by a diamond.

Under the influence of slowly varying parameters μ, the stability properties sketched above lead to a well-pronounced hysteresis behavior (Fig. 2.1). After the circulation broke down in the saddle-node bifurcation, a reduction of the freshwater flux μ does not result in an instantaneous return to the positive overturning solution, but the system stays

on the haline branch until the freshwater flux μ changes sign and the thermal and haline driving forces act in the same direction. The result is a jump from zero overturning to strong positive overturning as one passes through $\mu = 0$. A similar hysteresis experiment, where the freshwater flux μ was slowly increased and decreased linearly by $\Delta\mu = \pm 0.04$ starting from $\mu = 0$ with a velocity $d\mu/d\tilde{t} = 4 \cdot 10^{-5}$ is depicted in Fig. 2.1. Here the overturning $(x-y)$ is shown depending on the freshwater flux μ. The bifurcation at $\mu_c = 0.03$ is clearly visible, as is the hysteresis behavior of the circulation. Henceforth the focus will be on the solution with positive overturning, as this is the situation in today's ocean.

2.2.3 Model Reduction

In order to allow an analytical treatment, the system is reduced to one dimension.

If we assume that the system contains widely differing response times, the behavior of the system on short timescales may be of minor importance for the long term evolution of the slow variables. In this case variables can be separated, "slaving" the fast variables to the slow variables. By this "adiabatic elimination" (Gardiner, 1994) the dimensionality of the system is reduced to one. In principle, this approach is not justified, if the goal is as realistic a description of reality as possible. Realistic temperature gradients are smaller that ΔT_0. On the other hand, the qualitative properties of the system, namely the saddle-node bifurcation and the hysteresis behavior, are retained in the reduced system.

In the case investigated here, the following system of Langevin stochastic differential equations (SDE) is considered:

$$dx = (-|x-y|x + \gamma(1-x))\,dt \tag{2.9}$$

$$dy = (-|x-y|y + \mu)\,dt + \sigma\,dW. \tag{2.10}$$

Under the assumption that the temperature relaxation timescale $\tau = 1/\gamma$ is very short, corresponding to γ very large, temperature relaxation happens instantly constraining x to $x = 1$ if one considers the long timescales only. Therefore the system (2.9, 2.10) can be reduced to a one-dimensional SDE in y only:

$$dy = (-|1-y|y + \mu)\,dt + \sigma\,dW. \tag{2.11}$$

In the case of positive overturning ($y < 1$) this corresponds to

$$dy = \left(y^2 - y + \mu\right)dt + \sigma\,dW, \tag{2.12}$$

which has the deterministic steady state solutions

$$y_{1,2} = \frac{1}{2} \pm \sqrt{\frac{1}{4} - \mu} \tag{2.13}$$

with y_1 an unstable and $y_2 = y_0 = 1/2 - \sqrt{1/4 - \mu}$ a stable fixed point.

Please note that the system described by Eq. 2.11 is very similar to the one investigated by Cessi (1994). The only difference is that Cessi parameterized the volume transport by the square of the density difference and not by the absolute value used here.

This SDE retains the relevant features of the full system of SDEs. The system undergoes a saddle-node bifurcation at the critical freshwater flux $\mu_c = 0.25$ and again observes a hysteresis behavior as in Fig. 2.1. Due to the large values of γ assumed in the adiabatic approximation, the bifurcation point is now at a much higher value of the freshwater flux μ than in the full system (2.7, 2.8), i.e. the bifurcation is at $\mu_c = 0.25$ instead of $\mu_c = 0.03$ in the full system.

In the following model simulations, the model equations are integrated using an explicit Euler scheme (Kloeden and Platen, 1999) with a timestep of 0.1 (nondimensional) "years". Initial sensitivity experiments have shown that the convergence properties do not improve using smaller timesteps.

2.2.4 Freshwater Flux Variability

The freshwater flux μ is composed of a multitude of factors. It contains all processes that influence the salinity balance both in the equatorial Atlantic and in the deepwater formation areas in the high northern latitudes, with the exception of freshwater transport by the THC. For the Labrador sea, which is one of two deepwater formation areas for the North Atlantic THC (Warren, 1981), Houghton and Visbeck estimate that the major contributors to the freshwater balance of that area are advective transport, sea ice melting, continental runoff, precipitation and evaporation (Houghton and Visbeck, 2002). In addition to these, there is also wind-driven transport, which could have an influence. The freshwater flux μ is composed of all of these factors, minus the advective transport by the THC. This transport is described explicitly by the Stommel model.

In order to assess the magnitude of σ, the variance of the quantities composing μ has to be estimated. Estimates for these factors are difficult to obtain and notoriously unreliable, and the variance of these quantities is rarely even considered. Nonetheless a few estimates exist.

Walsh and Portis estimate from reanalysis data that the standard deviation of annual averages of precipitation P and evaporation E over the North Atlantic is typically about 10-20% of the mean (Walsh and Portis, 1999), while Houghton and Visbeck report that

interannual variations in the Labrador current are about 30% of the mean (Houghton and Visbeck, 2002). In addition there is an estimate of the variability of the winter sea ice concentration in the Labrador sea by Deser et al. (2002).

Apparently sea ice anomalies are preceded by freshwater anomalies (Houghton and Visbeck, 2002) and are therefore correlated with these. It also seems plausible that the interannual variations of P and E are not entirely uncorrelated. If precipitation is anomalously large one year, evaporation must also be anomalously large, though not necessarily in the same location. With regard to the advective transport we simply don't know, how representative the Labrador current is for the advective freshwater transport within the entire North Atlantic basin.

The variance of such a sum of random processes is the sum of the variances, if the processes are independent and uncorrelated. If the processes are correlated, on the other hand, the variance is much harder to quantify, since the processes are no longer independent and their correlation has to be taken into account.

Therefore it is only possible to give an estimate for the minimum of σ by using the variability of precipitation P as an indicator for the total variability, as the sea ice concentration and advective transport influences and their correlations are very difficult to quantify.

In the model it is assumed that precipitation is a white noise process. In reality, precipitation is not an uncorrelated white noise process, but rather a correlated red noise process with an autocorrelation e-folding time or decorrelation timescale of a couple of days (e. g. Joseph et al., 2000). In the model (Eq. 2.11) a white noise process has been substituted for the red noise process of precipitation. This is possible if the timescales of the processes differ widely, which is the case here, since the model integration timestep is 0.1 years.

The noise amplitude σ of an equivalent white noise process driving the ocean model can be assessed by comparing the variances of two simple linear models: One that is driven by white noise and one that is driven by red noise. A model y driven by white noise $\sigma\dot{W}$ has variance

$$\mathrm{var}(y) = \frac{\sigma^2}{2\delta} \tag{2.14}$$

with δ the inverse decorrelation timescale of the model. A model y' driven by a red noise process z, on the other hand, has the variance $\mathrm{var}(y') = \lambda^2/(2\alpha\delta(\alpha+\delta))$, if z has the variance $\mathrm{var}(z) = \lambda^2/2\alpha$. Here, α is the inverse decorrelation timescale of the red noise process z driving the model, δ is the same as for the model driven by white noise, and

λ is the amplitude of the white noise process generating the red noise. From comparing these quantities it becomes obvious that $\sigma^2 = \lambda^2/(\alpha(\alpha+\delta))$ and therefore

$$\sigma = \sqrt{\frac{2}{(\alpha+\delta)}\mathrm{var}(z)}.$$

Walsh and Portis report the standard deviation of annual averages of precipitation. The variance of such annual averages is of course much lower than the variance of the original process. If we assume the original process to be a piecewise constant timeseries, we can estimate that the variance of a process $\bar{z}$, where N values have been averaged, is $1/N$ times the variance of the original process z. Numerical experiments show that this relationship holds well for the actual red-noise process, if a segment length of twice the decorrelation timescale τ is assumed. This gives the relation $\mathrm{var}(z) = N\,\mathrm{var}(\bar{z})$ for the variances, with N given by $N = (T/2\tau) = \alpha T/2$ and T the averaging time.

Walsh and Portis estimate that the standard deviation of precipitation and evaporation is about 10-20% of the mean, corresponding to a variance $\mathrm{var}(\bar{z}) = (\beta\mu)^2$ with μ the mean freshwater flux and $0.1 \leq \beta \leq 0.2$. If we assume that rain has a decorrelation timescale τ of about a week, $\tau = 1/\alpha \approx 1/50\,\mathrm{yr}$ and therefore $\alpha \approx 50\,\mathrm{yr}^{-1}$. The inverse decorrelation timescale δ of the ocean model can be assessed from the linearized model presented in section 2.3. From Eq. 2.16 it is obvious that $\delta = 2\sqrt{\Delta\mu}$. As $0 \leq \Delta\mu \leq 0.25$, we get $0 \leq \delta \leq 1$. From these considerations it follows that

$$\sigma = \sqrt{\frac{2}{(\alpha+\delta)}\frac{\alpha}{2}T(\beta\mu)^2} \approx \sqrt{T}\beta\mu. \tag{2.15}$$

The maximum mean freshwater flux μ in the reduced Stommel model is $\mu = \mu_c = 0.25$, giving a range from $\sigma = 2.5\times10^{-2}$ to $\sigma = 5\times10^{-2}$ for σ. In the following model simulations a value of $\sigma = 2.5\times10^{-2}$ will therefore be used, unless another value is specified explicitly.

2.3 Spectral changes at the bifurcation

In the deterministic case, it is possible to asses the distance to the bifurcation point on the basis of a measured steady state overturning q. This would require, however, a perfect knowledge of q itself as well as of all the model parameters.

The stochastic model formulation on the other hand reveals additional information because fluctuations are included, the properties of which might be used for indicating the distance to the bifurcation.

The spectrum of the system described by Eq. 2.12 can be calculated analytically by using small noise expansion (Gardiner, 1994), essentially a linearization of the system around the steady state solution $y_0 = \langle y(t) \rangle$. The prerequisite for applying this approximation is that the noise amplitude is sufficiently small, i.e. the influence of the noise on the system behavior is small compared to the deterministic influences.

The dynamics of the perturbation $\tilde{y} = y - y_0$ is given by the linearization of Eq. 2.12 around y_0:

$$\dot{\tilde{y}} = (2y_0 - 1)\tilde{y} + \sigma\dot{W}. \tag{2.16}$$

Equation 2.16 describes an Ornstein-Uhlenbeck Process. The spectrum of this process is (Gardiner, 1994)

$$S(\omega) = \frac{\sigma^2}{(2y_0 - 1)^2 + \omega^2}. \tag{2.17}$$

Using the deterministic steady state solution (2.13) and the distance $\Delta\mu = \mu_c - \mu$ from the critical freshwater flux μ_c, the dependence of the power spectral density on the distance to the bifurcation point $\Delta\mu$ is obtained:

$$S(\omega, \Delta\mu) = \frac{\sigma^2}{4\Delta\mu + \omega^2}. \tag{2.18}$$

Plotting the power spectral density calculated from the timeseries of overturning data, a shift in spectral properties due to the lurking bifurcation can be seen. It is clearly visible from Fig. 2.2 that the spectrum changes as the system is moved towards the bifurcation point. Far away from the bifurcation, one obtains a red spectrum with a cutoff frequency (the frequency, where the spectrum changes from a horizontal to a decreasing shape) of approx. 10^{-1} (please note that frequency is given in nondimensional units, as time is nondimensional), while the magnitude of the spectrum in the limit $\omega \to 0$ is approx. 8×10^{-4}. Close to the bifurcation, the cutoff frequency decreases to approx. 2×10^{-2} at $\Delta\mu = 0.02$, while the magnitude of the spectrum in the limit $\omega \to 0$ increases by about an order of magnitude to approx. 8×10^{-3}.

Obviously the decorrelation time of the overturning increases as one gets closer to the bifurcation, which results in a change in cutoff frequency. This also implies that the probability density function widens and that the amplitude of fluctuations increases.

In Fig. 2.2 both measured and theoretically estimated spectra of the overturning are shown for different distances to the bifurcation point $\Delta\mu$. Comparing these it is obvious that both measured and calculated spectrum agree very closely.

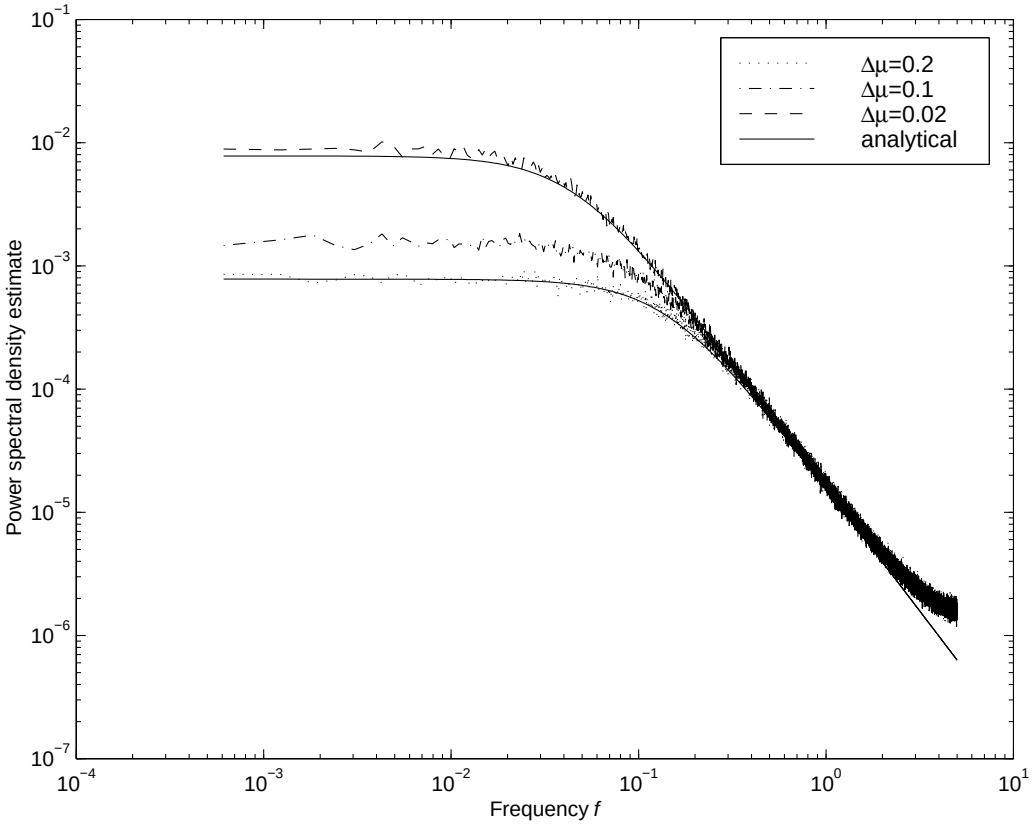

Figure 2.2: Power spectral density estimate of overturning in adiabatically reduced model at distances to bifurcation point $\Delta\mu = 0.2$, $\Delta\mu = 0.1$, $\Delta\mu = 0.02$ and corresponding theoretical spectrum. The analytical spectrum for $\Delta\mu = 0.1$ has been left out for clarity. The frequency denoted on the abscissa refers to nondimensional time.

By transforming the system to an Ornstein-Uhlenbeck process we are now capable of discussing the mechanism leading to increased decorrelation times, i. e. smaller cutoff frequencies.

Physically a larger mean freshwater flux μ, corresponding to a smaller distance to the bifurcation point $\Delta\mu$, leads to an increase of the steady-state salinity gradient y_0 (see Eq. 2.13 for comparison). The increase in y_0 in turn reduces the overturning $q = 1 - y$. Thus the salt-advection feedback (Rahmstorf et al., 1996) that stabilizes the circulation is decreased in strength and small deviations from the steady state change the advection term in Eq. 2.11 very little, which leads to a very slow relaxation to the steady state, thus allowing larger deviations from y_0 and increasing the decorrelation time. The power spectral density changes towards a "redder" spectrum. The magnitude of the spectrum in the limit $\omega \to 0$ is inversely proportional to $\Delta\mu$, while the cutoff frequency is proportional to the square root.

While the change in spectral properties as a system is moved closer to a bifurcation certainly lends itself nicely to visualization, this may, depending on the investigation conducted, not be the most reliable method for estimating the distance to the bifurcation point. The increase in decorrelation time used to determine $\Delta\mu$ could also be obtained by other techniques of timeseries analysis, e. g. by determining the autocorrelation.

2.4 Probability density at the bifurcation

In order to gain further insight into the processes that take place as the system approaches the bifurcation, it seems valuable to also look into the changes of the probability density function (pdf) of the process. While the Langevin equation describes the temporal evolution of the system itself as a diffusion process, the Fokker-Planck equation describes the temporal evolution of the pdf. The Fokker-Planck equation is equivalent to the Langevin SDE, but it examines a different aspect of the system properties.

The Fokker-Planck equation

$$\frac{\partial}{\partial t} p(y,t) = \hat{L}_{\mathrm{FP}} p(y,t) \tag{2.19}$$

is a partial differential equation describing the temporal evolution of the probability density function p. $\hat{L}_{\mathrm{FP}}$ is the Fokker-Planck operator

$$\hat{L}_{\mathrm{FP}} = -\frac{\partial}{\partial y}(-\nabla f(y)) + \frac{\sigma^2}{2}\frac{\partial^2}{\partial y^2} \tag{2.20}$$

with

$$f(y) = -\left(\frac{y^3}{3} - \frac{y^2}{2} + \mu y\right) \tag{2.21}$$

being the potential for the adiabatically reduced system (2.12) in the vicinity of the potential minimum. If the system is close to the steady-state solution y_0, a steady state probability density function can be calculated from the Fokker-Planck equation using the potential solution (Gardiner, 1994). This solution is

$$p_{\mathrm{stat}}(y) = N \exp\left(-\frac{2}{\sigma^2} f(y)\right) \tag{2.22}$$

with a normalization constant N and the potential (2.21). An analogue to this system is the motion of an overdamped particle in a potential well driven by a Brownian forcing.

It can be assumed that this *Ansatz* can be used as long as the mean first exit time from the quasi-stationary state is much longer than the timescales under consideration. Strictly speaking, this method of solution is not applicable because the system is not

in a stationary state, but only in a quasi-stationary state. As outlined in section 2.5, this assumption is valid as long as the system is not so close to the bifurcation that a breakdown of the circulation is inevitable.

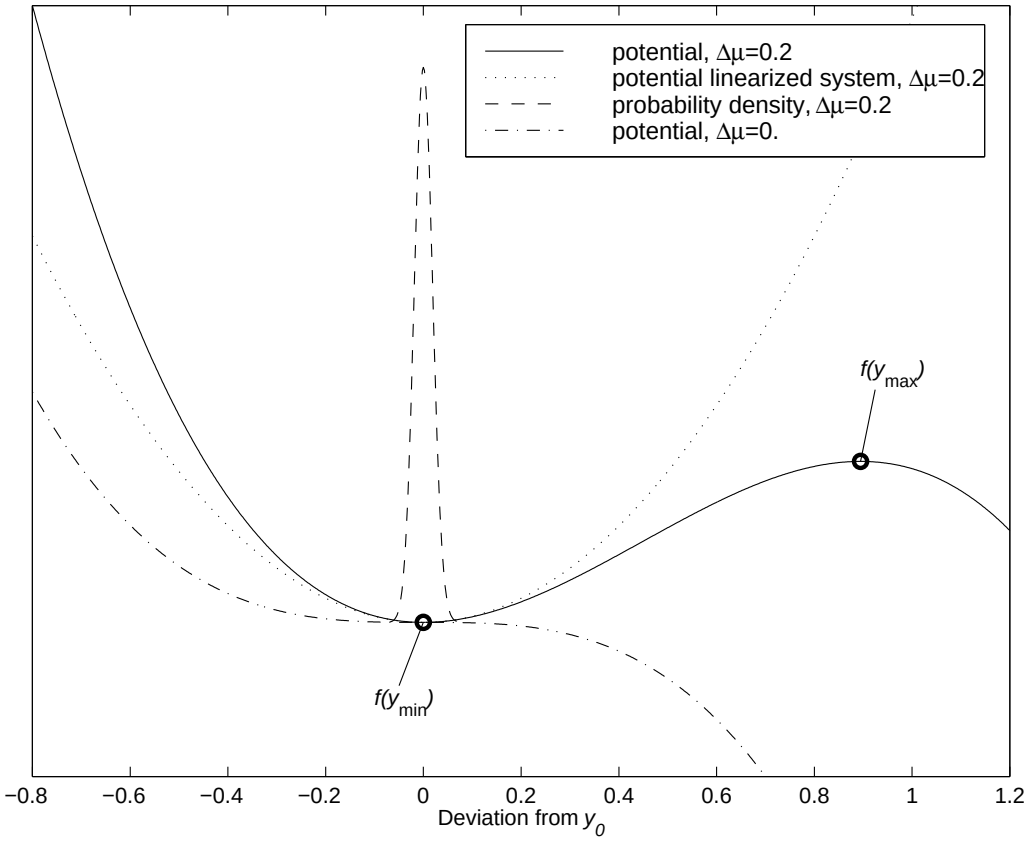

Figure 2.3: Potential and probability density function at distance to bifurcation point $\Delta\mu = 0.2$ and potential at the bifurcation point $\Delta\mu = 0$. The potentials have been transformed by an additive constant, so that they agree in y_0. Noise amplitude σ was $\sigma = 2.5 \cdot 10^{-2}$. Potential minimum $f(y_{\min})$ and potential maximum $f(y_{\max})$ are marked with circles. The pdf is obviously constrained to an area, where potential and linearization still agree.

The adiabatically reduced system (2.12) corresponds to the cubic potential (2.21). Far away from the bifurcation point, there is a well-defi ned potential-well. This is shown quite clearly in Fig. 2.3, where the potential is plotted for $\Delta\mu = 0.2$ and $\Delta\mu = 0$. At $\Delta\mu = 0.2$ the pdf is tightly constrained within the potential-well. As the system moves closer to the bifurcation, the potential difference $\Delta f = f(y_{\max}) - f(y_{\min})$ decreases, until it vanishes at the deterministic bifurcation point μ_c. The pdf broadens and the probability current across the local maximum $f(y_{\max})$ increases.

The approach to a deterministic saddle-node bifurcation corresponds to a decrease of the potential difference between local minimum (corresponding to the stable fixed point in the deterministic system) and local maximum (corresponding to the unstable fixed point) of the stochastic potential, until the potential difference is zero at the deterministic bifurcation point. This flattening of the potential again reflects the vanishing restoring force.

The linearized system (2.16) corresponds to a parabolic potential. As the system approaches the bifurcation, the parabola widens. Therefore the change in the spectrum can be explained by the widening of the parabolic potential, whereas the bifurcation itself is the vanishing of the potential well.

2.5 Stability of the THC

As the stochastic system approaches the bifurcation, its stability decreases gradually. Even if the deterministic bifurcation point has not been reached, there still is a finite probability that the stochastic system will leave the potential well and cross over to the haline-driven reverse equilibrium circulation (Monahan, 2002).

If the goal of detecting a lurking bifurcation is to provide means for control, the bifurcation has to be detected at large enough a distance to the bifurcation point. Very close to the bifurcation, however, the system will not be stable for very long. If this method is to make sense, the circulation has to be stable long enough to provide enough time for a meaningful measurement and for moving the system away from the bifurcation again, if it is too close to it. Therefore it is necessary to assess the dependence of the lifetime of the quasistationary state of the THC on the bifurcation parameter. In addition the stationary solution developed in the last section does not make any sense, if the quasistationary system is not stable on the timescales under consideration.

Within the framework of Fokker-Planck equation and probability density, the lifetime of the quasistationary state of the system can be described by the mean first exit time from the potential well, which is the time, when the system leaves the potential well for the first time in the ensemble mean. Physically, this is the average time the system stays in the stable equilibrium solution despite the forcing by the stochastic process. In this section the dependence of the mean first exit time on the bifurcation parameter is investigated.

Some arbitrary area in configuration space is considered that contains the current maximum of the pdf. The mean first exit time from the potential well can be calculated from the probability density p and the probability current J. The probability current can

also be understood as the probability divided by the mean first exit time τ. Therefore the mean first exit time can be calculated from

$$\tau = \frac{P}{J} = \frac{2}{\sigma^2} \int_{y_1}^{y_2} \exp\left(-\frac{2}{\sigma^2} f(y)\right) dy \int_{y_{\min}}^{A} \exp\left(\frac{2}{\sigma^2} f(y)\right) dy \tag{2.23}$$

with $f(y)$ given by Eq. 2.21 (Risken, 1996). The probability P that the system is within the potential well is determined by the first integral in Eq. 2.23, whereas the inverse of the probability current from the potential minimum at $y_{\min}$ to a point A outside the potential well is estimated in the second integral. The integration boundaries $y_{1,2}$ are the boundaries of the area in configuration space considered, while A is located outside the potential well, somewhat larger than $y_{\max}$. The exact location of A is arbitrary, since it is assumed that the transition from $y_{\max}$ to A is much faster than the mean first exit time. The integrals in Eq. 2.23 can be evaluated numerically.

If the potential difference $\Delta f = f(y_{\max}) - f(y_{\min})$ is much larger that the diffusion coefficient $D = \sigma^2/2$, it is also possible to obtain an analytical expression for the mean first exit time by using Kramers' formula (Risken, 1996). Thus an insight into the dependence of the system's stability on the distance from the bifurcation point can be gained. In the case under consideration here, Kramers' escape time is

$$\tau(\sigma, \Delta\mu) = 2\pi (4\Delta\mu)^{-\frac{1}{2}} \exp\left(\frac{1}{3\sigma^2} (4\Delta\mu)^{\frac{3}{2}}\right). \tag{2.24}$$

The mean first exit time τ grows stronger than exponentially with distance $\Delta\mu$, while it decreases with rising noise variance σ^2. As one can see from Fig. 2.4, this approximation is not valid very close to the bifurcation point. In that case, the mean first exit time has to be calculated numerically.

In order to compare these results with model simulations, an ensemble experiment of 1000 model simulations for every parameter combination considered is conducted. The model equation (2.12) is integrated forward in time, and the time when the system leaves the potential well is considered the first exit time. The mean first exit time τ is given by the ensemble mean. These simulations are performed at noise amplitudes of $\sigma = 2.5 \times 10^{-2}$, $\sigma = 5 \times 10^{-2}$ and $\sigma = 7.5 \times 10^{-2}$ with mean freshwater fluxes μ ranging from $\mu = 0.23$ to $\mu = 0.25$, corresponding to $\Delta\mu = 0.02$ and $\Delta\mu = 0$.

The results obtained by numerical integration of Eq. 2.23 and by model simulation were nearly identical. Thus we have plotted the mean first exit times obtained by numerical integration and by the analytical approximation in Fig. 2.4. From this figure it is obvious that the analytical approximation is not applicable below $\Delta\mu = 1.1 \times 10^2$ at $\sigma = 7.5 \times 10^{-2}$, while it can be used closer to the bifurcation point, if the noise strength is lower. At larger distances from the bifurcation point all methods give similar answers.

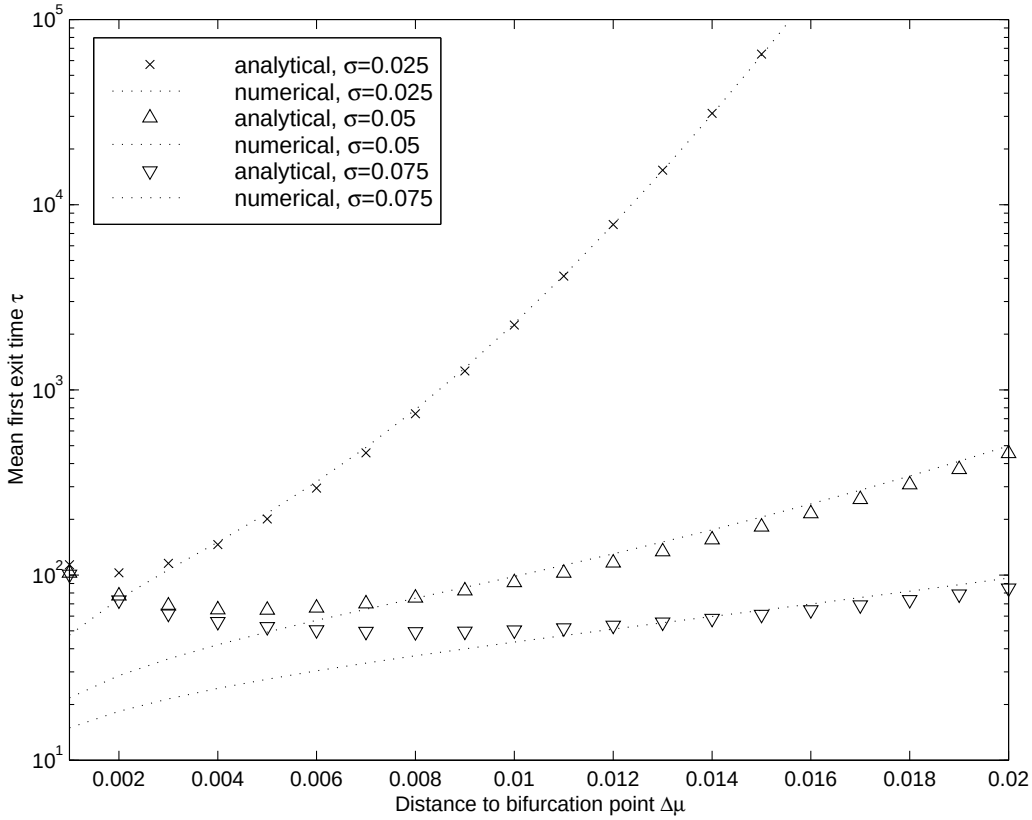

Figure 2.4: Nondimensional mean first exit times in the vicinity of the bifurcation point, calculated analytically and numerically for three noise amplitudes σ.

When it comes to a discussion of the stability of the THC, three timescales are of major interest. First a mean first exit time of about 10^4 years is relevant, as that is the age of the Holocene, and the THC has been relatively stable for that long, which can be inferred from North Atlantic sediment data (Bond et al., 1997). If we assume that conditions have been relatively stable during the Holocene until the begin of industrialization, this value of the mean first exit time is the minimum distance possible for preindustrial conditions. The second relevant timescale is the time needed to obtain a meaningful measurement, while the third timescale is the time needed to change the mean freshwater input μ, if it is determined that we are too close to a breakdown of the THC. We estimate both the second and the third timescale to be in the range of $10^2 - 10^3$ years.

As an illustration of the information that can be gained by using the *Ansatz* developed in this section, the distances to the bifurcation point that correspond to these timescales will be estimated. The analysis is of course not directly applicable to the real THC, but only to the simplified model. For convenience, we now assume that a nondimensional

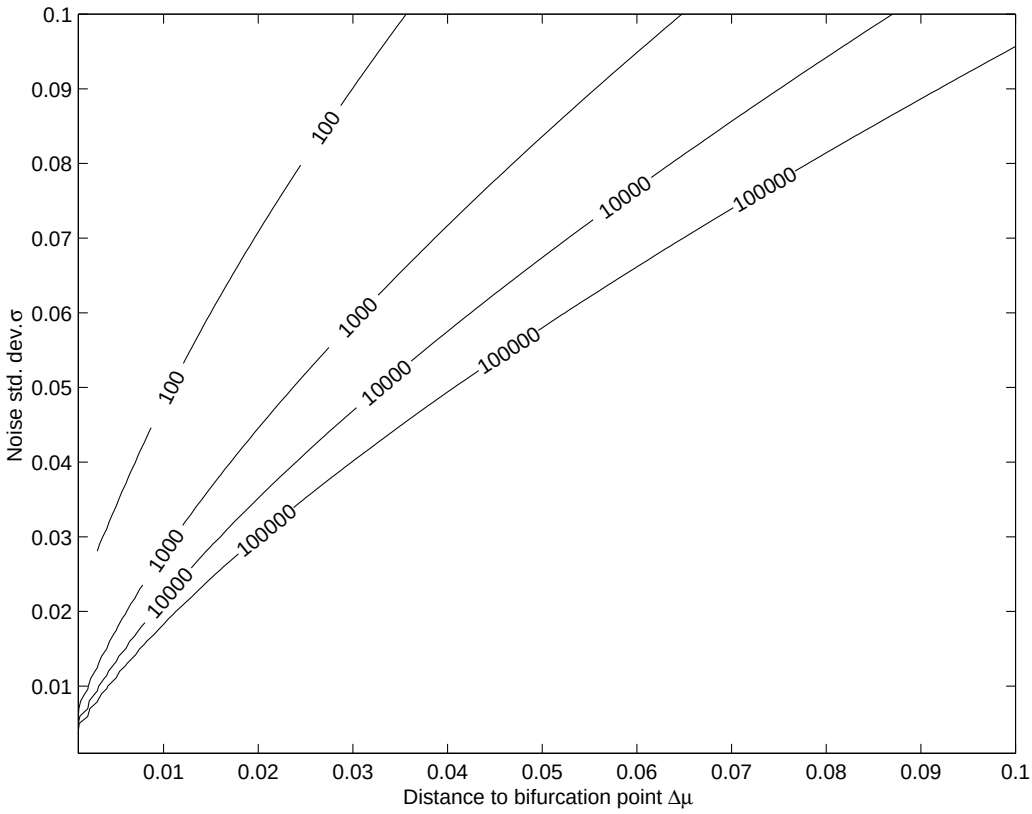

Figure 2.5: Nondimensional mean first exit time from the potential well for varying noise strength σ and distance to bifurcation point $\Delta\mu$. Calculated from the analytical approximation, where it is valid. The mean first exit time is given in nondimensional time units. Large decorrelation times also allow for the notion of quasistationary states. For sensible parameter combinations the mean first exit times are always much larger than decorrelation times.

timestep is equal to one year. The error introduced by this simplification is small, as the actual length of a timestep is equal to 1.66 yr.

From Fig. 2.5, where the mean first exit time obtained analytically is shown depending on the distance to the bifurcation point $\Delta\mu$ and on the noise amplitude σ, it can be seen that a mean first exit time of 10^4 years is reached at $\Delta\mu = 0.07$, corresponding to $\mu = 0.18$, if the noise standard deviation is comparatively high at $\sigma = 7.5 \times 10^{-2}$. With $\sigma = 5 \times 10^{-2}$, this time is reached at $\Delta\mu \approx 0.033$, corresponding to $\mu = 0.217$, while $\Delta\mu \approx 0.013$ at $\sigma = 2.5 \times 10^{-2}$.

A mean first exit time of 10^3 years is reached at $\Delta\mu = 0.052$ for $\sigma = 7.5 \times 10^{-2}$. Therefore the mean freshwater flux μ must be smaller than $\mu = 0.198$, if we want to be able to still measure and control the system. This minimum permissible distance to

the bifurcation point decreases with smaller noise standard deviations to $\Delta\mu = 0.023$ at $\sigma = 5 \times 10^{-2}$ and $\Delta\mu = 0.008$ for $\sigma = 2.5 \times 10^{-2}$.

2.6 Beyond the simplified Stommel model

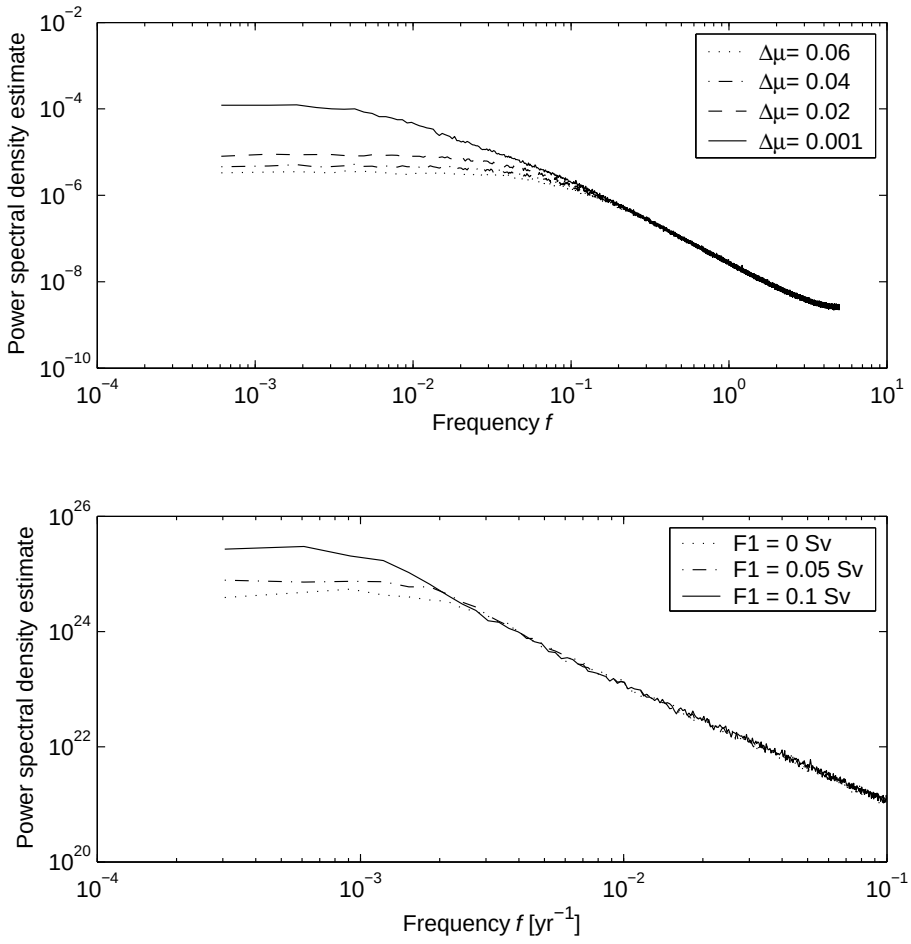

Figure 2.6: Power spectral density of overturning at different mean freshwater fluxes in less simplified box models. Upper panel: Full Stommel model, legend gives distance to bifurcation point $\Delta\mu$, frequency is nondimensional. Lower panel: Four box model of the interhemispheric THC, salinity only, legend gives mean freshwater flux F_1.

The change in the spectrum as the system is moved closer to the saddle-node bifurcation is caused by a decrease in the strength of the advective feedback stabilizing the THC. The advective feedback mechanism is clearly not a property that is restricted to the simple box model the experiments were performed with. Therefore it can be assumed

that the changes in the spectrum that are observed in a very simple box model also occur in more comprehensive models, if the strength of the advective feedback is reduced.

We have performed experiments similar to the ones we described in section 2.3 with two less simplified box models. First the full Stommel model including the temperature dynamics was used, as in equations 2.7 and 2.8. The upper panel of Fig. 2.6 shows the power spectral density at different distances to the bifurcation point $\Delta\mu$. Clearly the power spectrum changes in a manner similar to the simplified Stommel model as the system gets closer to the bifurcation point.

In addition these, experiments were performed with a salinity-only version of an interhemispheric four-box model of the THC (Titz et al., 2002), which is very similar to the other well-known interhemispheric three- and four-box models (Rooth, 1982, Rahmstorf, 1996, Rahmstorf and Ganopolski, 1999b, Scott et al., 1999, Titz et al., 2002). These models describe an interhemispheric thermohaline circulation, where the strength of the overturning is dependent on the density gradient between the northern and the southern box of the model. The equatorial box, which is much warmer than the polar boxes, has no influence on the steady state circulation, it only affects the dynamics of changes in circulation strength. In this type of model a modified bifurcation behavior occurs: If there also is a freshwater transport above a certain threshold between the equatorial and the northern box of the model, a Hopf bifurcation can occur (Titz et al., 2002). The model is modified by adding a stochastic freshwater flux between the southern and the equatorial box of the model, and experiments at different mean freshwater fluxes are performed, while the freshwater flux between the equatorial and the northern box is kept below the critical value for the Hopf bifurcation. The power spectral density of the overturning is shown in the lower part of Fig. 2.6. Again there are distinct changes in the power spectrum as the system approaches the bifurcation point.

Due to the lack of a suitable GCM it has not yet been possible to test whether the effect described here also occurs in full-scale GCMs, but GCM experiments have shown that the overturning decreases with an increase of the freshwater flux into the Atlantic basin (Rahmstorf, 1996). Decreased overturning implies decreased advection and therefore a decrease in the strength of the advective feedback.

Von Storch et al. have investigated the spectral characteristics of the deep-ocean mass-transport (von Storch et al., 2000). They found no evidence against the assumption that the THC has a red spectrum. In fact they found a power spectral density $S(\omega)$ proportional to ω^{-2} in a frequency range from $\omega = 1/20\,\mathrm{yr}^{-1}$ to $\omega = 1/500\,\mathrm{yr}^{-1}$. Longer timescales, where a red spectrum would level off, could not be resolved due to the short timeseries they had available.

Knutti and Stocker have published results from experiments with a model of intermediate complexity (Knutti and Stocker, 2002), where they report that the variability of the overturning increases strongly in the vicinity of the critical threshold where the THC collapses. Tziperman has reported a similar increase in variance close to the instability threshold in experiments with a comprehensive 3D ocean-atmosphere model (Tziperman, 2000). This increase in variability is also predicted by our model, as implied by Eq. 2.14.

Finally, we show in a separate publication (Held and Kleinen, 2004) that a slightly modified version of our method can also be applied to an earth system model of intermediate complexity. The model CLIMBER-2 (Petoukhov et al., 2000, Ganopolski et al., 2001) consists of a zonally averaged ocean model, which is coupled to a coarse-resolution atmospheric model, and a simple biosphere model.

A bifurcation is characterized by the fact, that the equilibrium solutions of the system under consideration change at the bifurcation. In general there is a control parameter μ, and at a critical value μ_c of the control parameter, an equilibrium solution vanishes or is created. When discussing bifurcations in the climate system, it is implicitly assumed that the quasi-stationary dynamics of the climate system can be simplified as an equilibrium of a nonlinear dynamical system which is perturbed by noise. In the small noise limit, which we consider in this chapter, the response to the noise forcing can be approximated by linear modes.

A fundamental property of bifurcations is the fact that one mode, the "critical mode", becomes unstable at the bifurcation, which leads to a vanishing of the smallest decay rate (Wiggins, 1990). Since the variance in the linear approximation of the small noise limit increases as $\Delta\mu = \mu_c - \mu \rightarrow 0$, this critical mode can be approximated by the leading empirical orthogonal function (EOF) (von Storch and Zwiers, 1999).

Hence we attempted to determine the critical mode in the ocean model of CLIMBER-2. We perturbed the current-day climate the model simulates by adding a freshwater flux to the North-Atlantic region. We thus created a quasi-stationary state, where the ocean was very close to the bifurcation point. By performing a principal component analysis of the salinity field, we determined the leading EOF, which approximates the critical mode.

We then created different quasi-stationary states by adding different freshwater fluxes to the North-Atlantic and projected the salinity field onto the EOF approximating the critical mode. The timeseries of the corresponding principal component can then be used to determine the proximity to the bifurcation, since it also displays increasing decorrelation times as the system approaches the bifurcation.

While all of these characteristics are no conclusive evidence that the behavior we are describing also occurs in the real ocean, they are consistent with the predictions by our model. We therefore feel confident that our results can also be applied to the real ocean.

2.7 Summary and Conclusions

In this chapter we have demonstrated how the spectral properties and the probability density change as the THC moves closer to the bifurcation point in a stochastic modification of the Stommel-model. As the system approaches the bifurcation point, the spectrum becomes "redder". The magnitude of the power spectral density in the limit of zero frequency increases inversely proportional to the distance to the bifurcation point $\Delta\mu$, while the cutoff frequency decreases proportionally to the square root.

The mechanism described above is a generic property of the advective feedback mechanism and the saddle-node bifurcation and is therefore independent of the exact values of model parameters. The spectral characteristics of the overturning in GCMs and the observed increase in variance of the overturning close to the instability threshold support the hypothesis that the mechanism described above is also valid for more comprehensive models, even though this would have to be confirmed by experiments. The method presented above could have a wide range of applicability to all systems that contain a saddle-node bifurcation or a feedback mechanism similar to the advective feedback of the THC.

Rahmstorf estimated the distance from the bifurcation point by fitting a deterministic four-box-model to a GCM hysteresis run of the THC (Rahmstorf, 1996). A similar approach could also be used to estimate the distance to the bifurcation point in the real climate system, but it needs the total overturning strength as an input, which is very difficult to measure accurately. Any error in measuring the total overturning would lead to an error in the estimate of the distance to the bifurcation point, which makes an additional independent approach desirable.

Rather than average values of total overturning, our method requires the cutoff frequency of red overturning power spectra as an input, or, equivalently, the decorrelation time in overturning time series. Therefore, the proposed method allows an independent estimate of the actual overturning, for a two-fold reason.

First, the cutoff frequency only requires decorrelation properties of overturning time series as an input, not the total overturning, nor its total variability. Therefore, a time series of a representative fraction of overturning would be sufficient. In addition, fluctuations of salinity and temperature differences show the same change in the power spectral

density as one gets close to the bifurcation. Therefore the distance from the bifurcation point could also be estimated by measuring the fluctuations in either of these quantities.

Second, the proposed method adds information with respect to another source of uncertainty: results obtained with a simple model have to be transferred back to the real world system. This transfer is problematical with both methods, the one proposed here, and the "traditional" based on time-averaged, total overturning estimates. The model parameters, which contain considerable uncertainty, facilitate this transfer. From a simple argument of units it becomes evident that our proposed method is sensitive to an alternative set of parameter uncertainties compared to the traditional method. Our method rests on cutoff frequencies, and hence decorrelation times of the overturning, and thereby introduces the unit of "time" into the analysis, whereas the "traditional" scheme relies on the total measured overturning, which is not in itself time-dependent. Therefore, the focus of sensitivity in parameter space is different for both methods, and the method proposed here is therefore a source of supplementary information on the state of the system.

What can be obtained from consecutive measurements without a transformation back to the "real world" is a prediction of a trend in the bifurcation parameter. This may be worth something already, even if the absolute distance to the bifurcation point contains a certain margin of error.

A problem appears, if the actual threshold in the climate system is not determined by the advective processes described by the Stommel model, but by a shutdown of convection before the saddle-node bifurcation is reached. If this is true, the distance from the saddle-node bifurcation can still be estimated, but this will not be relevant for the climate system. An estimate of the distance from the point, where convection shuts down, may also be possible, but this has not been investigated so far.

It remains questionable, whether this indicator can be used as a warning indicator for THC shutdown dangers due to global warming, since timeseries length requirements are still quite high compared to the timescales during which climate change will occur within the near future. Nevertheless, it may still be able to improve our understanding of the THC by using paleo information on the Holocene THC in order to determine the state of the THC during preindustrial conditions, as outlined in Held and Kleinen (2004). In addition, this indicator could be used for further applications. Since the changes in spectral properties are a generic feature of the saddle-node bifurcation, the indicator could also be valuable for the assessment of different systems, e. g. the Indian Monsoon, where a saddle-node bifurcation may play a role (Zickfeld, 2003), or for the detection of transitions in ecosystems (Scheffer and Carpenter, 2003). In addition, it can be shown that similar changes in the spectrum occur at pitchfork and transcritical bifurcations.

This chapter illustrates that the variability of climatic variables contains important information that is not accessible, if only averaged values are considered. Stochastic information is therefore able to reduce uncertainty about the state of the system.

Chapter 3

Probabilistic extension of the Tolerable Windows Approach

3.1 Introduction

The *tolerable windows approach* (TWA) (Petschel-Held et al., 1999, Bruckner et al., 1999, 2003b, Toth, 2003, Toth et al., 2003a,b), also called the *guardrail approach*, is an approach to the integrated assessment of climate change (IA).

The assessment of climate change initially started out as a work done along disciplinary lines. Atmospheric scientists and oceanographers worked on atmospheric and ocean models. Hydrologists and ecologists attempted to assess the impacts of climate change on water supply, ecosystems and food production. Economists and engineers tried to evaluate the feasibility and costs of emission reduction strategies. Since all of these were disconnected activities, they involved diverse and often contradictory assumptions. This led to difficulties in comparing results and reduced policy relevance. In the late 1980s, first attempts were made to integrate these elements into a consistent framework. Out of these first attempts grew what now is called *integrated assessment* (Bruckner et al., 1999).

In the integrated assessment of climate change an attempt is made to evaluate the whole chain of cause and effect of climate change, ranging from the anthropogeneous emissions of greenhouse gases, over the changes in climate these emissions cause, to the impacts the induced climate change will have. Prototypically, this is done in a comprehensive and coordinated analysis. Since this mainly involves the *future* changes in climate, a strong emphasis is placed on models as tools for IA.

Formally the integrated assessment of climate change is a control problem with the basic formulation

$$\dot{\mathbf{x}} = \mathbf{f}(\mathbf{x}, t; \mathbf{u}). \tag{3.1}$$

In this equation $\mathbf{x} \in \mathbb{R}^n$ is the state vector of the system, and $\mathbf{u} \in \mathbb{U}$ is a vector of control variables that can be freely chosen in $\mathbb{U}$. In the climate change problem, $\mathbf{u}$ could be the reductions in CO_2 emissions, or the emissions themselves. With the help of this basic equation, three basic approaches to the integrated assessment of climate change can be distinguished (adapted from Weyant et al., 1996):

- Policy evaluation modeling: in policy evaluation modeling the physical, ecologic economic and social consequences of *predefined* climate protection strategies are evaluated. Formally, a single control function $\mathbf{u}(\cdot)$ is specifi ed as an input, and the solutions $\mathbf{x}(\cdot)$ are sought.
  A representative of this approach is the IMAGE family of models (Rotmans et al., 1989, Alcamo et al., 1998).

- Policy optimization modeling: in policy optimization modeling it is attempted to determine control vectors in such a way that a predefi ned goal function is maximized. This function may be determined by costs and benefi ts of climate protection strategies in a single metric, i. e. US $, but other defi nitions are possible as well. After defi ning a goal function $J(t) = \int_0^t c(\mathbf{x}, t')dt'$, solutions $\tilde{\mathbf{u}}(\cdot)$ are sought, such that
  $$\tilde{\mathbf{u}}(\cdot) = \arg\max_u(t) \int_0^t c(\mathbf{x}, t')dt' \text{ with } \dot{\mathbf{x}} = \mathbf{f}(\mathbf{x}, t; \mathbf{u}). \tag{3.2}$$
  Policy optimization modeling usually takes place either as *cost-benefit analysis* or, in cases where additional constraints are acknowledged, as *cost-effectiveness analysis*. Typical representatives of this approach are the models DICE (Nordhaus, 1994), RICE (Nordhaus and Yang, 1996) and SIAM (Hasselmann et al., 1997).

- Policy guidance modeling: policy guidance modeling aims to determine the *complete set* of climate protection strategies $\mathbf{u}(\cdot)$ that are compatible with normative constraints, formally defi ned as $\mathbf{h}(\mathbf{x}, t; \mathbf{u}) \leq \mathbf{0}$. These constraints may be set in order to limit the impacts of climate change, but they may also limit the costs of emission reduction or any other element that is represented in the coupled assessment model. This problem can formally be represented as a differential inclusion (Aubin and Cellina, 1984, Deimling, 1992)
  $$\dot{\mathbf{x}} \in \mathbb{F}(\mathbf{x}, t) \text{ with } \mathbb{F} := \{\mathbf{f}(\mathbf{x}, t; \mathbf{u}) | \mathbf{u} \in \mathbb{U}\} \tag{3.3}$$

under the condition

$$\mathbf{h}(\mathbf{x}, t; \mathbf{u}) \leq 0. \tag{3.4}$$

A possible solution to this problem is the *funnel*, the set of all states that can be reached by trajectories that are compatible with the constraints. A projection of the funnel on the plane defined by the time axis and an emission axis is called an *emission corridor*.

Representatives of this approach are the *safe landing analysis* (Swart et al., 1998), which partly fulfills the abovementioned characteristics, and the *tolerable windows approach*.

The *tolerable windows approach* (TWA) (Petschel-Held et al., 1999, Bruckner et al., 1999, Toth, 2003, Bruckner et al., 2003b) is a representative of the policy guidance modeling approach. The TWA was originally proposed by the German Advisory Council on Global Change (WBGU, 1995) during the preparations for the 1st Conference of the Parties (COP) to the United Nations Framework Convention on Climate Change (UNFCCC) in Berlin. Its main objective is to support climate change decision-making by separating scientific analysis from the normative setting of climate protection targets (Petschel-Held et al., 1999, Bruckner et al., 2003b).

A major motivation for the TWA stems from Article 2 of the UNFCCC. This article calls for the stabilization of greenhouse gas concentrations at levels that prevents dangerous anthropogenic interference with the climate system (United Nations, 1995). The TWA is an approach that enables an operationalization of Article 2, since it aims to determine the maneuvering space humanity has, if it wants to avoid "dangerous anthropogenic interference". In the TWA the integrated assessment process starts by assessing which impacts of climate change or mitigation measures are undesirable. These impacts are then excluded by setting normative constraints, "guardrails" in the language of the TWA. This step is seen as a normative decision to be taken by the policy-maker seeking policy advice, guided by the scientific assessment, but not a scientific decision in itself. In a subsequent step, the TWA then determines sets of emission reduction strategies that are compatible with the predefined guardrails.

The impacts of climate change are very important in the TWA, and impacts can therefore be represented as climate impact response functions (CIRF) (Bruckner et al., 1999, Füssel et al., 2003). CIRFs are derived from climate impact assessments and indicate how the system under consideration reacts to climate change. Therefore impacts of climate change need not be expressed in monetary terms, as in policy optimization modeling, but they can rather be expressed in a metric that is suitable to the impact under consideration.

Since uncertainty is present in every link of the chain of cause and effect in IA, uncertainty needs to be represented adequately in the TWA. First steps of considering uncertainty in the TWA have been made. Toth et al. (2003b) have presented emission corridors that arise, if parameters in the model or guardrail settings are varied. Similarly, Zickfeld and Bruckner (2003) have determined emission corridors for various probabilities of a collapse of the thermohaline circulation, as well as for different climate sensitivities, while Kriegler and Bruckner (2004) have investigated the sensitivity of emission corridors to changes in various parameters.

While these studies have performed the first steps in considering uncertainty in the TWA, this chapter aims at modifying the conceptual framework in order to fully consider probabilistic uncertainty within an extended TWA. The extension of the deterministic TWA to a probabilistic TWA has two advantages. First, the natural variability of climate and impacts can be considered explicitly. Second, in cases of parameter uncertainty, where probability distributions for uncertain parameters are known, the information known about these uncertainties can be utilized fully. This allows a further improvement in policy advice applications, since the uncertainty can be considered explicitly, which facilitates its communication.

In section 3.2 a stochastic extension to the ICLIPS climate model will be presented, and the consequences of uncertainty for the TWA will be explored. In section 3.3 the conceptual framework of a probabilistic TWA will be developed, while a first application will be shown in section 3.4. The chapter will end with a summary and some conclusions in section 3.5.

3.2 The TWA under probabilistic uncertainty

3.2.1 Two concepts

Two concepts are important for an understanding of the TWA, and they are therefore introduced here. One of the most important concepts in the TWA is the *guardrail*. Originally, the TWA even got it's name from it, since it was called "*Leitplankenansatz*", German for guardrail approach, when it was first conceived.

A guardrail is a limit to climate change, an impact of climate change, or to climate protection measures. Guardrails are conceived to be *normative* limits that are not to be exceeded by climate change or the mitigation of climate change. In the policy advice application the TWA is intended for, the positioning of guardrails is understood to be a normative decision by the policymaker seeking policy advice, guided by scientific advice, but not a scientific decision in itself (e. g. Bruckner et al., 1999).

The exact definition of a guardrail, however, needs to take the important characteristics of the impact under consideration into account. Since an important aim of Article 2 in the UNFCCC is the prevention of dangerous climate change, the "cause of dangerousness" needs to be taken into account.

In general, impacts of climate change can be classified according to the climatic characteristics that are important. Those characteristics that cause an impact to be dangerous therefore need to be taken into account, as will be shown in some examples.

The original set of guardrails investigated by the WBGU (1995) was based on two principles, the "Preservation of Creation" and the prevention of excessive cost. The prevention of excessive cost was considered by limiting emission reductions to a maximal reduction rate, but a guardrail insuring the preservation of creation was set by an expert judgment. A possible interpretation of the first principle is that ecological damages are to be limited. Since there was (and still is) no generally accepted and all-encompassing model that would be able to relate a given climate change to the ecological impacts it would induce, the global mean temperature was used as a rough indicator of climate change consequences. Since the biosphere has evolved during the Quaternary, is was stipulated that the global mean temperature should not leave the range of global mean temperature during the Quaternary plus a certain margin. The WBGU then decided on a guardrail of 2°C above preindustrial temperature.

It is obvious that it would be too narrow an interpretation of a guardrail derived from such considerations to stipulate that the 2°C limit is not ever to be exceeded. A short excursion, where the 2°C guardrail is slightly violated in one year due to natural variability, would not matter at all, since the overall goal, the preservation of creation, could still be reached. The guardrail would in this case rather be set in terms of the mean climate change than in terms of annual values. An inclusion of the natural variability in global mean temperature would therefore be excessive in this case, whereas uncertainty in climate sensitivity definitely is relevant to the problem and should be included in the assessment.

A guardrail that is set to prevent a collapse of the North Atlantic THC is an entirely different matter. For this case, section 2.5 in chapter 2 has shown that the probability of leaving the basin of attraction of the stable solution, roughly the inverse of the mean first exit time, increases as the system is moved closer to the bifurcation point, i. e. the probability of a collapse of the THC increases with climate change. In addition, even a single very large freshwater flux event might cause the collapse. Natural variability should therefore be taken into account in an assessment, as well as uncertainty in climate sensitivity, but the exact definition of the guardrail might then entail a limit to the maximum annual freshwater flux, but not necessarily a probabilistic guardrail.

A similar case are guardrails that are set to limit decreases in agricultural yield. Mearns et al. (1997) have shown that changes in agricultural yield due to climate change depend on changes in variability as well as changes in mean. Here the number of very cold days in winter may have an effect, as well as the length of dry spells in any season, and numerous other influences may be relevant as well. A guardrail definition for this type of impact should therefore also take natural variability into account.

Finally, another impact that could be considered are changes in the probability of single events happening, like the changes in the probability of flood events investigated in chapter 4. The most important factor for changes in flooding probability are changes in the extreme precipitation events. Both a change in the magnitude of the largest extremes and a change in the frequency of a large event of a defined magnitude will lead to an increase of the probability of a flood event happening. Therefore the variability is important here as well, but is not necessarily the variance that is important, but rather the size of the largest fluctuations.

The examples given therefore allow the following classification of the role climatic characteristics play in impacts of climate change:

1. there are some impacts where changes in mean are much more important than the variance, or higher order moments, as the example of the WBGU-guardrail shows.

2. in other impacts of climate change, changes in variance may be equally important

3. there are some impacts of climate change, where higher order moments, like the skewness or the tail of a probability distribution play the dominant role.

Definitions of guardrails need to take these characteristics into account.

The second important concept is an *emission corridor* or, more generally, the different possible solutions to the TWA. In the following, it is assumed that the behavior of the system under consideration can be described by the time evolution of a vector of state variables $\mathbf{x}(t) \in \mathbb{R}^n$. This vector might, for example, contain global mean temperature, greenhouse gas concentration, gross domestic product and agricultural yield. The time evolution of this vector $\mathbf{x}(t)$ depends on a vector $\mathbf{u}(t) \in \mathbb{R}^m$ of control variables. In the climate change problem that is considered here, these are the greenhouse gas emissions, but in principle the approach is of a generic nature, so that any other control variable could be used as well. The evolution of the system can then be modeled as a set of differential equations

$$\dot{\mathbf{x}} = \mathbf{f}(\mathbf{x}, t; \mathbf{u}), \tag{3.5}$$

with a state vector $\mathbf{x} \in \mathbb{R}^n$, a control vector $\mathbf{u} \in \mathbb{U} \subseteq \mathbb{R}^m$, and an initial state $\mathbf{x}_0$. The guardrails or constraints can in the deterministic case usually be formulated as a vector of inequalities

$$\mathbf{h}(\mathbf{x}, t; \mathbf{u}) \leq \mathbf{0}. \tag{3.6}$$

The goal of the TWA is the determination of the set of all emission strategies $\mathbf{u}(\cdot)$ that are compatible with the predefined constraints. Mathematically, this problem is equivalent to the differential inclusion (Aubin and Cellina, 1984, Aubin and Frankowska, 1990)

$$\dot{\mathbf{x}} \in \mathbb{F}(\mathbf{x}, t) \;\; \text{with } \mathbb{F} := \{\mathbf{f}(\mathbf{x}, t; \mathbf{u}) | \mathbf{u} \in \mathbb{U}\} \tag{3.7}$$

under the condition

$$\mathbf{h}(\mathbf{x}, t; \mathbf{u}) \leq 0 \quad \forall t \in [0, t_e] \tag{3.8}$$

subject to $\mathbf{x}(t = 0) = \mathbf{x}_0$, $\mathbb{F} \in \mathbb{R}^n \times \mathbb{R}^m$.

Different concepts exist for definitions of what can be considered a solution to equations 3.7 and 3.8. Following Bruckner et al. (2003b), the following solution concepts can be identified.

A single state trajectory $\mathbf{x}(\cdot)$ starting from $\mathbf{x}_0$ and fulfilling simultaneously Eq. 3.5 and 3.6 is called an *admissible trajectory* driven by a corresponding *admissible control path* $\mathbf{u}(\cdot)$. The comprehensive solution to the problem would then be provided by the *bundle of all admissible trajectories* $\mathfrak{S}(\mathbf{x}_0)$, which corresponds to a *bundle of admissible control paths*. This bundle of admissible control paths is the set of all emission reduction strategies sought. The actual determination of this bundle is currently not possible, however (Bruckner et al., 2003b).

While the focus for the bundles of admissible trajectories / control paths is on the different *trajectories*, the set of *admissible points* in either state or control space can also be determined and is given by

$$\begin{aligned} \Gamma(\mathbf{x}_0) &\equiv \{(t, \mathbf{x}(t)) \mid t \in [0, t_e], \mathbf{x}(\cdot) \in \mathfrak{S}(\mathbf{x}_0)\} \\ &\subseteq [0, t_e] \times \mathbb{R}^n. \end{aligned}$$

$\Gamma(\mathbf{x}_0)$ is called the *funnel*. It is the set of points one obtains when plotting all admissible trajectories. This approach simplifies the problem, since it is no longer necessary to determine all the admissible trajectories, but only the admissible states, and it is possible to determine the boundary of the funnel without knowing $\mathfrak{S}(\mathbf{x}_0)$. It has to be stressed, though, that the funnel contains less information than the bundle. The funnel contains the admissible states, but the information how these states are connected is lost.

Finally, one can select one component of either the state or the control vector and project the funnel onto a plane defined by the time axis and the axis of the respective variable. These projections are called *necessary corridors*. Unfortunately, these corridors do not contain the full information contained in the bundles of admissible trajectories and control paths, but they rather are necessary conditions for trajectories and control paths to be admissible. This implies that every trajectory or control path that leaves the corridor violates at least one of the guardrails and is therefore not admissible, while not every trajectory lying completely within the corridor is necessarily admissible. The fact that an emission path lies completely within the corridor does not insure that none of the constraints is violated. This has to be verified on a case by case basis. While it is possible to derive sufficient subsets of the emission corridor (Kriegler and Bruckner, 2004), these subsets are not complete, and it is currently not possible to derive complete sufficient subsets.

Since the emissions of CO_2 are the most important control variable in the climate change problem considered here, the typical results of TWA-based analyses are *emission corridors*, i. e. projections of the funnel of admissible emissions on the plane defined by a time and an emission axis.

3.2.2 Uncertainty in the integrated assessment of climate change

There have been numerous attempts at classifying the uncertainties inherent in the coupled system of humanity and climate. Some of these attempts are based on more general theories and concepts. In control theory, for example, one distinguishes *aleatory* and *epistemic* uncertainty (Paté-Cornell, 1996). This classification can be found in the integrated assessment of climate change, e. g. in publications by Rotmans and van Asselt (2001), who distinguish between internal variability of the system on the one hand, and unknowns on the other hand. On the basis of these coarse categories, one can distinguish different causes of uncertainty, e. g. random chance inherent in natural processes, or the diversity of human values and behavior.

In another typology, Toth et al. (2003b) distinguish between uncertainties in processes, uncertainty about the predictions of future development, and uncertainty about values and political decisions. This classification of uncertainties is based on the distinction between the different relations to the decision-making process for climate protection strategies.

In the integrated assessment of climate change, uncertainty has so far mostly been considered for *parameter uncertainty*, i. e. uncertainty about climatic processes that can be represented as uncertain parameters in models. Tol (1999), for example, has investigated probability distributions for uncertain parameters in a policy optimization model,

which has also been done by Nordhaus (1994) and Plambeck et al. (1997). Dowlatabadi (2000) and van Asselt and Rotmans (1996) have also investigated parameter uncertainties, with the latter not assuming probability distributions for parameters, but instead investigating the consequences of different cultural perspectives by different actors on the choice of parameters. Finally, Lempert et al. (2000) have investigated the influence of climate *variability* in a policy evaluation model.

With respect to policy guidance modeling, the consideration of uncertainty has been limited so far. What has been done in the past is a sensitivity analysis exploring the sensitivity of emission corridors with respect to uncertain parameter settings, as in Toth et al. (2003b), Zickfeld and Bruckner (2003), Zickfeld (2003), and Kriegler and Bruckner (2004). In all of these cases, it was just possible to test certain parameter settings and to derive the different emission corridors arising out of variations of single parameters, but a more comprehensive treatment of uncertainty remains desirable.

For the purposes of this thesis, three types of uncertainty in the integrated assessment of climate change can be distinguished: uncertainty that is caused by natural variability, uncertainty caused by insufficient knowledge, and uncertainty caused by the unpredictability of human society.

The latter uncertainty is in part anticipated by the TWA, since the TWA doesn't try to predict the future development of human society. By determining the set of emission reduction strategies that is compatible with the predefined guardrails it maps the "maneuvering space" humanity has, if certain impacts are to be avoided. Therefore the uncertainty about the future development of human society is considered by not making predictions about it.

The other two causes of uncertainty can be considered in a TWA that is extended to a probabilistic framework. Here, stochastic information may improve on the deterministic TWA.

Uncertainty caused by insufficient knowledge is impossible to consider comprehensively, since insufficient knowledge implies that we just don't know everything that is important. What can be considered in a practical application is uncertainty that can be expressed as uncertainty in model parameters. If all that is known about an uncertain parameter is a possible range of values, then stochastic information will not help much in considering it, but if a probability distribution of model parameter values is known, then stochastic information can help in considering the uncertainty in a probabilistic TWA.

Uncertainty caused by variability can be considered in the probabilistic TWA as well, as will be shown later in this chapter.

The probabilistic TWA considers *probabilistic uncertainty* in the integrated assessment of climate change. Probabilistic uncertainty is the term we are using for uncertainty

that either arises through the consideration of natural variability, which leads to a probability distribution for the outcomes of an ensemble of experiments, or uncertainty that can be represented by the consideration of probability distributions for uncertain parameters. While the underlying causes of these two sources of uncertainty may be different, the consideration of them leads to similar experiments and results. Both types of uncertainty can be considered in Monte-Carlo experiments (Press et al., 1997) – in the first case sampling from different realizations of the stochastic process, and in the second case sampling from the probability distribution of uncertain parameters –, and both types of uncertainty lead to similar results for experiments. Experiments do not return a single solution, but a probability distribution of experiment outcomes.

The application of the probabilistic TWA will be demonstrated by considering uncertainty in the climate sensitivity, and by considering uncertainty arising through the natural variability of global mean temperature.

One of the key uncertain factors in the assessment of changes in climate is the *equilibrium climate sensitivity* T_{2xCO_2}. The equilibrium climate sensitivity, also simply called climate sensitivity, is the change in global mean temperature that results when the climate system, or a climate model, attains a new equilibrium after a forcing change resulting from a doubling of the atmospheric CO_2 concentration (Cubasch et al., 2001). There are various estimates for T_{2xCO_2}.

The estimate of climate sensitivity published by the IPCC is the range $T_{2xCO_2} \in [1.5°C, 4.5°C]$ (Cubasch et al., 2001), without any further specification of probability distribution or most probable value. However, a few estimates of a probability distribution for T_{2xCO_2} exist, which were derived by various means, e. g. the estimates by Morgan and Keith (1995), Webster and Sokolov (2000), Andronova and Schlesinger (2001), Gregory et al. (2002), and Forest et al. (2002). Of these distributions, the ones by Andronova and Schlesinger (2001) and Forest et al. (2002) are considered here.

Andronova and Schlesinger (2001) used a simple climate/ocean model, the observed near-surface temperature record, and a bootstrap technique to objectively estimate a probability density function (pdf) for T_{2xCO_2}. Their climate model was able to consider five different mechanisms for radiative forcing. These were the radiative forcing by all greenhouse gases other than tropospheric ozone, the forcing by tropospheric ozone, the direct and indirect forcing by sulfate aerosols, the forcing by volcanoes, and the changes in forcing due to changes in solar irradiance. They considered 16 different combinations of these forcing mechanisms. For each combination of forcing mechanisms, they determined the changes in global mean near-surface temperature resulting from the forcing mechanisms and compared them to observations. In addition, they considered the uncertainty arising from natural variability by using a bootstrap-resampling approach.

Thus they derived probability distributions for the climate sensitivity T_{2xCO_2}. The probability distributions for the 16 different combinations of forcing mechanisms roughly fall into three classes. The class T1 does not consider the radiative forcing by aerosols, whereas the other two classes do. The T2 and T3 class estimates differ in their consideration of solar forcing. While the T2 class of estimates considers the solar irradiance forcing, the T3 class does not. Since the T1 class of estimates does not consider the aerosol forcing and it's maximum in probability density is at the very low end of the IPCC range, it will not be considered here, but the T2 and T3 class estimates will be considered.

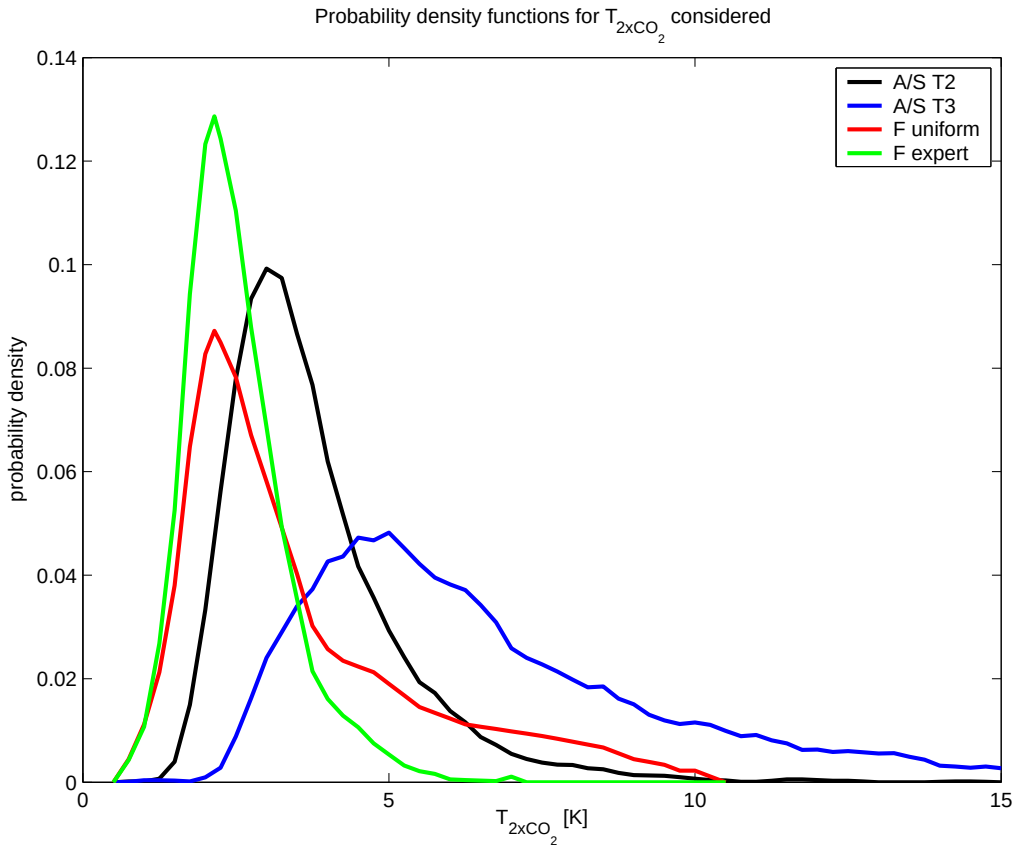

Figure 3.1: Estimates for climate sensitivity T_{2xCO_2} by Andronova and Schlesinger (2001) (A/S T2 and T3), and Forest et al. (2002) (F uniform and expert).

Finally, Forest et al. (2002) derived joint probability distributions for three uncertain properties of the climate system. They used an optimal fingerprinting approach for comparing simulations of a climate model of intermediate complexity with three diagnostics of recent climate observations derived from the upper-air temperature record,

the surface temperature record, and the record of ocean temperatures. In climate model simulations, they systematically varied the climate sensitivity, the rate of heat uptake by the deep ocean, and the strength of the anthropogenic aerosol forcing in order to assess, which simulations match the observed climate record. By using a Bayesian updating scheme, they utilized each diagnostic to update the probability distribution for T_{2xCO_2}, starting from either an expert prior distribution or a uniform prior distribution. Both of the posterior distributions published will be considered.

The probability distributions considered are shown in Fig. 3.1. The estimated probability distributions by Andronova and Schlesinger are shown in black for the T2 class of estimates and in blue for the T3 class, while the estimates by Forest et al. are shown in red for the uniform prior and in green for the expert prior. While both distributions by Forest et al. have the maximum probability density at 2.15K, the maximum in probability density is located at 3.0K for the Andronova and Schlesinger T2 distribution and at 4.75K for the T3 distribution. For the Forest et al. estimates probability density is higher than Andronova and Schlesinger's at low values of T_{2xCO_2}, while it doesn't reach as large values at high T_{2xCO_2}. The pdf generated from a uniform prior assigns higher probabilities to high values of T_{2xCO_2} than the one generated from an expert prior.

The Andronova and Schlesinger T3 distribution gives comparatively high probabilities to high values of T_{2xCO_2}, with values as large as 15K still getting non-zero probabilities. Such high climate sensitivities appear to be quite improbable, but they cannot be ruled out with certainty so far, as was recently shown by Stainforth et al. (2005). Stainforth et al. (2005) performed a large ensemble experiment with a GCM, where they varied a number of uncertain parameters. The climate sensitivities produced by this ensemble were in a range from 1.9 to 11.5K, highlighting that such high climate sensitivities can also be reproduced by GCMs and cannot be ruled out with certainty.

In the future, it may be possible to narrow the range of possible climate sensitivities by constraining climate sensitivity with proxy data from climate states other than the current, e. g. the last glacial maximum, but this work is currently ongoing, and only preliminary results are available. For example, von Deimling et al. (2004) report that they can exclude climate sensitivities $> 4.7°$C, since these are inconsistent with current understanding of the climate at the last glacial maximum. As is apparent from a comparison with Fig. 3.1, these estimates will *considerably* reduce the uncertainty in climate sensitivity.

3.2.3 The ICLIPS climate model

When exploring the consequences of probabilistic uncertainty for the TWA, two sources of uncertainty will be considered. On the one hand, probability distributions for climate

sensitivity will be considered, and on the other hand the natural variability in global mean temperature will be investigated. For this purpose the ICLIPS climate model will be employed, which has to be adapted to the question investigated.

The ICLIPS climate model, originally published in Petschel-Held et al. (1999) and described in more detail by Kriegler and Bruckner (2004), is a reduced-form climate model with very low requirements with regard to computational resources. These low requirements allow extensive ensemble experiments in order to explore the consequences of probabilistic uncertainty for the TWA. The model describes the climate response to anthropogenic forcing, with CO_2 emissions considered as the only greenhouse gas.

The model consists of a very simple carbon cycle coupled to a temperature equation. The carbon cycle approximates a pulse-response model that has been calibrated against carbon cycle and GCM experiments (Maier-Reimer and Hasselmann, 1987, Hasselmann et al., 1997).

The ICLIPS climate model is made up of the three differential equations

$$\dot{F} = E \tag{3.9}$$

$$\dot{C} = \beta E + BF - \gamma C \tag{3.10}$$

$$\dot{T} = \mu \ln\left(\frac{C}{C_{pi}}\right) - \alpha(T - T_{pi}) \tag{3.11}$$

for the cumulative emissions F, the CO_2 concentration C and the global mean temperature T. Inputs and parameters to the climate model are the CO_2 emissions E in GtC, the CO_2 emission to concentration conversion factor β, the atmospheric retention factor $B/(\beta\gamma)$, and the carbon cycle response parameter γ in equation 3.10. In equation 3.11, there are the parameters μ and α, and the preindustrial CO_2 concentration C_{pi} and temperature T_{pi}. The parameters μ and α can be identified as

$$\mu = \frac{Q_{2xCO_2}}{c_{oc} \times \ln 2}, \qquad \alpha = \frac{Q_{2xCO_2}}{c_{oc} \times T_{2xCO_2}} \tag{3.12}$$

with Q_{2xCO_2} the radiative forcing at a doubling of CO_2, and c_{oc} the effective oceanic heat capacity (Kriegler and Bruckner, 2004). The parameter values used are summarized in Table 3.1, as well as initial (1990) and preindustrial conditions.

In order to be able to consider the sources of uncertainty under investigation, the deterministic model presented above has to be modified to a stochastic formulation in order to simulate the natural variability in global mean temperature.

If one considers the global mean temperature T_{GM}, as it is simulated by large 3D GCMs, it becomes apparent that this quantity displays a certain variability. Collins et al. (2001) report that the global mean temperature in the GCM HadCM 3 has a standard

Parameter	value	Initial condition	value
β	$0.47\frac{\text{ppm}}{\text{GtC}}$	E_0	$7.9\frac{\text{GtC}}{\text{a}}$
B	$1.51\times10^{-3}\frac{\text{ppm}}{\text{GtC a}}$	F_0	426GtC
γ	0.0215a^{-1}	C_0	360ppm
c_{oc}	$43.6\frac{\text{Wa}}{\text{m}^2\text{K}}$	C_{pi}	280ppm
T_{2xCO_2}	3K	T_{pi}	14.6°C
Q_{2xCO_2}	$3.7\frac{\text{W}}{\text{m}^2}$		

Table 3.1: Model parameter values, initial conditions and preindustrial values used in the ICLIPS model. Values are set following Kriegler and Bruckner (2004) with the exception of c_{oc}, which was changed to reflect IPCC TAR. All values except T_{2xCO_2} are held constant in the ensemble experiments.

deviation of 0.12K, whereas T_{GM} in HadCM 2 had a standard deviation of 0.13K. A stochastic extension to the ICLIPS climate model has therefore been implemented. This extension reproduces the natural variability in global mean temperature T_{GM} shown by HadCM 3.

In order to correctly simulate the natural variability in T_{GM}, Eq. 3.11 has to be modified to a stochastic formulation

$$\dot{T} = \mu \ln\left(\frac{C}{C_{pi}}\right) - \alpha\,(T - T_{pi}) + \sigma\xi. \tag{3.13}$$

In this equation, the stochastic extension is the term $\sigma\xi$. It consists of a white noise process ξ with standard deviation σ. By using this extension to the original model, the variance of T_{GM} can be reproduced.

The second uncertain element that will be investigated is the uncertainty in climate sensitivity. Considering Eq. 3.12 it is obvious that a probability distribution for T_{2xCO_2} results in a probability distribution for α.

3.2.4 Consequences of uncertainty for the TWA

The consideration of probabilistic uncertainty in the TWA has profound consequences for the conceptual framework, as we will explore in the following paragraphs.

As a reference for comparison, an emission trajectory was determined using the deterministic model setup. The emission trajectory was chosen in such a way, that a temperature guardrail $\Delta T \leq 2.5$K was observed, i. e. the temperature change ΔT in the deterministic model was limited to $\Delta T = 2.5$K.

The emission trajectory is shown in Fig. 3.2, on the left, along with the corresponding temperature trajectory. The emissions, shown in green, rise quickly at first, reaching a

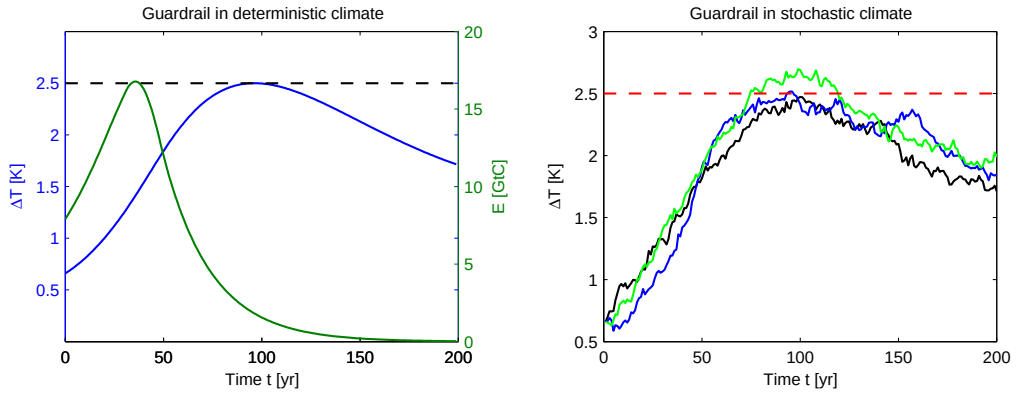

Figure 3.2: Consequences of natural variability for the TWA. Left: One climate trajectory observing guardrail $\Delta T \leq 2.5$K in deterministic TWA. Shown are change in global mean temperature ΔT (blue) and CO_2 emissions E (green). Right: Three realizations of the same CO_2 emissions trajectory from a stochastic climate model. While the guardrail is observed in the deterministic system, this depends on the realization of the stochastic process in the stochastic system. Therefore there is some probability of exceeding the guardrail in the stochastic case.

maximum at time $t = 38$, and are then reduced in an exponential decay. The temperature change ΔT, shown in blue, also rises initially, until maximum warming is reached at time $t = 99$. Afterwards, temperature falls slowly, but temperature does not reach a stationary state at the end of the time horizon. As a temperature guardrail limiting ΔT to $\Delta T = 2.5$K was set, the maximum temperature change at $t = 99$ is $\Delta T = 2.5$K.

If the stochastic climate model that reproduces the natural variability of the global mean temperature, as in equations 3.9 to 3.13, is now driven by the same emission trajectory, the temperature guardrail will not necessarily be observed. The climate trajectories stemming from three realizations of the stochastic process ξ are shown on the right of Fig. 3.2. It is obvious that not all realizations of the stochastic process observe the guardrail. While the realization shown in black observes the guardrail, the realization shown in green grossly violates the guardrail, and the realization shown in blue slightly violates it. This clearly demonstrates that it is dependent on the realization whether the guardrail is observed in the presence of variability. Therefore a certain probability exists, that the guardrail is violated. This probability is given by the cumulative distribution, and it turns out to be $P = 0.5$ due to the symmetric nature of the Gaussian distribution of the white noise.

As argued in section 3.2.1, a small violation of the guardrail, as in the case of the temperature guardrail shown in Fig. 3.2, may not be relevant to the larger problem at hand. In the case of the global mean temperature, a slight deviation will probably not

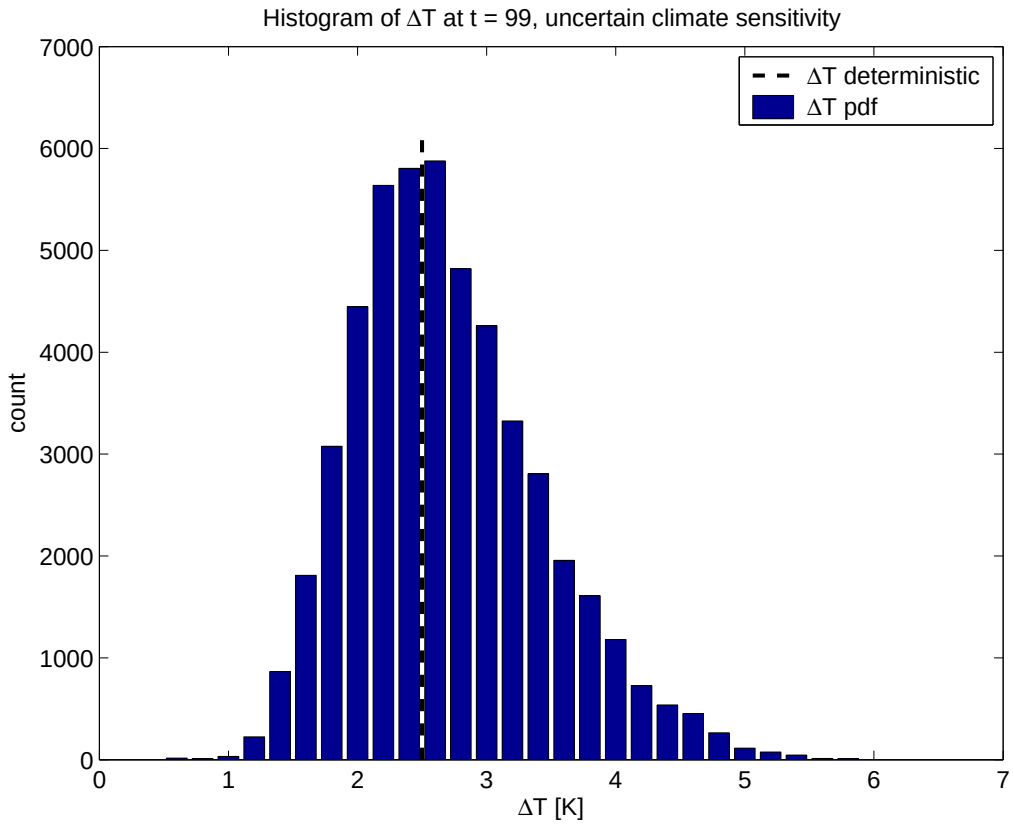

Figure 3.3: Histogram of temperature change ΔT at time $t = 99$ with T_{2xCO_2} sampled from the Andronova and Schlesinger T2 probability distribution.

be all that important, and the guardrail could also be defined in terms of e. g. ten year averages. On the other hand, there are impacts of climate change, where the variability of climatic variables plays a major role. Mearns et al. (1997) have shown that changes in the variability of temperature and precipitation may strongly affect agricultural yield. Similarly, changes in extreme precipitation events may cause changes in flooding probabilities (Becker and Grünewald, 2003, Booij, 2002, Shabalova et al., 2003). In these cases, the variability plays a major role and therefore needs to be taken into account for guardrail definitions. The need for the consideration of natural variability therefore depends on the problem under consideration.

The second source of uncertainty considered is uncertainty in climate sensitivity. A probability distribution for the climate sensitivity T_{2xCO_2} now leads to a probability distribution for the parameter α in Eq. 3.11. In order to explore the effect of this uncertainty on the TWA, a Monte-Carlo scheme is employed to sample from the T2 probability distribution estimate by Andronova and Schlesinger (2001).

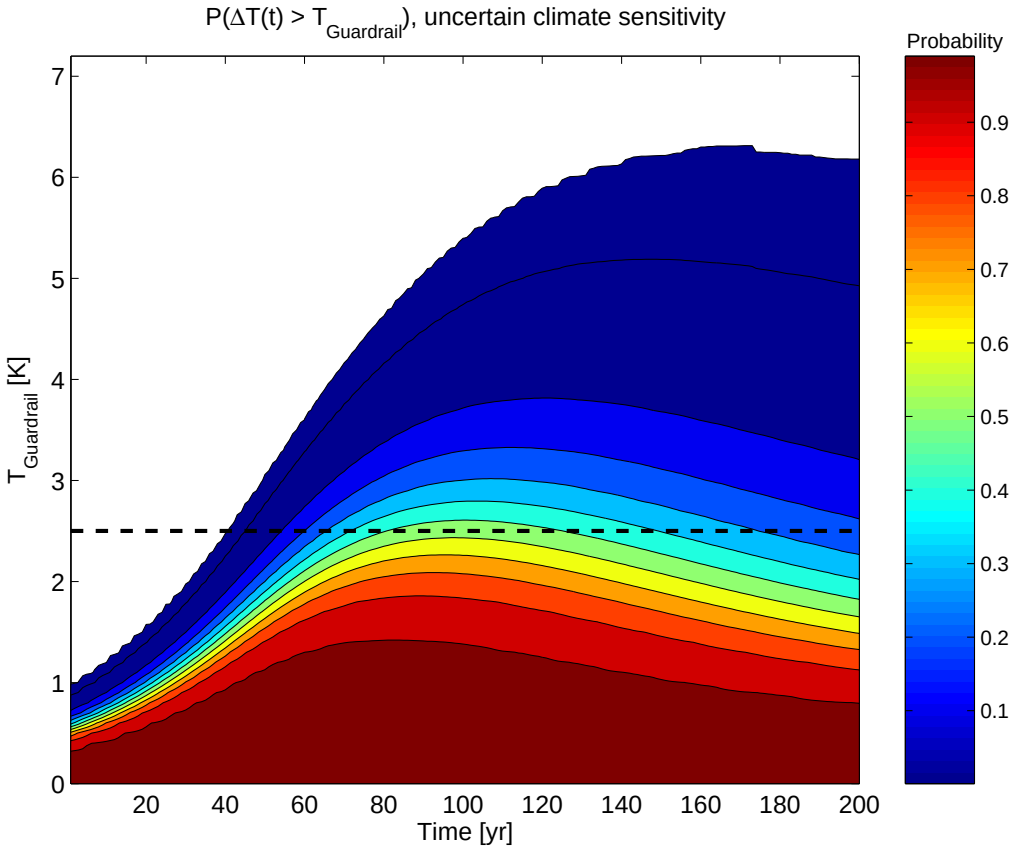

Figure 3.4: Cumulative probability of temperature change $\Delta T\,(t)$ exceeding $T_{Guardrail}$ over the time horizon of the integration, shown as color. Climate sensitivity is sampled from the T2 probability distribution by Andronova and Schlesinger, natural variability is not considered.

The climate model is driven by the emission scenario shown in Fig. 3.2 and the probability distribution is determined for temperature change ΔT at time $t = 99$, which is the time of maximum warming in the deterministic scenario shown in Fig. 3.2. As shown in Fig. 3.3, the temperature change ΔT varies widely around the deterministic temperature change of $\Delta T = 2.5$K, which is also the temperature guardrail assumed in the deterministic scenario, and most of the probability distribution is located at higher temperatures. The temperature change at the time of maximum warming, which varies with with the respective climate sensitivity, ranges from 0.72 K, relative to the preindustrial climate, to a warm 7.27 K reached at $t = 200$ for the largest climate sensitivity in the ensemble.

The consequences of this uncertainty in climate sensitivity for the TWA are profound. Fig. 3.4 shows the cumulative distribution of temperature change ΔT over the time horizon of the integration. The contour plot shows $P\,(\Delta T\,(t) > T_{Guardrail})$, the prob-

ability of exceeding the temperature change $T_{Guardrail}$, shown on the abscissa, at time t. According to this figure, the deterministic guardrail of 2.5K has a maximum probability $P \approx 0.56$ of being exceeded at $t \approx 100$.

Finally, it is also possible to consider both sources of uncertainty by using Monte-Carlo techniques. In this case, one samples from the probability distribution for climate sensitivity and from the realizations of the stochastic process representing natural variability. Since $P(\Delta T(t) > T_{Guardrail})$, the cumulative distribution function, is virtually identical to the on shown in Fig. 3.4, it is not shown here. In this case the maximum probability of exceeding the deterministic guardrail is about $P \approx 0.56$ at time $t = 97$.

3.3 The probabilistic TWA

3.3.1 Probabilistic guardrails

As shown in the last section, the deterministic TWA is not able to fully cope with the uncertainty that is inherent in the climate change problem. The consideration of uncertainty leads to a certain probability that a guardrail will be violated, even though it may be observed in the deterministic case.

In order to solve this problem, the TWA therefore has to be extended to a probabilistic TWA. This has three consequences:

1. the conceptual framework of the TWA has to be extended in such a way, that probabilities can be considered, especially with regard to guardrails

2. the model framework and solution algorithms have to be adapted to a probabilistic formulation

3. climate impact response functions (CIRFs) have to be derived that incorporate probabilities.

Part of the second point has already been addressed in section 3.2.3, and we will come back to solution algorithms in section 3.3.3. The third point will be addressed in section 3.3.2, as well as in chapter 4 of this thesis. This leaves the first point to be addressed here.

Section 3.2.4 has shown that deterministic guardrails under probabilistic uncertainty lead to a non-zero probability that the guardrail will be violated. Therefore the concept of a guardrail used in the TWA has to be extended in such a way that probabilities can be considered. This allows the consideration of probabilistic uncertainty, i. e. uncertainty that can be expressed as a probability distribution, and of natural variability. Uncertainty

that cannot be expressed as a probability distribution would need a different type of extension, e. g. Kriegler (2005).

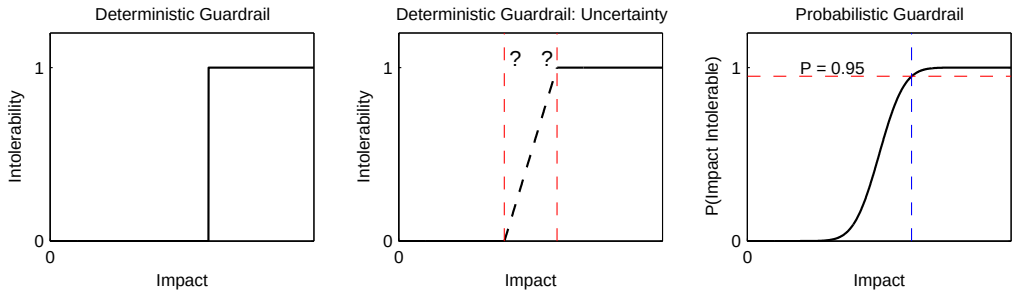

Figure 3.5: Conceptual visualization of a guardrail. Left: deterministic guardrail. Middle: deterministic guardrail in the presence of uncertainty. Right: probabilistic guardrail.

In the deterministic TWA, a guardrail is envisioned as a binary decision. A decisionmaker decides, which impact level is tolerable and which is intolerable. Therefore the outcome of this is binary: either an impact level is tolerable, or not. The guardrail in the deterministic TWA is then placed at the impact level where the transition between tolerability and intolerability takes place. Such a situation is sketched in the left hand panel of Fig. 3.5. In this case the TWA aims to insure $I \leq I_{Guardrail}$, with I the impact under consideration and $I_{Guardrail}$ the impact guardrail, which is set, where the intolerability of I changes from 0 to 1.

Expressed in terms of probabilities, the deterministic TWA therefore assumes the probability of observing the guardrail as

$$P\left(I \leq I_{Guardrail}\right) \in \{0,1\}: \tag{3.14}$$

The probability of staying below the guardrail is either zero or one.

The situation where the deterministic TWA reaches its limit is shown in the middle of Fig. 3.5. If there is uncertainty, whether a certain impact level is tolerable or not, the placement of the guardrail becomes a grave problem. One could either place the guardrail at the highest impact where one is still certain that the impact is tolerable, or one might place the guardrail at the lowest impact where one is certain that the impact is intolerable, or one might place the guardrail somewhere in between. This uncertainty in placing the guardrail may arise out of cognitive uncertainty (the decisionmaker simply doesn't know, what is (in)tolerable), but it also arises if probabilistic uncertainty is considered explicitly. If one looks further at the chain of cause and effect in climate

change, this situation could also arise, if the relation between climate change and impact of climate change, the CIRF, becomes uncertain.

Another situation, where this problem could become relevant, is a multi-actor situation. The TWA was conceived with a single-actor perspective in mind, where a single decisionmaker is asking for policy advice. This single actor may be able make a single normative decision, which impacts are intolerable, but if more decisionmakers come into play, they might make different normative settings.

One solution to this conceptual problem is shown on the right of Fig. 3.5. This is a sketch of a probabilistic guardrail. Contrary to a deterministic guardrail, it is not just a single impact level dividing tolerable from intolerable, but it is a tuple of impact level and probability limit. In this situation, the decisionmaker does not just specify $I_{Guardrail}$, but also a probability guardrail $P_{Guardrail}$. $P_{Guardrail}$ could either be a limit to the probability of reaching a certain impact level, or it could be a limit to the probability of a certain impact level being intolerable. In addition, $P_{Guardrail}$ could also be derived by determining the different $I_{Guardrail}$, where a number of decisionmakers would put the guardrail, and using this information to obtain a probability distribution. This approach could therefore also extend the single-actor perspective currently employed by the TWA.

These new probabilistic guardrails can now be properly expressed conceptually. In the case of probabilistic uncertainty, Eq. 3.14 becomes

$$P\left(I \leq I_{Guardrail}\right) \in [0,1]\,, \tag{3.15}$$

the probability of observing the guardrail is no longer either zero or one, but it is any value in between. The new probabilistic guardrail can then be formulated as

$$P\left(I \leq I_{Guardrail}\right) \geq P_{Guardrail}\,. \tag{3.16}$$

The guardrail now consists of the impact limit $I_{Guardrail}$ and the probability limit $P_{Guardrail}$. Please note that the notation is somewhat arbitrary. Here, we decided to determine $P\left(I \leq I_{Guardrail}\right)$, and therefore P must be larger than $P_{Guardrail}$, which will probably be some comparatively large value, e. g. $P_{Guardrail} = 0.9$. It could also be done vice versa and would be equally valid, as long as it is done consistently.

3.3.2 Probabilistic CIRFs

In the TWA, guardrails are set to limit impacts of climate change. *Climate impact response functions* (CIRFs) (Bruckner et al., 1999, Füssel et al., 2003, Füssel, 2003) have been developed to facilitate the setting of guardrails. CIRFs indicate the relationship between climate change and the impacts of climate change. They can formally be rep-

resented as $I = I(C,S)$ with the impact I, the relevant climatic variables C, and the signifi cant socio-economic variables S. What is hidden by the seemingly simple relation sketched above, is that a CIRF is a representation of highly aggregated information that has usually been obtained by detailed impact assessment studies. In principle, any impact of climate change that can be evaluated by assessment studies can be used to generate a CIRF. Therefore CIRFs can not only be determined for impacts of climate change in the natural environment, but also for socio-economic impacts.

CIRFs can be used in a number of ways. First of all, they can be used as a tool to give information about the likely impacts of a certain climate state or a climate change scenario. Second, they can be used to gain an overview of the overall response to climate change of the impact considered. This allows the identifi cation of threshold values, where qualitative changes in impact response occur, e. g. nonlinear responses to forcing. Third, they allow the setting of guardrails in climate impact space in order to allow the determination of the set of climate protection strategies that do not violate the guardrail within the TWA. The latter would not be possible without CIRFs, since the determination of the set-valued solutions to the TWA already incurs a huge numerical cost, which would become prohibitive, if impact models had to be coupled on-line into the integrated assessment model.

So far, CIRFs have been determined for climate change impacts on natural vegetation, agricultural production and freshwater availability (Füssel et al., 2003, Füssel, 2003). These CIRFs were defi ned within a deterministic framework. In the probabilistic TWA, CIRFs may need to be defi ned in terms of probabilities.

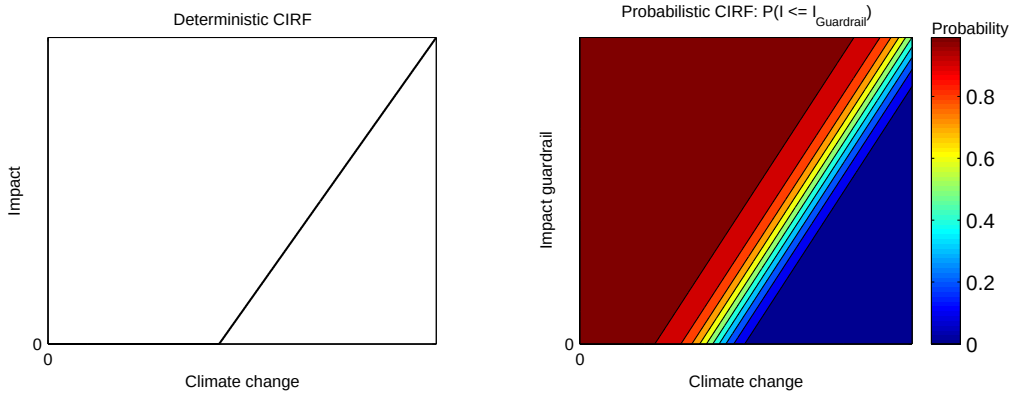

Figure 3.6: Conceptual visualization of a CIRF. Left: deterministic CIRF, right: probabilistic CIRF. The probabilistic CIRF is the probability that the impact I stays below an impact guardrail $I_{Guardrail}$.

In the deterministic case, a cartoon of which is shown on the left of Fig. 3.6, CIRFs can be visualized as some function relating I to C (and S).

In the presence of uncertainty, this becomes more complicated. In cases where the uncertainty arises through uncertain parameters, for which a probability distribution can be determined, or where the uncertainty arises through natural variability, a probabilistic CIRF, similar to the one depicted on the right of Fig. 3.6, can be derived. This kind of CIRF can be understood as the probability $P(I_{Guardrail}) = P(I(C,S) \leq I_{Guardrail})$ that the impact $I(C,S)$ is smaller than some impact guardrail $I_{Guardrail}$. Therefore the figure has to be interpreted as follows: one looks at a certain impact level $I_{Guardrail}$, shown as "Impact guardrail" in the plot, and a certain amount of climate change C. The color shown in the plot then gives $P(I(C,S) \leq I_{Guardrail})$ at the climate change C one is looking at. In addition, a probabilistic CIRF can also be used to indicate how probabilities of extreme events change. This will be demonstrated in chapter 4.

This probabilistic CIRF can then be used in the probabilistic TWA to set probabilistic guardrails.

3.3.3 Calculation of emission corridors

The last sections have shown how the deterministic TWA can be extended conceptually to enable the consideration of probabilistic uncertainty. In the probabilistic TWA, the guardrail is no longer a simple limit $I_{Guardrail}$ to an impact I, but the guardrail becomes a combination of impact- and probability limit, which can be expressed as $P(I \leq I_{Guardrail}) \geq P_{Guardrail}$. In addition, the CIRFs describing the impacts may have to be modified in such a manner, that $P(I_{Guardrail}) = P(I(C,S) \leq I_{Guardrail})$ can be determined.

Such modifications to the conceptual foundations of the approach also call for a modification of the way solution are determined. We begin this by reviewing the deterministic approach to determining solutions.

As described in section 3.2.1, a typical result of a TWA-based analysis is an emission corridor. For the case of the deterministic TWA an algorithm for the approximation of emission corridors has been developed (Leimbach and Bruckner, 2001, Bruckner et al., 2003b). In this case it is sufficient to calculate the upper and the lower boundary of the emission corridor. As a further approximation, this can be done for a finite number of points $t \in \{t_1, t_2, ..., t_n\}$ with $t_n \leq t_e$.

Once again it is assumed that the evolution of the system can be modeled as a set of differential equations

$$\dot{\mathbf{x}} = \mathbf{f}(\mathbf{x}, t; \mathbf{u}), \tag{3.17}$$

with a state vector $\mathbf{x} \in \mathbb{R}^n$, a control vector $\mathbf{u} \in \mathbb{U} \subseteq \mathbb{R}^m$, and an initial state $\mathbf{x}_0$, whereas the guardrails can be formulated as a vector of inequalities

$$\mathbf{h}(\mathbf{x}, t; \mathbf{u}) \leq \mathbf{0}. \tag{3.18}$$

For the determination of an emission corridor the control variables are the emissions, and the upper (lower) boundary of the emission corridor can be determined by successively maximizing (minimizing) the emissions $E(t_i)$ at time t_i subject to the dynamical constraints (Eq. 3.17) and the additional constraints provided by the guardrails (Eq. 3.18). The maximal (minimal) emissions $E(t_i)$ are then determined numerically by a constrained optimization algorithm, such as the algorithms implemented in GAMS or MATLAB.

For the case of the probabilistic TWA, this algorithm can be used as well, with minor modifications. Within the framework described in equations 3.17 to 3.18, two elements can be identified that may be subject to probabilistic uncertainty:

1. The system of differential equations describing the coupled socio-economic-climate system (Eq. 3.17) is transformed to a system of stochastic differential equations

$$d\xi = \mathbf{f}(\xi, t; \mathbf{u})\, dt + \mathbf{g}(\xi, t; \mathbf{u})\, d\mathbf{W}(t) \tag{3.19}$$

   with a state vector $\xi(t)$, a drift term $\mathbf{f}(\cdot)$, a diffusion term $\mathbf{g}(\cdot)$ and a Wiener process $\mathbf{W}(t)$.

2. The deterministic constraints (Eq. 3.18) become stochastic constraints

$$\mathbf{h}(\mathbf{x}, \eta, t; \mathbf{u}) \leq \mathbf{0} \quad \forall\, t \in [0, t_e], \tag{3.20}$$

   that are dependent on a stochastic term $\eta(t)$.

In this case, the trajectories $\xi(\cdot)$ that solve the system of differential equations (Eq. 3.19) and still fulfill the constraints (Eq. 3.20), are the solutions to the stochastic differential inclusion (Aubin et al., 2000)

$$d\xi \in \mathbb{F}(\xi, dt \oplus d\mathbf{W}), \qquad \mathbb{F} \in \mathbb{R}^n \times \mathbb{R}^m \tag{3.21}$$

with

$$\mathbb{F}(\xi, dt \oplus d\mathbf{W}) := \{\mathbf{f}(\xi, t; \mathbf{u})\, dt + \mathbf{g}(\xi, t; \mathbf{u})\, d\mathbf{W} \mid \mathbf{u}(t) \in \mathbb{U}(\mathbf{x})\}$$

under the constraint condition

$$P\left(\mathbf{h}\left(\mathbf{x},\eta,t;\mathbf{u}\right)\leq\mathbf{0}\right)\geq P_{Guardrail}. \tag{3.22}$$

This probabilistic constraint condition limits the probability P of observing the guardrail to the limiting probability guardrail $P_{Guardrail}$.

As in the deterministic case it will in general not be possible to determine an exact solution, i. e. the *bundle of control paths*, to this problem, but the algorithm for approximating the *emission corridor* can be adapted to the probabilistic problem. As in the deterministic case a numerical implementation of the model describing the evolution of the coupled system is a prerequisite to the determination of emission corridors. Depending on the nature of the problem, this may either be a deterministic formulation as in Eq. 3.17 or a stochastic implementation as in Eq. 3.19.

For considering the probabilistic constraints, the probability $P\left(\mathbf{h}\left(\mathbf{x},\eta,t;\mathbf{u}\right)\leq\mathbf{0}\right)$ has to be determined by some method, e. g. by using Monte-Carlo techniques. If one considers a probabilistic formulation for the dynamical system, such as in the examples shown in section 3.2.4, $P\left(\mathbf{h}\left(\mathbf{x},\eta,t;\mathbf{u}\right)\leq\mathbf{0}\right)$ can be determined by calculating the time evolution of an ensemble of realizations of either the climate sensitivity or the stochastic process ξ (or both). If, on the other hand, the guardrails in Eq. 3.18 become probabilistic, while the dynamical system itself remains deterministic, then an ensemble of realizations of the process considered in the guardrail can be used to determine $P\left(\mathbf{h}\left(\mathbf{x},\eta,t;\mathbf{u}\right)\leq\mathbf{0}\right)$.

For the determination of the emission corridors that will be shown in section 3.4, both a deterministic and a stochastic version of the ICLIPS model, as in Eq. 3.9-3.13, have been implemented. In order to consider a probability distribution for the climate sensitivity, the deterministic version is used and an ensemble of model configurations is generated by sampling from the probability distribution for T_{2xCO_2}. $P\left(\mathbf{h}\left(\mathbf{x},\eta,t;\mathbf{u}\right)\leq\mathbf{0}\right)$ can then be determined from the frequency of experiment outcomes. For the consideration of natural variability, on the other hand, the stochastic version is used, and an ensemble of realizations of the stochastic process is generated. $P\left(\mathbf{h}\left(\mathbf{x},\eta,t;\mathbf{u}\right)\leq\mathbf{0}\right)$ can again be determined from the frequency of experiment outcomes.

The consideration of both sources of uncertainty then becomes a straightforward task: the stochastic version of the model is used, and an ensemble of of model configurations is generated by sampling from the pdf for T_{2xCO_2}. This ensemble then samples from the realizations of the stochastic process, and $P\left(\mathbf{h}\left(\mathbf{x},\eta,t;\mathbf{u}\right)\leq\mathbf{0}\right)$ is once again determined from the experiment outcomes. In this case, as in all cases where multiple sources of uncertainty are considered, care must be taken in choosing an appropriate sampling strategy to insure that the uncertainty is properly taken into account.

The algorithm described above has been implemented in MATLAB using the constrained optimization routine provided. As in the deterministic case, the emissions $E(t_i)$ are maximized (minimized) at times $t_i \in \{t_1, t_2, ..., t_n\}$ for the determination of the upper (lower) boundary of the emission corridor. In section 3.4 the probability of observing a temperature guardrail T_{Guard} is considered as a climate constraint, therefore $P(\Delta T \leq T_{Guard})$ is determined by sampling from the probability distribution for climate sensitivity *and* by sampling from the realizations of the stochastic process as described above.

In the case of the very simple system considered here, a more elegant solution to the determination of $P(\mathbf{h}(\mathbf{x}, \eta, t; \mathbf{u}) \leq \mathbf{0})$ could probably be found. Our aim here was to develop the conceptual framework of a probabilistic TWA, though, and therefore a method that can be applied to a wide range of problems was used. In addition, the consideration of different realizations also allows the propagation of uncertainty through the chain of cause and effect in climate change, which is in most cases not possible using analytical solutions.

3.4 Emission corridors in the probabilistic TWA

The uncertainties considered, uncertainty in climate sensitivity and natural variability in global mean temperature, lead to a probability distribution for the warming realized under a defined greenhouse gas forcing scenario. In this section, emission corridors will therefore be determined, limiting the temperature change to a temperature guardrail T_{Guard} that has to be observed with a probability $P(\Delta T \leq T_{Guard}) \geq P_{Guard}$ larger than or equal to the probability guardrail P_{Guard}.

Following Kriegler and Bruckner (2004), additional guardrails are set for these corridors. The change in emissions is parameterized as $\dot{E} = gE$, and the maximal emission reduction is limited to 4% p.a., as large emission reductions may be very costly or even impossible to obtain. Second, the rate of change in emission reduction is limited, as a certain inertia in the socio-economic system has to be assumed. We are assuming a transition timescale of $t_{trans} = 20$ yrs from the initial rate of change in emissions g_0 to the maximal emission reduction $g_{max} = -0.04$. It is also assumed that the growth rate in emissions does not rise again after emission reductions have started, for plausibility reasons. The latter two constraints can be summarized as $0 \leq \dot{g} \leq -(g_0 + g_{max})/t_{trans}$. The initial rate of change in emissions g_0 is determined by the optimization algorithm, but bounded to be between 1% p.a. and 3% p.a., the range of the late 20th century rise in emissions.

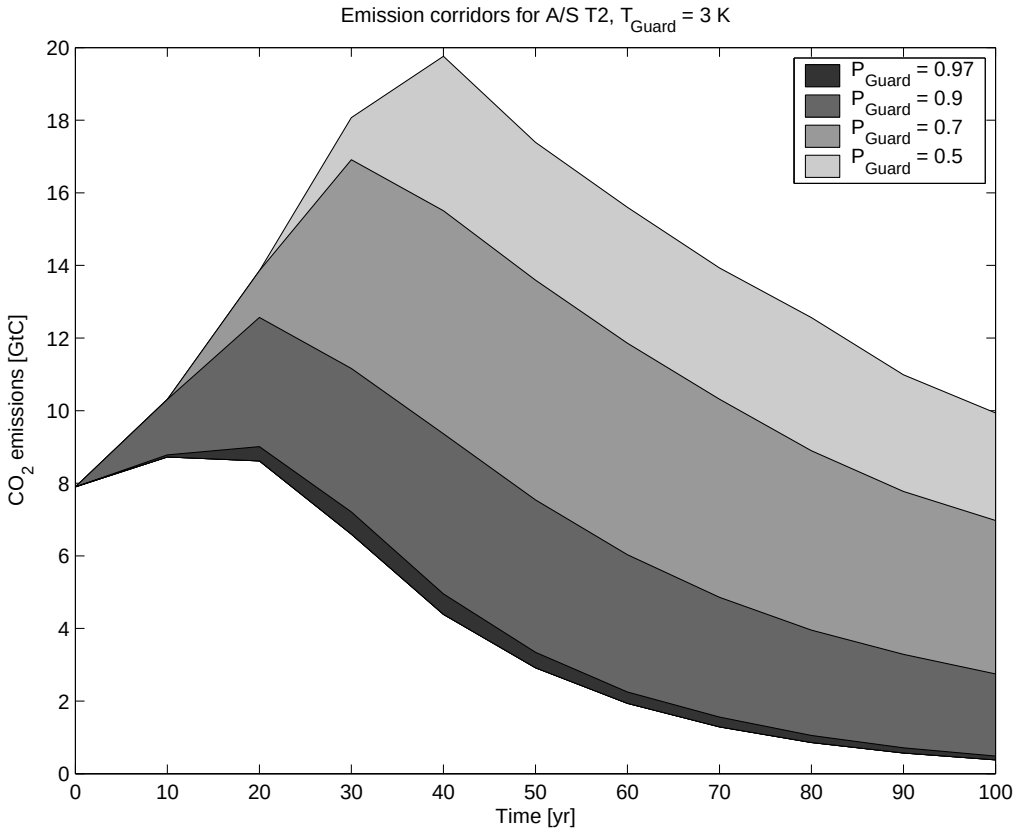

Figure 3.7: Emission corridors for temperature guardrail $T_{Guard} = 3$K and probabilities $P(\Delta T \leq T_{Guard}) \geq P_{Guard} = 0.97$, 0.9, 0.7 and 0.5. Climate sensitivity is sampled from the A/S T2 distribution.

The probability guardrail considered has a large influence on the overall size of emission corridors. Fig. 3.7 shows the consequences of differing limits to the probability of exceeding the temperature guardrail. The emission corridor is shown as shaded area. Please note that the corridors shown here are additive, in the sense that the larger corridors consist of the total area between the upper boundary of the corridor and the lower boundary of the shaded area in the plot. Here, the temperature guardrail is set to $T_{Guard} = 3$K, and corridors are derived for probabilities of observing the temperature guardrail of $P(\Delta T \leq T_{Guard}) \geq P_{Guard} = 0.97$, 0.9, 0.7 and 0.5. Climate sensitivity is sampled the Andronova and Schlesinger T2 distribution. It is obvious that the emission corridor shrinks for higher probability guardrails. While a probability guardrail $P_{Guard} = 0.5$ allows a maximum in emissions of nearly 20 GtC, $P_{Guard} = 0.97$ allows less than 9 GtC.

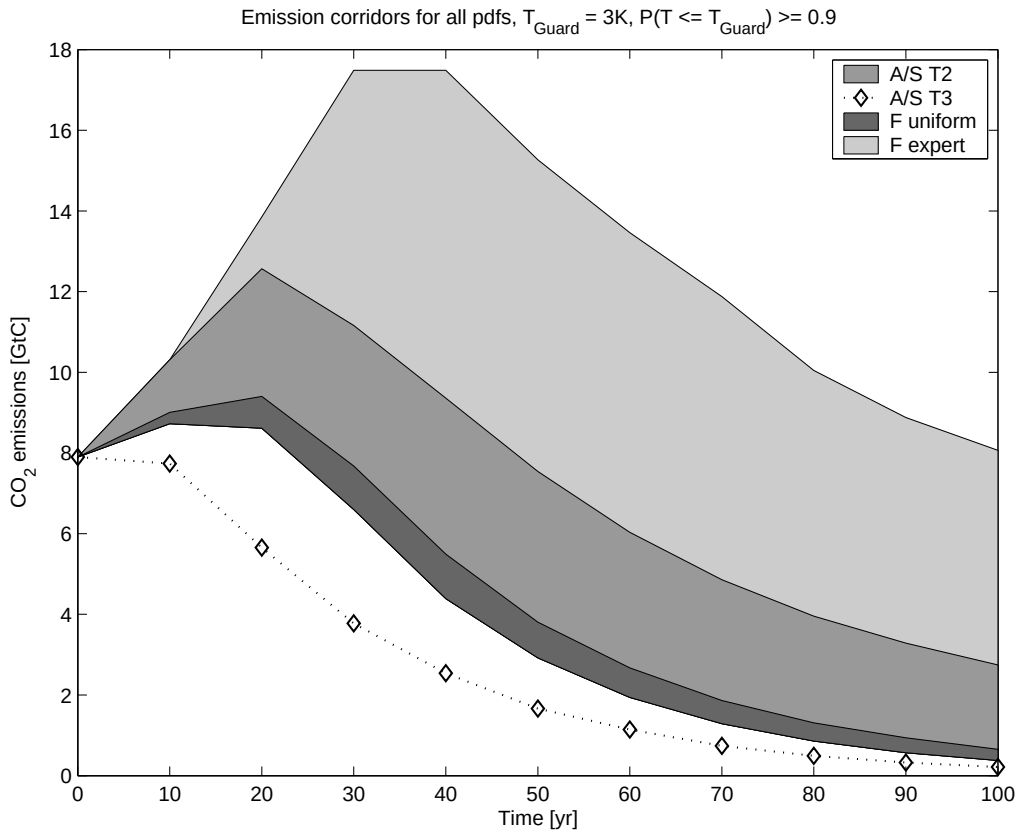

Figure 3.8: Emission corridors for $T_{Guard} = 3$K, $P_{Guard} = 0.9$, all probability distributions considered.

Another important question is the influence of the probability distribution for climate sensitivity on the emission corridors. For guardrails $T_{Guard} = 3$K, $P_{Guard} = 0.9$, this is shown in Fig. 3.8. In this case emission corridors were obtained for all the pdfs considered. As could be expected after considering the pdfs shown in Fig. 3.1, the Forest et al. pdf from an expert prior yields the largest emission corridor, with maximal emissions of about 17.5 GtC allowed, while the A/S T2 and the Forest et al. uniform pdfs yield viable emission corridors, with a maximum of about 12.5 GtC and 9.4 GtC allowed, respectively. The most interesting case is the A/S T3 estimate, shown as a dotted line in Fig. 3.8. This dotted line shows the hypothetical upper boundary of the emission corridor, but since the upper boundary is located *below* the lower boundary, the emission corridor is an empty set. If the A/S T3 estimate had to be assumed for the probability distribution of climate sensitivity, it would therefore be impossible to keep climate change below 3K with a high probability of not exceeding this value. Compared

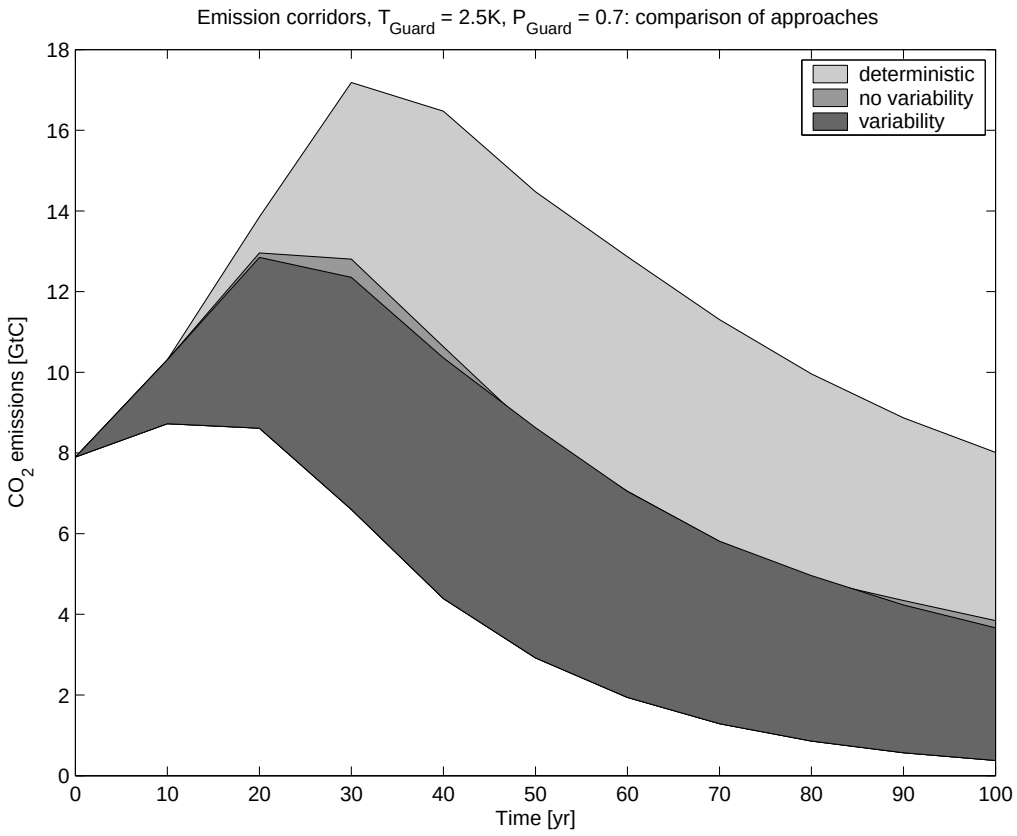

Figure 3.9: Comparison of emission corridors. Temperature guardrail is $T_{Guard} = 2.5$K, probability guardrail is $P_{Guard} = 0.7$. Shown are deterministic corridor with $T_{2xCO_2} = 3$K, probabilistic corridor with no consideration of natural variability, and probabilistic corridor with consideration of natural variability and uncertainty in T_{2xCO_2} (A/S T2 estimate).

to the other estimates, the high probability of high values for climate sensitivity leads to a low probability of observing the $T_{Guard} = 3$K guardrail.

The main difference between the Forest et al. estimates from a uniform and an expert prior, as shown in Fig. 3.1, is that the distribution generated from a uniform prior has a heavy tail, i. e. comparatively high probabilities for high values of climate sensitivity, even though the maximal probability density is located at the same value of T_{2xCO_2}. The consequence of this difference is a dramatically smaller emission corridor available in the case of the heavy tailed distribution.

For comparison, Fig. 3.9 shows emission corridors for the deterministic case, as well as for the probabilistic case (based on the A/S T2 estimate) with and without consideration of natural variability in. The corridor for the deterministic case was derived for a climate sensitivity $T_{2xCO_2} = 3$K, and the guardrail settings were a temperature guardrail

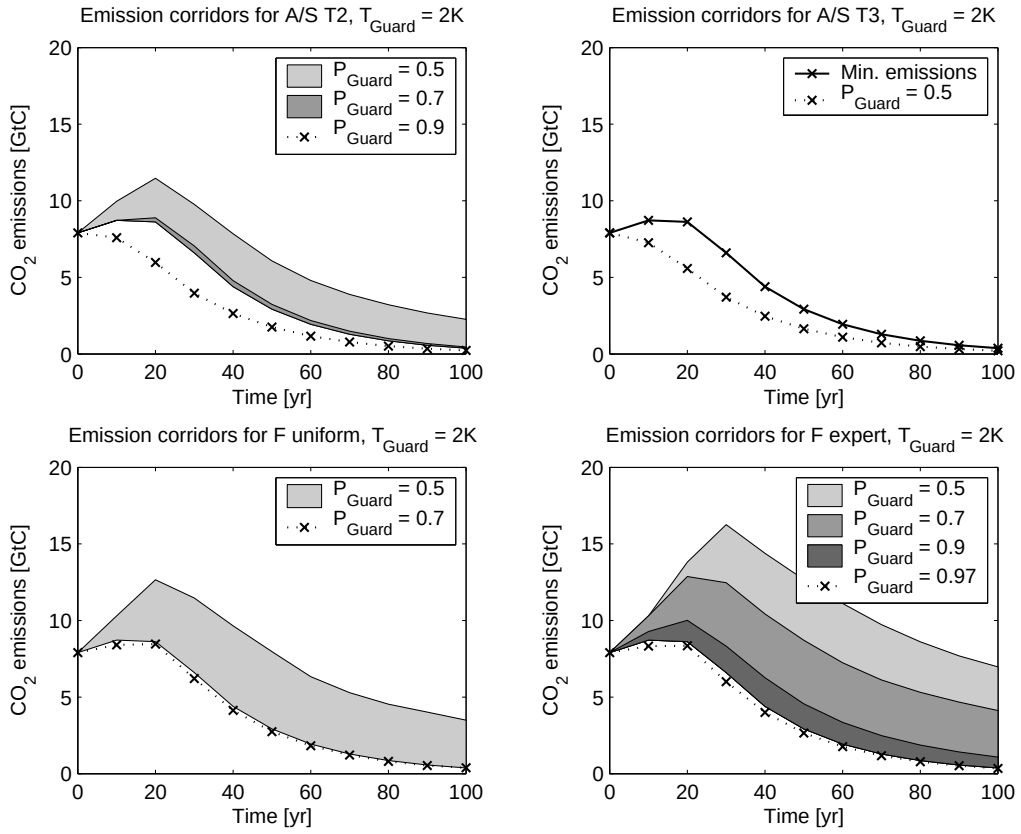

Figure 3.10: Emission corridors for a climate protection target $T_{Guard} = 2K$ for all probability distributions considered. Probability guardrails P_{Guard} are shown in legend.

$T_{Guard} = 2.5$K with a probability guardrail $P_{Guard} = 0.7$. The deterministic case yields a much larger corridor, but the size of this corridor is very sensitive to the choice of climate sensitivity. The difference between the probabilistic corridors, on the other hand, is very small, with the corridor that considers natural variability slightly smaller than the one that does not. Therefore the consideration of the uncertainty in climate sensitivity appears to be more important than the consideration of natural variability in this case, but this is very much dependent on the problem under consideration. As soon as guardrail settings other than limits to the global mean temperature change are considered, the natural variability may turn out to be the main factor.

Finally, the matter of emission corridors limiting temperature change to 2°C remains an interesting question. A climate protection target of limiting temperature change to 2°C above the preindustrial climate was proposed by the German advisory council on climate change in 1995 (WBGU, 1995), and this target was later adopted by the European Union. Fig. 3.10 shows emission corridors for a guardrail setting $T_{Guard} = 2K$ for

all the probability distributions considered. For each probability distribution, the emission corridors for all probability guardrails up to the lowest setting, where the corridor was an empty set, were determined. The fi gure therefore allows a comparison of the consequences of the probability distributions for the 2°C climate protection target. If A/S T2 is the "real" probability distribution, the target can be met with a probability $P = 0.7$, while it cannot be met for the A/S T3 distribution. Similarly, the Forest et al. distribution from a uniform prior yields just a $P_{Guard} = 0.5$ corridor, whereas the distribution from an expert prior yields viable corridors up to $P_{Guard} = 0.9$. Concentrating on the A/S T2 and the Forest et al. expert distributions, it becomes apparent that emission corridors that give high probabilities of staying within the temperature guardrail are quite small. Therefore emission reductions will have to happen soon, unless we are willing accept a non-negligible probability of violating the climate protection target. On the other hand, a probability guardrail $P_{Guard} = 0.9$ implies that there still is a probability $P = 0.1$ that the guardrail will be violated. Therefore even emission reduction strategies conforming to the most ambitious corridor determined do not insure that targets will be met with certainty.

3.5 Summary and conclusions

This chapter has demonstrated how the "traditional" deterministic tolerable windows approach can be extended to a probabilistic TWA. This extension improves the deterministic TWA because it allows the consideration of probabilistic uncertainty, i. e. uncertainty that can be expressed as a probability distribution or that arises through natural variability.

This extension of the TWA involves changes to the modeling framework and solution algorithms, but most important of all is a different understanding of guardrails. While guardrails in the deterministic TWA are single values dividing tolerable impacts from intolerable, a probabilistic TWA forces us to also consider a probability limit. Therefore the guardrail now involves two numbers, not one: An impact guardrail and a probability guardrail. The impact guardrail is – as before – an impact level that is considered a boundary that divides tolerable impacts of climate change from intolerable impacts, but in addition we need to specify a probability guardrail that specifi es the minimum probability of staying below the impact guardrail that the policymaker is willing to accept.

This conceptual change is more important than it may appear, because at the current state of climate change science there is very little certainty. Therefore it just isn't possible to exclude impacts of climate change with certainty, but the maximum one can hope for is a certain probability for having excluded the impact of climate change one is concerned

about. Scientific policy advice will therefore gain from the explicit consideration of uncertainty.

We were able to demonstrate the probabilistic TWA by determining emission corridors that limit the change in global mean temperature to 2, 2.5 and 3K, with various probabilities of observing the guardrail. For this the uncertainty in climate sensitivity was included by considering various estimates of probability distributions for climate sensitivity, and natural variability was also included as an additional source of uncertainty.

In general, emission corridors shrink, if uncertainty is considered and higher probabilities of observing the guardrail are enforced. The higher the probability of observing the guardrail, the smaller the corridor. This may be obvious to the reader who has already given some thought to this problem, but the finding is important enough to be repeated here.

While the guardrails used here may not be the most interesting – or the most relevant – ones, this chapter serves as an illustration of the conceptual framework. Applications of the probabilistic TWA to more pressing issues will surely follow, since the groundwork has now been laid.

One observation with respect to the emission corridors shown needs to be made, though. The European Union has repeatedly stated a goal of limiting global warming to 2°C above preindustrial. Fig. 3.10 shows emission corridors for a temperature guardrail $T_{Guard} = 2$K and all the probability distributions considered. Depending on the probability distribution of climate sensitivity, this goal can be met with varying probabilities of staying within the tolerable window, but high probabilities can only be assured if the probability distribution is one of the more benign ones. In addition, strong efforts to curb global warming have to made soon, since the emission corridors, the "maneuvering space" of humanity, are comparatively small.

Chapter 4

Integrated assessment of changes in flooding probability

4.1 Introduction

The integrated assessment of climate change needs to take into account both the costs and the benefits of climate protection measures. Whereas the first mainly relates to issues of energy production, the latter is associated with avoided damages from climate change. Whereas many integrated assessment models consider the costs of mean climate change, the effects of extreme events are often neglected. This is despite the fact that there is an increasing trend of economic losses due to "atmospheric" natural disasters (Berz, 1999). The Mississippi flood of 1993, for example, has caused economic losses of about $US 12 bn., whereas the losses of the 2002 summer floods in Europe are estimated to be about EUR 30 bn. (Munich Re, 2004). Both numbers are of the same order of magnitude as the estimated damage costs in the water sector for both regions for an increase in global mean temperature of about 1-2.5°C (Tol, 2002). This indicates that extreme floods, which appear in the "midfield" in the statistics of economic losses due to natural hazards (Berz, 1999), should be an essential component of integrated assessment.

For the recent global warming of the 20th century, no significant trends could be observed with regard to increases in annual maximum flows (Kundzewicz et al., 2003). For great events, i. e. 100-year floods, however, an increasing risk was detected in 29 basins larger than 20000km^2 by Milly et al. (2002). In spite of major uncertainties, there are some studies, including Working Group II of the IPCC TAR, which claim an increase of major flooding probability for future warming (Kundzewicz and Schellnhuber, 2004, Milly et al., 2002). Other studies show similar results with a rather heterogeneous geographical distribution of changes in flooding probabilities (Arora and Boer, 2001,

Arnell, 1999a). Yet, in some highly vulnerable regions a significant increase of flooding probabilities has been found under global warming, e. g. for Bangladesh (Mirza, 2002), central Asia and eastern China (Arnell, 1999a). All of these studies are restricted to climate change induced shifts in flooding probabilities and do not take into account other major factors relevant for changes in flooding intensities and frequencies. These factors include land-use changes, modification of streamflows by various water-management schemes like dams or dykes, or, when it comes to the actual damages, the relocation of infrastructure or settlements. On the one hand, this makes assessments easier, but on the other hand it might give biased results.

For a flood component of an integrated assessment model (IAM), it is generally not sufficient to model the shifts in flooding probabilities only. In addition, one needs to map those probabilities to actual damages, where the specific measure of damage depends on the overall framework of the IAM. In case of a cost-benefit approach, for example, the flood model needs to give a monetary output. Within other frameworks, e. g. the tolerable windows approach (TWA), damages need to be calculated in a decision relevant measure, which doesn't need to be directly related to monetary costs.

Another difficulty in the development of an integrated assessment module of flood changes is due to computational requirements of those models, in particular if the overall model includes the decision making with respect to climate mitigation endogenously in the model. These computational costs ask for so-called reduced-form models, which mimic the outcomes of more detailed models, yet are much faster to compute.

Within the first part of this chapter (sections 4.2-4.5), such a reduced-form model is developed, based on simplified descriptions of regional patterns of climate change and on a highly reduced scheme for runoff computation. As "output" variable, the model computes the number of people affected by a pre-defined shift of flooding probability, e. g. a once in 50 years event shifts to a once in 25 years event. These shifts are computed for large river basins with an area of more than $2.5 \times 10^4\,\mathrm{km}^2$, and the "other major factors" affecting flooding probabilities are also neglected.

In the final section, a first application of the model within the tolerable windows approach is presented. The model is used to generate a probabilistic climate impact response function (CIRF), which allows to set probabilistic guardrails. Thus emission corridors are computed, where the number of people affected by changes in flooding probability is limited.

Parts of this chapter have been submitted for publication in Climatic Change (Kleinen and Petschel-Held, 2004).

4.2 Model description

4.2.1 Aims and scope

We are aiming to develop a reduced-form model that is able to incorporate the probabilities of large-scale flooding in an integrated assessment modeling framework. This model will be used to determine CIRFs that can be used to estimate the effects of climate change on flooding probabilities and their consequences. While floods may have a multitude of causes, ranging from blocking of river passages by ice or debris via land-use changes and river regulation to large precipitation events, most of these causes are not directly related to climate change. Due to climate change, the hydrological characteristics of the atmosphere may change. Higher temperatures cause an increase in evaporation, and the moisture capacity of the atmosphere increases as well (Trenberth et al., 2003). This may lead to increases in precipitation. As the non-climatic causes for flooding mentioned above can not easily be incorporated in the type of model we are aiming at, the analysis will focus on the climate change related causes. In addition, we have to restrict the type of floods we are attempting to model. Local, sudden floods ('flash floods') occur in small catchments and are mainly caused by localized intense precipitation events. While changes in the characteristics of these events are to be expected in a changed climate, we regard an integrated assessment of changes in probability of flash floods as too ambitious on a global scale for the time being. Extensive, long-lasting floods ('plain floods'), on the other hand, occur in larger catchments (Bronstert et al., 2002). These floods may be caused by extreme short-term precipitation events, especially in mountainous areas, but they may also be caused by large-scale rainfall lasting several days or weeks. The latter is the type of flood we are attempting to model.

The assessment conducted is global in scope. Therefore, a compromise has to be made with regard to the temporal and spatial scales that can be resolved. While high spatial resolutions allow assessments on the scale of small river basins, or even sub-basins, they also lead to high requirements with respect to computing time, input data and validation data. Similarly, high temporal resolution could allow the simulation of flash-floods, and similarly fast events, and might generally improve the fidelity of model results, but again the requirements with respect to data and computational resources are very demanding.

For the assessment of changes in flooding probability on the scale of large river basins, a spatial resolution of 0.5° seems to be a reasonable compromise, as well as a temporal resolution of one month. Vörösmarty et al. (2000) estimate that river basins with drainage areas $\geq 2.5 \times 10^4\,\mathrm{km}^2$ can be modeled reasonably at a spatial resolution of 0.5°, and climate data are readily available at this resolution, e. g. the "CRU" data by

New et al. (2000), the data by Willmott and Matsuura (2001) or data by Leemans and Cramer (1991). These data have a temporal resolution of one month, which allows the resolution of the annual cycle, while fast events like flash-floods can not be investigated at this timescale. As gauge records from a large number of streamflow gauges with a global coverage also use the monthly time scale, the model uses a timestep of one month for calculation.

In addition to the choice of resolution, a few other simplifications are made. The model will neglect the temporal dynamics of river routing, as this does not seem relevant at a temporal resolution of one month. At this temporal scale, water traveling at $0.5\,\mathrm{m/s}$ moves approximately 1300 km during one timestep (Vörösmarty et al., 2000). The mean travel times therefore exceed one timestep for the very largest rivers only. The consideration of river routing would therefore only influence results for these river systems. In addition, river routing will not change significantly due to climate change, neglecting possible changes in the timing of flows. The soil storage of moisture and evaporation from water bodies are also neglected. While these factors may degrade model results, especially with regard to the simulation of the annual cycle of runoff, the sensitivity analysis in section 4.4.3 suggests that the simulation of floods would not be improved by the reductions in runoff implied by these factors.

4.2.2 Downscaling of climate change

The climate components of many IA models, e. g. the models DICE (Nordhaus, 1994), MERGE (Manne et al., 1995), MiniCAM (Edmonds et al., 1996) and SIAM (Hasselmann et al., 1997), are intended for the evaluation of large numbers of climate change scenarios. In some cases, they are also coupled to economic models, which obtain solutions by optimizing some predefined goal-function. Therefore the climate models employed in such a framework must be run a large number of times. This limits the computational resources such a model may consume. Therefore a typical climate model for integrated assessment applications only calculates the change in global mean temperature ΔT_{GM}, while the spatial distribution of temperature change and changes in other climatic variables have to be inferred from this.

The impact of climate change we want to assess here not only requires a more explicit spatial resolution, but it also needs to take into account climate variability, and not just the changes in mean climate. The modeling approach is therefore divided into a "mean" and a "variability" part.

Geographically explicit changes in mean climate can be calculated by using the pattern-scaling approach (Mitchell et al., 1999, Mitchell, 2003, Füssel, 2003). In this approach geographically explicit patterns of climate change obtained from GCM ex-

periments are scaled by ΔT_{GM} calculated by the simple climate model included in the integrated assessment model. Despite the apparent simplicity of the approach, results obtained in this way are surprisingly accurate (Mitchell, 2003).

In this investigation climate change patterns are used that were obtained by an EOF analysis of output from a number of GCM experiments (Bruckner et al., 2003a, Füssel, 2003). In order to reflect the pertaining uncertainty about the spatial aspects of climate change, patterns of temperature and precipitation change from three different GCMs are used, i. e. the GCMs HadCM 2 (Johns et al., 1997), ECHAM 3 (Voss et al., 1998) and ECHAM 4 (Roeckner et al., 1996). These patterns of monthly climate change are scaled by the change in global mean temperature ΔT_{GM} and applied to the climatology. Accordingly, the geographically explicit changes in mean temperature and precipitation are generated as follows:

$$T_{changed}(r,m,t) = T_C(r,m) + k\Delta T_{GM}(t) \times T_P(r,m) \quad (4.1)$$

$$P_{changed}(r,m,t) = P_C(r,m) \times (1 + k\Delta T_{GM}(t) \times P_P(r,m)) \quad (4.2)$$

with $\Delta T_{GM}(t)$ the change in global mean temperature in year t, k the scaling factor relating the scaling of the patterns to $\Delta T_{GM}(t)$, $T_C(r,m)$ the temperature climatology in location r and month m, $P_C(r,m)$ the precipitation climatology, $T_P(r,m)$ the temperature change pattern and $P_P(r,m)$ the pattern of precipitation change. While $\Delta T_{GM}(t)$ is the annual change in global mean temperature, T_C, T_P, P_C and P_P are monthly fields on a spatial grid. The calculations in Eq. 4.1 and 4.2 therefore have to be performed for each month and each grid-cell.

The climate change patterns generated by different GCMs are used because there still is fundamental uncertainty about the global distribution of changes in temperature and precipitation. Due to the different model formulations, different GCMs predict different geographical distributions of climate change. This uncertainty is fundamental and cannot be resolved at the current state of climate science. If either the geographical distribution of climate change predicted by different GCMs converged, reducing the uncertainty, or if probability distributions for the geographical distribution of climate change were available, this uncertainty could be resolved explicitly and a common climate change pattern could be used. As this is currently not possible, different patterns have to be used and evaluated independently in order to take the uncertainty inherent in climate change projections into account. This uncertainty is also the reason for not using patterns generated by more recent models. While the representation of changed climate states may have improved in each of the GCMs concerned, the uncertainty through different

regional climate change projections by different GCMs remains. Use of more recent GCM patterns would therefore not reduce the uncertainty inherent in the projections.

While pattern scaling gives the geographically explicit changes in the mean climate, a representation of the variability of precipitation and evaporation is also necessary for the evaluation of changes in probabilities of fboding. An estimate of variability can be obtained in a number of ways. Besides the vast uncertainties to be expected in each method, most of the approaches, e. g. high resolution GCMs (Hennessy et al., 1997, Voss et al., 2002), statistical downscaling (e. g. Xu (1999), Wilby and Wigley (1997), Wilby et al. (1998)) or stochastic weather generators (e. g. Cameron et al. (2000), Hutchinson (1995), Wilks and Wilby (1999)) are computationally expensive.

Therefore we chose a resampling approach, similar to the one used by Alcamo et al. (2001) for the GLASS model. This approach is based on data of observed climatic variables on a 0.5° grid with monthly resolution. Both a climatology and the deviations from the climatology are determined from the data, and the deviations from the climatology are used as "templates" of spatio-temporal variability patterns.

As source of climate data, the CRU-PIK dataset by Österle et al. (2003) is used (see section 4.3.2). From this dataset, the monthly climatology for the years 1961-1990 is determined, as well as the deviations from the climatology with $T'(m,t) = T(m,t) - T_C(m)$ and $P'(m,t) = P(m,t)/P_C(m)$ the temperature and precipitation deviation patterns for year t and month m.

In more detail, the "complete" climate is calculated as follows. A climate model is used to calculate the change in global mean temperature $\Delta T_{GM}(t)$ in year t. Currently the deterministic ICLIPS climate model is used for this purpose, as described in chapter 3, Eq. 3.9-3.11, but in principle any other climate model giving $\Delta T_{GM}(t)$ could be used as well. $\Delta T_{GM}(t)$ is then used to scale the patterns for temperature and precipitation, which are applied to the climatology in order to obtain the spatial distribution of the mean climate for $\Delta T_{GM}(t)$. This mean climate is then perturbed by a variability pattern from the sequence of 20th century deviations from the climatology in order to represent natural variability.

The global temperature and precipitation fi elds in a particular month m within year t are thus computed via

$$T(r,m,t) = T_C(r,m) + k\Delta T_{GM}(t) \times T_P(r,m) + T'\left(r,m,t'\right) \quad (4.3)$$

$$P(r,m,t) = \left(P_C(r,m) \times \left(1 + k\Delta T_{GM}(t) \times P_P(r,m)\right)\right) \times P'\left(r,m,t'\right) \quad (4.4)$$

with $T_C(r,m)$ the climatological temperature in month m in location r, $P_C(r,m)$ the climatological precipitation, $T_P(r,m)$ and $P_P(r,m)$ temperature and precipitation cli-

mate change patterns obtained from GCM runs, $\Delta T_{GM}(t)$ the change in global mean temperature in year t and k the scaling factor relating the scaling of the patterns to $\Delta T_{GM}(t)$. $T'(r,m,t')$ and $P'(r,m,t')$ are the deviations from the climatology described above, where the time t' refers to the sequence of deviations from climatology during the 20th century.

The advantage of this approach is that the measured variability of the climatic variables under consideration is well represented, including all spatial and temporal correlations.

The main drawback is that variability is assumed to stay the same in a changed climate – exactly the same for temperature due to the additivity of the deviation pattern and somewhat increased in the case of precipitation due to the multiplicity of the precipitation deviation patterns. While this drawback makes the application of the method to a future changed climate somewhat questionable, we are assuming that this approach can still give major insights into the effects of global warming on flooding probabilities.

4.2.3 Runoff calculation

Runoff is calculated using a simplification of Thornthwaite's formula (Thornthwaite, 1948) as the difference between precipitation and evaporation

$$R(r,m,t) = P(r,m,t) - E(r,m,t) - \Delta S(r,m,t), \tag{4.5}$$

with runoff R, precipitation P, evaporation E and the change in soil storage ΔS, all in location r, month m of year t. $\Delta S = 0$ is assumed, since the storage of moisture in the soil is neglected. This is based on the reasonable assumption that soil will be saturated during the large precipitation events that lead to large-scale flooding.

At temperatures below 0°C, it is assumed that precipitation falls as snow, which is removed from the precipitation field and stored until temperatures rise above freezing again. At temperatures above freezing, the accumulated snow melts and is added to the precipitation field again. Using W for the accumulated snow and T for the temperature, this is expressed as

$$\begin{aligned} W(r,m,t) &= W(r,m,t) + P(r,m,t) \wedge P(r,m,t) = 0 \quad \forall \quad T(r,m,t) < 0^\circ\mathrm{C} \\ P(r,m,t) &= P(r,m,t) + W(r,m,t) \wedge W(r,m,t) = 0 \quad \forall \quad T(r,m,t) \geq 0^\circ\mathrm{C}. \end{aligned}$$

Due to data constraints, the calculation of evaporation has to be done by a scheme that does not depend on very detailed climatological data. Therefore the Hamon scheme (Hamon, 1963) for potential evaporation E_p is used, as it is only dependent on temper-

ature data. In intercomparisons of different evaporation schemes (Federer et al., 1996, Vörösmarty et al., 1998) the Hamon scheme was found to have comparatively little bias (i. e. a systematic over- or underestimation of E_p) and to be well suited to a large range of surface types. On the other hand, the Hamon scheme is a purely empirical formulation that has been derived for present climatic conditions, which makes it questionable whether it is still applicable in a drastically changed climate (Vörösmarty et al., 1998). Nonetheless, the Hamon scheme will be used in the model, since most other evaporation schemes evaluated by Federer et al. had a larger bias and requirements with regard to input data that can not be fulfilled by present climate models suitable for integrated assessment.

In the Hamon scheme, potential evaporation E_p (in mm) is calculated as

$$E_p(T,\Lambda) = \frac{715.5 \times \Lambda \times e(T)}{T + 273.2} \tag{4.6}$$

with T the mean air temperature in °C, Λ the day length as fraction of day and $e(T)$ the saturated vapor pressure (in kPa) at temperature T. As the model uses monthly timesteps and available input data have monthly resolution, the monthly evaporation is calculated. This choice of temporal resolution suits the assessment by Federer et al. (1996) that the scheme is not very sensitive to the use of data with low time resolution.

In principle, evapotranspiration changes in a climate with elevated levels of CO_2. However, estimates of this effect vary and strongly depend on vegetation type (Lockwood, 1999). This effect is therefore disregarded here.

Finally, the actual evaporation E_a is calculated from the potential evaporation E_p using

$$E_a = \begin{cases} E_p & \forall E_p \leq P \\ P & \forall E_p > P. \end{cases} \tag{4.7}$$

Once again, this formulation assumes that soil and plants have no storage capacity for moisture.

The procedure described above gives the amount of runoff per grid cell. Subsequently this is multiplied by grid cell area and summed up over all grid cells belonging to a river basin in order to obtain the total monthly runoff for each river basin considered.

4.3 Data and Methods

4.3.1 River basin description

The evaluation of changes in the probability of large-scale flooding events only makes sense on the scale of river basins. The river basin description in our model is based on the

STN-30p dataset, a dataset of major river basins (Fekete et al., 1999, Vörösmarty et al., 2000). It is derived from a GIS-based analysis of global topographic fields, has a resolution of 0.5° and lists the grid cells belonging to the drainage areas of 6152 individual river basins.

As Vörösmarty et al. (2000) estimate that the accuracy of the data is better for river basins with drainage areas $\geq 2.5 \times 10^4 \mathrm{km}^2$, river basins below that size are excluded from the analysis. The scenario for future population growth described in section 4.3.3 guided the choice of river basins for the assessment of future climates: Of those river basins large enough, the river basins with the largest populations were chosen. The exception were a few basins, like the Nile and Chang Jiang, where the assessment would not be meaningful due to large dams that limit the danger of flooding. The assessment takes place in 83 river basins, where about 50% of world population in 2100 live. These basins are listed in appendix A.

4.3.2 Input and validation data

As source for climate data, the dataset by Österle et al. (2003) is used. This dataset is derived from the CRU timeseries dataset (New et al., 2000), a dataset of observed climatic variables (precipitation, daily mean temperature, diurnal temperature range, vapor pressure and cloud cover) interpolated to a 0.5° grid and covering the time range from 1901 to 1998 with monthly resolution. Österle et al. removed temporal inhomogeneities from the temperature and precipitation fields and extended the dataset to 2003. Henceforth, this dataset will be referred to as CRU-PIK.

For model validation, two datasets of streamflow gauge records were obtained. The first dataset lists monthly discharge data for world rivers excluding the former Soviet Union (Bodo, 2001a), based in large parts on the UNESCO (1974) dataset. The other dataset contains information on monthly discharge data for rivers in the former Soviet Union (Bodo, 2001b). These two datasets give monthly discharge data from 6883 streamflow gauge sites. Of these gauges, 1226 had drainage areas $\geq 2.5 \times 10^4 \mathrm{km}^2$, and of those gauges, 640 had records longer than 25 years, with only complete years considered.

The 640 gauge sites are located in 148 river basins. If there is more than one gauge site in a river basin, the site gauging the largest drainage area was chosen, unless there was another site with insignificantly smaller drainage area, but longer record length. About a third of the gauges (52) are at latitudes between 40°N and 60°N, all other 20° latitude bands north of 40°S still contain between 10 and 28 gauge sites, and 26 stations are located in the southern hemisphere. The latitudinal coverage of validation records therefore appears to be adequate.

4.3.3 Population scenario

The projected changes in flooding probability simulated by the model will in section 4.5.2 be aggregated to global numbers by considering the population affected by this change in flooding probability. Since this will affect the *future* population living in the river basins considered, a scenario giving geographically explicit projections of the changes in population is required.

Such a geographically explicit projection is not readily available, but has to be constructed. What is available are regionalized scenarios, giving the projected changes in population for a number of world regions, as well as geographically explicit datasets of current world population.

Lutz et al. (2004) have published scenarios for the future population in 13 world regions. Their projection is a probabilistic projection, in which they tried to quantify the uncertainty inherent in such projections. Therefore Lutz et al. (2004) published quantiles of the probability distribution of the future regional population, as well as a median value.

In order to derive a geographically explicit projection of future population, the median projection for the 13 world regions is used. The normalized change in population is determined for each of the 13 regions by dividing the projections for 2005-2100 by the population in 2000, as given by the projection. Thus the change in population, relative to 2000, is determined for each world region.

A geographically explicit dataset of current world population is available from CIESIN (2000). Using this data, the current population in each grid point is determined. In a subsequent step the geographically explicit population projection is determined. For each grid point belonging to one of the 13 regions, the population in 2000 is extrapolated to the future value by multiplying it with the regional population change factor determined from the Lutz et al. (2004) projection. It is therefore assumed that the population *distribution* within a region does not change.

This geographically explicit projection of the future population can now be used to determine the population living in a river basin by summing up the projected population for the grid points belonging to a basin.

4.3.4 Validation of annual and monthly runoff

The validation of simulated annual and monthly runoff may seem straightforward at first glance. One would assume that it is sufficient to take precipitation and temperature measurement data, determine the model output for the river basin area upstream of a gauge site, and compare the result with gauge records.

Such a model validation would certainly be possible, if perfect measurements of streamflow, precipitation and temperature were available. If this were the case, any discrepancies between model output and streamflow measurements would have to be regarded as model error. In reality, there may be quite large errors in the measured values, especially in the precipitation measurements (Adam and Lettenmaier, 2003, Fekete and Vörösmarty, 2004). In addition, those areas where higher quality measurements can be expected, are just those areas where it is very likely that streamflow characteristics have been changed by human intervention, since the highest measurement quality, the longest timeseries, and the highest density of measurement networks can be expected in the industrialized countries, where extensive fluvial management has taken place.

Fekete et al. (2002) investigated this problem in some detail. They compared runoff estimates from the "WBM" water balance model (Vörösmarty et al., 1996, 1998), driven by precipitation data from the Willmott and Matsuura (2001) climate data set, with streamflow measurements from selected streamflow gauging stations. They report large differences between simulated and measured streamflow, including some cases where measured streamflow actually exceeded the total measured precipitation.

Therefore the quality of the model is tested by comparing its results with the output of other models given similar input data. For this the *bias* of the mean annual streamflow was determined, defined as

$$bias = \frac{\bar{S} - \bar{O}}{\bar{O}} \times 100\%, \tag{4.8}$$

with $\bar{S}$ the mean modeled annual streamflow and $\bar{O}$ the corresponding observed annual streamflow. Though this *bias* is neglecting interannual variability of streamflows and thus is of limited use for our purpose here, it allows a far reaching comparison to other hydrological models.

In order to get better measures for model simulation quality, Willmott's index of agreement (Willmott, 1982) for the annual total runoff in the validation basins is also determined. The index of agreement d is defined as

$$d = 1 - \left[\frac{\sum_{i=1}^{N} (S_i - O_i)^2}{\sum_{i=1}^{N} \left(\left| S_i - \bar{O} \right| + \left| O_i - \bar{O} \right| \right)^2} \right] \tag{4.9}$$

with S_i the modeled value at time t_i, O_i the observed value at time t_i and $\bar{O}$ the mean observed value. It describes model quality with respect to variations, with $d = 0$ indicating complete disagreement, while $d = 1$ indicates complete agreement. It was proposed by Willmott because the correlation coefficient often used for such investigations is not consistently related to the quality of prediction (Willmott, 1982).

4.3.5 Validation of runoff extremes

The intended purpose of our model is not the accurate reproduction of the mean streamflows, but rather the assessment of probabilities of major flooding due to extreme precipitation. Therefore, model validation will focus on the validation of model simulated runoff extremes, even though annual and monthly runoff will also be evaluated.

The magnitude of the so-called "T-year flood" at a site, which is the amount of streamflow that has a probability $1/T$ of being exceeded in any one year, is commonly estimated by using either the annual maximum series (AMS) approach (Li et al., 1999) or the peak over threshold (POT) approach (Madsen et al., 1997). In both methods a suitable probability distribution is fitted to the timeseries in order to estimate the return period T of certain flood levels. In the POT approach, any flood peak larger than a threshold can be used for fitting the distribution, while the annual maximum is used for the AMS approach. In principle, we regard the POT approach as superior, but this approach requires well-defined flood peaks. As our model works on a monthly timescale, it produces just a single flood-peak per year in most river basins. Therefore the advantage of the POT approach, the ability to use more data than just the single annual maximum, does not come into play, and we thus make use of the AMS approach.

According to a recent review of probability distributions for the AMS approach (Li et al., 1999), various distribution functions are possible. Yet it is difficult to conclude which one is the most appropriate, as the choice of distribution function in mainly dependent on type of data and other factors. Of the distributions that were evaluated favorably by Li et al., the probability distribution that gives the best fit to the streamflow records we have available is the gamma distribution.

In order to obtain a measure of model performance, streamflow data and model results are normalized, and a gamma distribution is fitted to the annual maxima of streamflow (validation data) or runoff (model results). All available data are used for fitting the distribution, the timeframe considered therefore is variable for the validation data, while it is 100 years (1901-2000) for the model results.

From the gamma distribution, the magnitude of the 50-year maximum streamflow / runoff event is determined. The deviation

$$\Delta_{50yr} = \frac{(S_{50yr} - O_{50yr})}{O_{50yr}} \times 100\% \tag{4.10}$$

of the 50-year maximum event, expressed as a percentage of O_{50yr}, shows how well the model reproduces the streamflow extremes. In this equation S_{50yr} is the magnitude of the model-generated 50-year maximum runoff event, and O_{50yr} is the magnitude of the 50-year maximum streamflow event, as estimated from the gauge records.

As the change in probability of the 20th century 50-year maximum streamflow event will later be calculated, this measure gives the most direct indication of simulation quality for the intended purpose of the model.

4.3.6 Sensitivity analysis

In order to assess the model sensitivity to certain parameterizations, a sensitivity analysis is performed. Within the runoff balance (Eq. 4.5), five uncertain factors appear:

1. Some portion of precipitation may be converted to runoff instantly, without being available for evaporation.

2. Some portion of precipitation may be stored as soil water or converted to groundwater, removing it from the water balance equation.

3. Evaporation may be over- or underestimated by the simple parameterization used (Eq. 4.6).

4. Precipitation may be over- or underestimated in the dataset.

5. The neglect of changes in soil moisture.

Experiment	Equation	Formula	Reason
A	Eq. 4.5	$R_A = 0.1 \times P + (0.9 \times P - E)$	direct conversion of P to R
B	Eq. 4.5	$P_B = 0.9 \times P$	groundwater recharge
C	Eq. 4.5	$P_C = 1.1 \times P$	underestimation of P
D	Eq. 4.6	$E_{p,D} = 0.9 \times E_p$	overestimation of E_p
E	Eq. 4.6	$E_{p,E} = 1.1 \times E_p$	underestimation of E_p

Table 4.1: Sensitivity experiments performed. Listed are experiment identifier, equation modified, formula for the modification and the reason for performing the experiment.

In order to test the first four of these possibilities, a series of five sensitivity experiments was performed by changing the components of the runoff balance (Eq. 4.5). These experiments are listed in Table 4.1.

The fifth uncertain factor in Eq.4.5 is the neglect of changes in soil moisture. While this factor may have a large influence on model error, especially with respect to the monthly flows, it is not possible to test this without introducing soil dynamics into the model. This uncertain factor therefore had to be neglected in the quantitative analysis.

4.4 Model validation

4.4.1 Verification of annual and monthly runoff

In order to validate the model performance, the mean annual runoff is determined and compared to estimates from other models of similar scale.

Models of similar scale are the macro-scale hydrological models WBM (Vörösmarty et al., 1996), WGHM (Döll et al., 2003), VIC (Nijssen et al., 2001, Liang et al., 1994), and Macro-PDM (Arnell, 1999b, Meigh et al., 1999) on the one hand. On the other hand, one could also consider the land surface model of atmospheric GCMs (Russell and Miller, 1990, Oki et al., 1999), and the Dynamic General Vegetation Model LPJ (Gerten et al., 2004). Unfortunately, the publication of actual numbers for the error in single river basins, as opposed to plots summarizing the error, is not very common. We therefore restrict the detailed comparison of model error to the numbers published by Russell and Miller (1990) and Nijssen et al. (2001).

The simulation quality of these models varies widely, but is much improved, if the model parameters are tuned on a basin scale. For example, Döll et al. (2003) report a great increase in simulation quality after model tuning, similar to Nijssen et al. (2001). Since no tuning on the river basin scale takes place in our model, as there are no validation records available for some important river basins, the comparison is limited to the published errors before model tuning.

The simulation quality of the macro-scale models, where no such tuning on a basin scale takes place, generally is worse than desirable. Nijssen et al. (2001), for example, report biases ranging from -74.6% to 424.3%, with a median value of -18.1% for the untuned model, with increasing simulation quality after tuning. Similarly, Russell and Miller (1990) report biases ranging from -62.98% to 1018% with a median value of 33.93%.

Arnell (1999b) and Meigh et al. (1999) do not publish numbers for specific river basins, but judging from their plots, the biases range from about -50% to +20% for Arnell (1999b), where some tuning takes place for the whole continent of Europe, and from at least -50% to more than +50% for Meigh et al. (1999), but in both cases the median bias seems to be quite small.

In Table 4.2 the simulation error in the annual runoff is shown for those river basins, where either Russell and Miller (1990) or Nijssen et al. (2001) publish values for their models, and a direct comparison is therefore possible. While Nijssen et al. (2001) publish values for *bias*, Russell and Miller (1990) only publish values for mean annual runoff, both simulated and observed, and the *bias* has to be inferred from these. Overall, the *bias* of our model shows a similar spread of values as both Nijssen et al. and Russell

River	Δ_{50yr}[%]	d	$bias$[%]	$bias_N$[%]	$bias_R$[%]
Amazon	11.48	0.34	-30.79	-39.80	-62.98
Amur	11.11	0.86	-8.33	-45.90	-2.77
Chang Jiang	20.45	0.43	-32.98	-14.30	44.89
Colorado	n. a.	0.10	2120.39		315.00
Columbia	4.00	0.65	-19.90	-74.30	20.72
Danube	27.14	0.80	6.21	12.30	44.66
Dvina	0.64	0.75	-4.78	31.30	10.38
Fraser	25.18	0.75	-11.19		33.93
Indigirka	24.00	0.39	-56.75	-54.70	
Indus	3.49	0.60	40.06		26.05
Kolyma	1.12	0.50	-42.71	-32.00	376.06
Lena	9.77	0.36	-38.66	-68.20	5.84
Mackenzie	33.07	0.48	-20.28	-69.00	83.66
Magdalena	21.58	0.57	-24.58		32.49
Mekong	5.67	0.63	-12.12	-19.10	51.49
Mississippi	2.58	0.65	31.95	18.00	-10.86
Murray	-18.05	0.08	1490.34		431.82
Niger	25.19	0.12	336.75		82.81
Nile	16.55	0.05	508.47		606.02
Ob	18.90	0.73	7.11	46.50	30.91
Olenek	20.99	0.52	-40.97	-36.70	
Parana	10.22	0.28	93.26	6.20	
Pechora	12.42	0.48	-29.26	16.30	
Senegal	34.21	0.20	144.59	424.30	
Shatt el Arab	4.92	0.80	3.53		71.74
St. Lawrence	27.87	0.25	47.24		3.36
Volga	-13.33	0.53	26.90	83.60	
Yana	32.08	0.42	-52.28	-74.60	
Yenisei	12.69	0.28	-34.19	-44.40	-10.54
Yukon	-5.63	0.34	-48.87	104.80	152.31
Zambezi	-4.74	0.16	318.49		13.45

Table 4.2: Error in those river basins, where either Nijssen et al. (2001) or Russell and Miller (1990) publish values. Shown are Δ_{50yr}, index of agreement d and $bias$ for our model, $bias_N$ for Nijssen et al. and $bias_R$ for Russell and Miller. Δ_{50yr} is shown as not available for the Colorado basin, since it failed the Kolmogorov-Smirnov test in section 4.4.2.

and Miller, with the exception of the very extreme values our model produces in the Colorado and Murray basins.

Taking all validation basins into account, the *bias* for our model ranges from -68.8% to 2120.4%, with a median value of 9.5%, while the index of agreement *d* ranges from 0.05 to 0.93 with a median of 0.54.

In general the model overestimates runoff, 87 gauge sites (53%) show a positive *bias*. 98 of the 148 gauge records show an absolute *bias* below 50%, and 67 below 25%. 15 gauge records have a *bias* above 250%. A histogram of the distribution of *bias* is shown in Fig. 4.2, along with the results from the sensitivity analysis.

The Colorado and Murray basins, where model *bias* is particularly large, as well as the Nile and some other validation basins, are located in very dry areas, and therefore a number of processes that are not considered in our model become important. First of all there may be seepage from the river channel, and in addition the evaporation from open water may play a major role here, especially if the river runs through lakes or wetlands. For the Nile, Niger, Senegal and Orange similar problems are reported by Döll et al. (2003), while Oki et al. (1999) report such problems for the Colorado and Niger. In addition to these processes, basins like the Colorado are heavily managed by humans, and as these processes are not included in the model, they cannot be represented adequately either.

Model simulation quality with respect to the annual total runoff and the annual cycle of runoff therefore is comparable to other models of similar scope and scale, where no tuning on a river basin scale takes place, and a better performance would be desirable. We mainly attribute these performance problems to three causes. First of all, the Hamon scheme for the parameterization of potential evaporation (Eq. 4.6) basically rests on the assumption of uniform soil and vegetation characteristics. This leads to the potential evaporation scheme being more suitable to some river basins than to others. In addition, the neglect of soil storage of moisture and river routing may lead to additional errors, especially with regard to the timing of the annual cycle. Similarly, the simple parameterization of snow and snowmelt introduces additional errors into the model results.

4.4.2 Validation of runoff extremes

As reported in the methods section (section 4.3.5), the return period of extreme runoff events is commonly evaluated by fitting a suitable probability distribution to the annual maxima of runoff. In the case of the streamflow records available, a gamma distribution turns out to be most suitable. By performing a Kolmogorov-Smirnov test, we determine whether the gauge records are compatible with this hypothesis. At 5% significance level, only 2 out of the 148 gauge records are rejected. These are the Colorado and Rio

Grande basins, where extensive human influence on streamflow characteristics has to be assumed. These streamflow records are excluded from the subsequent analysis, leaving us with 146 gauge records for the validation of model extremes.

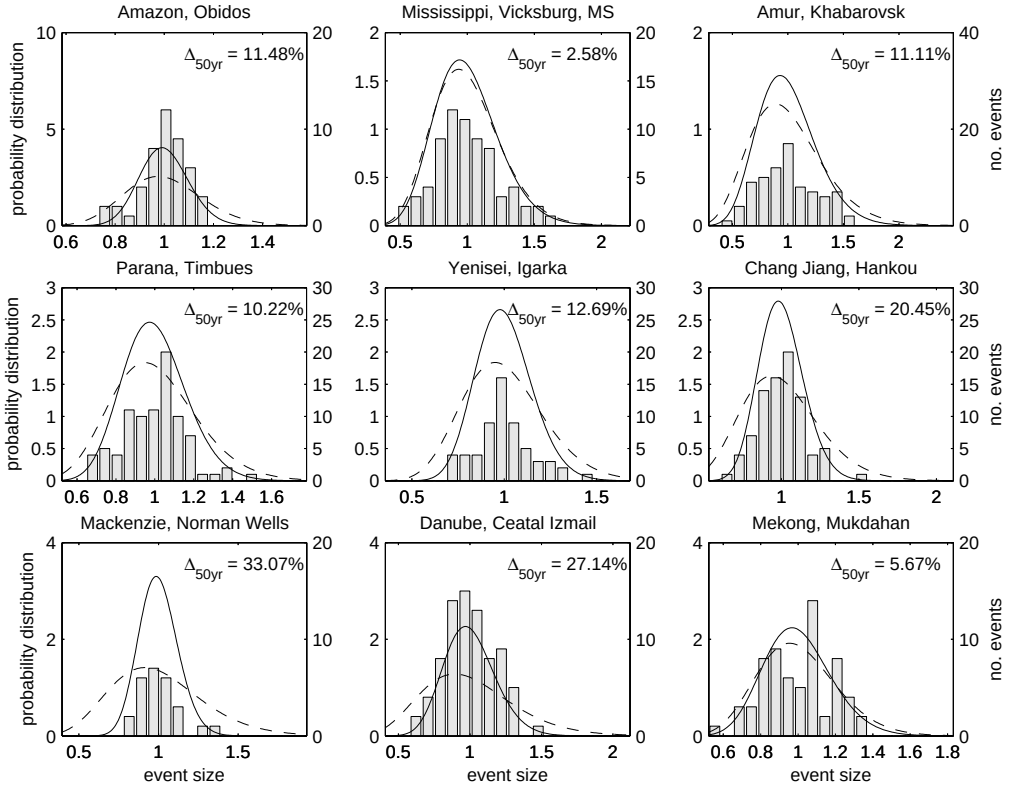

Figure 4.1: Probability distributions for extremes and histograms for measured extremes at selected gauge sites. Continuous line: fit to normalized gauge record annual maxima, dashed line: fit to normalized model annual maxima. Also shown: Δ_{50yr}.

As the mean flows the model simulates are biased (see section 4.4.1), the extremes can only be compared after a suitable normalization of the data. Streamflow data and model results are therefore normalized to a to a mean annual maximum streamflow / runoff of one, using

$$\tilde{S}_i = \frac{S_i}{\bar{S}} \qquad \text{and} \qquad \tilde{O}_i = \frac{O_i}{\bar{O}}$$

with S_i the model simulated annual maximum streamflow in year i, $\bar{S}$ the mean S_i and $\tilde{S}_i$ the normalized value. Similarly, O_i is the observed annual maximum streamflow in year i, $\bar{O}$ the mean O_i and $\tilde{O}_i$ the normalized value for year i.

After normalization the probability distributions fitted to these data are in comparatively good agreement with another. In order to give the reader an impression of model

simulation quality, plots of the estimated probability distributions at nine gauge sites are shown. Fig. 4.1 shows the probability distributions for the selected verification basins, as well as histograms of the number of annual maximum runoff events for the normalized event sizes, as estimated from streamflow measurements. While the probability distributions are similar in every case, some differences are apparent. In all cases the probability distributions for the model generated extremes are wider than the ones for the measured extremes. In addition the peak of the probability distribution is higher in the case of the measured extremes. Therefore the model overestimates the probability of events that are larger or smaller than the mean event, while it underestimates the probability of the mean event sizes.

In order to quantify these errors, the error Δ_{50yr} (Eq. 4.10) in the estimated 50-year extreme streamflow / runoff event is determined. Table 4.2 lists these values for selected river basins. The deviation of the 50-year extreme event ranges from an underestimation by -18.05% in the Murray to an overestimation by 34.21% in the Senegal. Taking all validation records considered into account, the deviation of the 50-year event between model and data is ranges from -36.11% to 47.02%, with a median value of 3.53%. In 87 out of the 146 records considered, the 50-year event is overestimated. The absolute value of Δ_{50yr} stays below 10% in 66 (45%) of the 146 gauge records, and it stays below 25% in 130 cases (89%). The error is never larger than 50%. A histogram of the distribution of Δ_{50yr} is shown in Fig. 4.2, lower panel, along with results from the sensitivity experiments.

All in all, the agreement of the model simulated extreme events with the extreme events estimated from streamflow records is surprisingly good considering the much larger bias in the mean flows. The error is below 10% in more than 45% of the gauge records evaluated, and no gauge displayed an error larger than 50%.

This good agreement of the probability distributions and of the 50-year max. runoff event, after an appropriate normalization, leads us to the conclusion that the current model appears to be suitable to the evaluation of future probabilities of high runoff events, as long as the intercomparison of current and future probabilities takes place within the model results. Even though the annual and monthly flows the model simulates may be biased, the agreement of probability distributions fitted to streamflow data and model results suggests that the probability of high runoff events relative to the (biased) mean flows is estimated more or less correctly.

4.4.3 Sensitivity analysis

The simple model formulation allows a thorough analysis, which of the factors in the runoff balance (Eq. 4.5) has the largest influence on model performance. The sensitivity

experiments undertaken are listed in Table 4.1. The model results of the sensitivity analysis runs are subjected to the same analysis as above, namely a validation of the model extremes and of the mean flows.

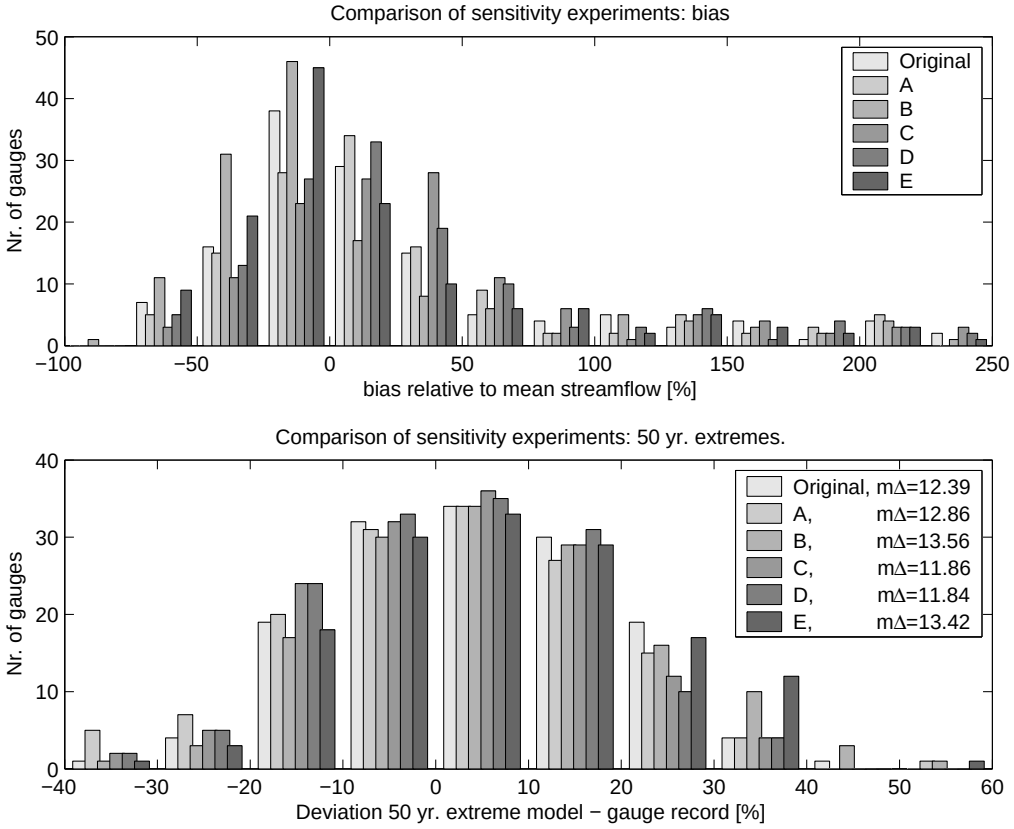

Figure 4.2: Upper panel: *bias* relative to mean streamflow for sensitivity experiments. 148 gauge records considered, but between 7 and 22 (depending on experiment) not shown due to *bias* $> 250\%$. Lower panel: deviation Δ_{50yr} of model simulated 50-year extremes from gauge record derived extremes, relative to gauge record derived extremes, for original configuration and sensitivity experiments. 146 gauge records considered. Legend also shows mean absolute Δ_{50yr} as mΔ.

Fig. 4.2, upper half, shows a histogram of the *bias* relative to the mean streamflows at the gauge sites for all 148 gauge records considered. The mean absolute *bias* is highest (145%) in experiment A, while it is lowest (80%) in experiment B. Model performance is improved in sensitivity experiments B and E, while it is worse than the original in sensitivity experiments A, C and D. As the model generally overestimates runoff, this was expected since precipitation is reduced in B and evaporation is enhanced in E.

Similarly, Fig. 4.2, lower half, shows a histogram of the deviations Δ_{50yr} of model simulated 50-year extremes from gauge record derived 50-year extremes, relative to the gauge record derived extremes, for the sensitivity experiments. The mean absolute Δ_{50yr} is shown as $m\Delta$ in the legend. Overall, the spread of the different cases in the sensitivity experiments is smaller for the extremes than for the means. The sensitivity experiments B and E performed worse than the original setup, while experiments A, C and D performed slightly better. The lowest mean absolute Δ_{50yr} (11.8%) is found in experiment D, while it is largest (13.6%) in experiment B.

Taking these results together, it seems recommendable to keep the original model setup. While sensitivity experiment D has the lowest mean absolute Δ_{50yr}, the result for the original setup is only slightly worse than that of experiment D. When looking at the mean flows, sensitivity experiments B and E perform best, while they perform worst when comparing the extremes. Choosing setup D would slightly improve performance with respect to the extremes, but it involves an arbitrary scaling of precipitation. While precipitation is generally underestimated by measurements, this underestimation is neither temporally nor geographically homogeneous, and reliable correction factors are not available for all regions (Arnell, 1999b).

Therefore there is no clear-cut "best" model configuration, and it seems best not to introduce arbitrary scaling factors. Hence we will keep the original, most simple model configuration in the following assessment of changed climates.

4.5 Changed probabilities for extreme runoff events under climate change

4.5.1 A single scenario experiment

As an example of the potential changes in probability of extreme runoff events, a synthetic temperature change scenario and the corresponding timeseries of annual maximum runoff are shown in Fig. 4.3. The top panel shows the change in global mean temperature, relative to the late 20th century, in the climate change scenario. As the CRU-PIK measurement data is used during the 20th century, climate change is not shown during this timeframe. During the 21st century, global mean temperature rises rapidly and peaks in 2080 at a global mean temperature change $\Delta T = 4$K. Afterwards temperature decreases again, but global mean temperature in 2200 is still about 2K higher than during the 20th century. As described in section 4.2.2, climate variability is assumed to be the same sequence of variability patterns as measured during the 20th century. The lower panels show annual maximum runoff in the Mississippi (middle panel) and Amazon

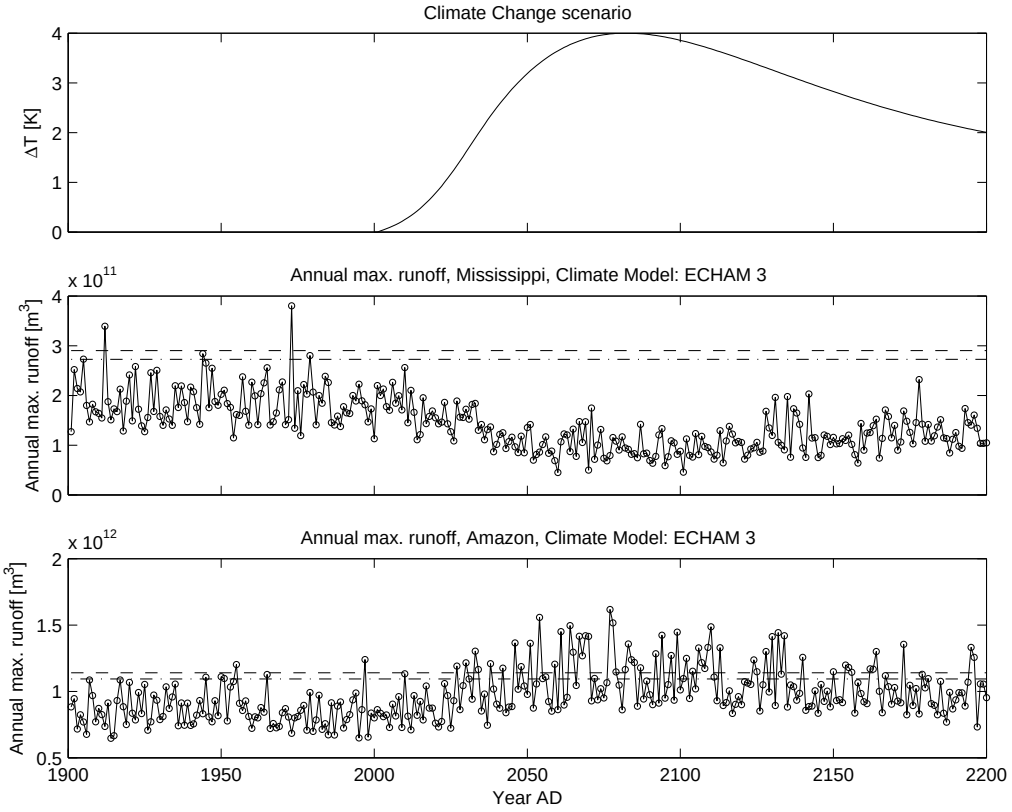

Figure 4.3: Consequences of climate change in two river basins. Top panel: climate change scenario, 20th century not shown because driven by CRU-PIK data. Lower panels: annual maximum runoff, model-generated, for the Mississippi (middle) and Amazon (bottom) basins. Also shown: 50-year maximum runoff event (dashed line) and 25-year max. runoff event (dash-dotted line).

(bottom) basins. Contrary to the runoff assessed in Sec. 4.4.1, the runoff shown in these plots is not the annual total summed up over sub-basins belonging to some streamflow gauge, but the runoff shown is the annual maximum monthly area-weighted sum of all the grid cells belonging to a drainage basin. The runoff timeseries is therefore comparable to the annual maximum streamflow timeseries given by a gauge located at the river mouth. The plots also show the level of the 50-year maximum runoff event during the 20th century (dashed line) and the level of the 25-year event (dash-dotted line). These are derived by fitting a gamma distribution to the model-generated annual maxima of runoff. Climate change patterns for this plot were derived from ECHAM 3.

It is clearly visible in Fig. 4.3 that the annual maxima of runoff in the Mississippi basin decrease in magnitude. Both the 25-year and the 50-year max. runoff events during the 20th century are never exceeded during the next centuries. The probability of

flooding therefore decreases in the Mississippi basin. In the Amazon basin, on the other hand, the picture is quite different. Here, the 25-year event is exceeded 65 times, while the 50-year event is exceeded 55 times during the 21st and 22nd centuries. If the system were in a stationary state, the 25-year event would become a 3.1-year event, while the 50-year event would become a 3.6-year event. The probability of major runoff events therefore clearly increases.

The model allows the determination of the change in flooding probability depending on the magnitude of global mean warming. We assess the changes in flooding probability for 83 of the largest river basins, where 50% of the projected world population in 2100 live. These basins are listed in appendix A.

To determine the change in flooding probability, 100 years of monthly runoff data are simulated for increased global mean temperatures, ranging from $\Delta T = 0.1$K to $\Delta T = 5$K in steps of 0.1K. As described above, a gamma distribution is fitted to the timeseries of annual maximum runoff, and thus the change in probability of a runoff event of equal magnitude to what was the 50-year maximum runoff event during the 20th century can be assessed. The event Q_{50yr} is determined, which is the magnitude of the 50-year flood during the 20th century, as simulated by the model. Subsequently, the probabilities $P(Q_{50yr})$ are determined for changed climate conditions.

Results of this assessment for nine large river basins are shown in Fig. 4.4 using climate change patterns generated by three different GCMs. While the probability $P(Q_{50yr})$ clearly increases in some river basins, there are other river basins where the magnitude of Q_{50yr} is never reached at all. Using the patterns generated by ECHAM 3, shown as dashed lines, the probability increases markedly with rising temperatures in the Amazon, Parana, Chang Jiang and Mekong basins. Other river basins, namely the Mississippi, Amur, Mackenzie and Danube river basins, experience a marked decrease in $P(Q_{50yr})$, while flooding probability in the Yenisei basin first increases and then decreases again. The climate change patterns produced by ECHAM 4, shown as dash-dotted lines, give a similar overall picture, with the exception of the Amur, Yenisei and Mackenzie basins. The most interesting of these cases are the Yenisei and the Mackenzie. While ECHAM 3 simulates an increase in $P(Q_{50yr})$ at temperature changes up to about 2K for the Yenisei basin, followed by a decrease, ECHAM 4 simulates a faster initial increase followed by a short decrease, which is again followed by an increase in probability. A similar behavior is apparent in the Mackenzie basin. Here, both models project an initial decrease in $P(Q_{50yr})$, but ECHAM 4 simulates an increase in probability at climate changes larger than 2.5K, while ECHAM 3 projects no further change in flooding probability. A more detailed analysis of model results reveals that this difference is due to changes in the annual cycle of model-generated runoff when driven by patterns generated by ECHAM 4.

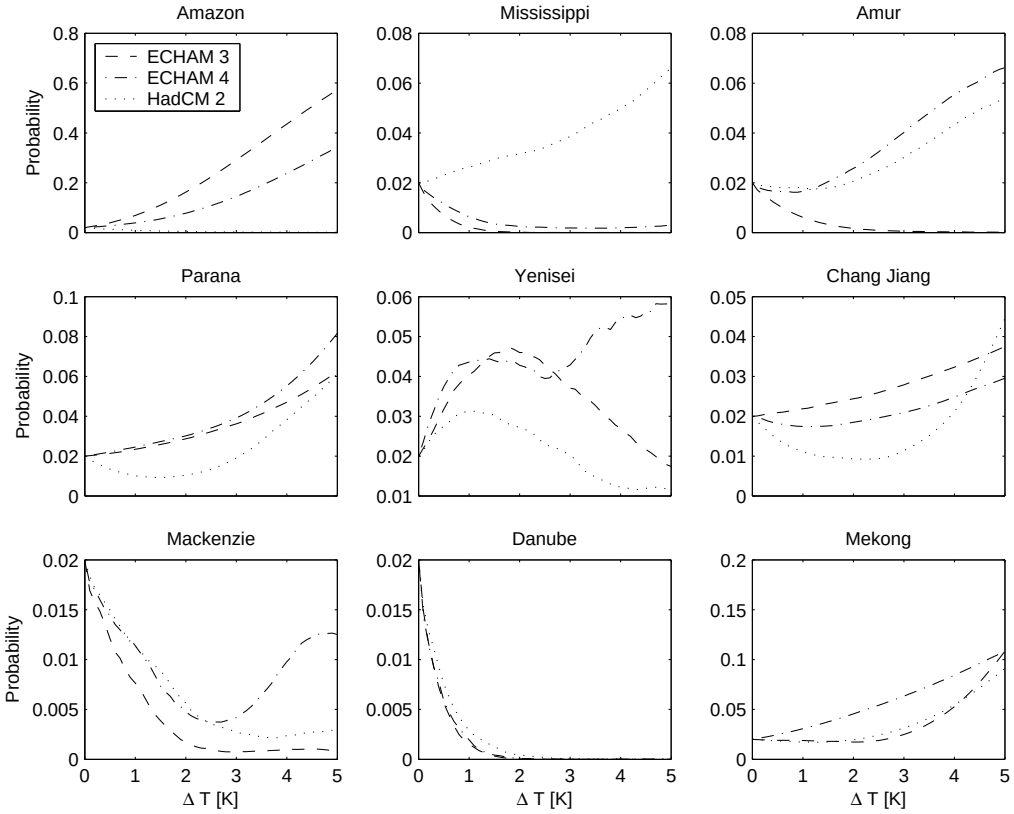

Figure 4.4: Changed probabilities for the 20th century 50-year max. runoff event Q_{50yr} ($P = 0.02$) for selected river basins, depending on change in global mean temperature ΔT. Determined using climate change patterns from ECHAM 3 (dashed line), ECHAM 4 (dash-dotted line) and HadCM 2 (dotted line).

While the patterns generated by ECHAM 3 induce that the annual maximum of runoff as generated by the model occurs in May, ECHAM 4 simulates a shift of the annual maximum of runoff to April, due to earlier snowmelt, and as evaporation is smaller in April due to both the shorter day length and lower temperatures, this generates increases in fboding probability. In the Amur basin the different projection by the two models is simply due to different precipitation projections, with ECHAM 4 simulating increases, while ECHAM 3 produces decreases in precipitation.

Looking at the climate change generated by HadCM 2, the largest difference to the ECHAM models occurs in the Mississippi basin, where HadCM 2 projects an increase in fboding probability, while the ECHAM models simulate a decrease. This is once again due to different precipitation patterns derived from the different models.

4.5.2 Climate Impact Response Function

For an application in the TWA, a climate impact response function (CIRF) can be determined by the model. Climate impact response functions (Füssel et al., 2003, Füssel, 2003) have been developed as reduced form models in order to enable the representation of the impacts of climate change in integrated assessment models. A CIRF is a representation of the relation between climate change on the one hand, and the impact(s) of climate change under consideration on the other hand.

In the case of a CIRF intended to limit changes in flooding probability, probabilities need to be taken into account in a probabilistic CIRF. In order to construct the CIRF, the magnitude Q_{50yr} of the 20th century 50-year flood event is used as a reference, and the new probability $P(Q_{50yr})$ of the Q_{50yr} event under changed climate conditions is determined.

The 50-year event is used for two reasons. First of all, we believe that it would be misleading to estimate the size of events that have an even smaller probability from a timeseries that is just 100 years long. Second, the amount of runoff that is reached or exceeded only once in 50 years is already so large that it seems plausible that this level will already cause major damage to infrastructure and endanger human lives. The 50-year event during the 20th century Q_{50yr} therefore seems to be a suitable benchmark to compare future climate states with.

Since the goal is the construction of a CIRF that indicates changes in flooding probability on a global scale, the results on the scale of single river basins have to be aggregated to this scale. Aggregating these changes in probability to a global level – after all this analysis was performed in 83 of the largest river basins – is nontrivial, as the aggregation of the change in probability over all river basins may very well mask the severity of the problem, as decreasing probabilities in some river basins may mask the strong increases in other river basins. Therefore the the population affected by increases in $P(Q_{50yr})$ is determined.

Using the projection of future population growth described in section 4.3.3, the future population living in the river basins analyzed can be determined. This may not quite represent the number of people that are actually affected by the change in flooding probability, as not all the people living in a river basin will experience the floods, but it seems safe to assume that the majority of the population living in a river basin lives close to the river and will therefore be affected by the change in flooding probability. Furthermore, the overall damage by a flood does affect an entire region, e. g. by demand for financing of the reconstruction of destroyed infrastructure.

The model therefore generates a four dimensional CIRF, with climate change, the change in $P(Q_{50yr})$, and the population affected by this change as the main dimensions,

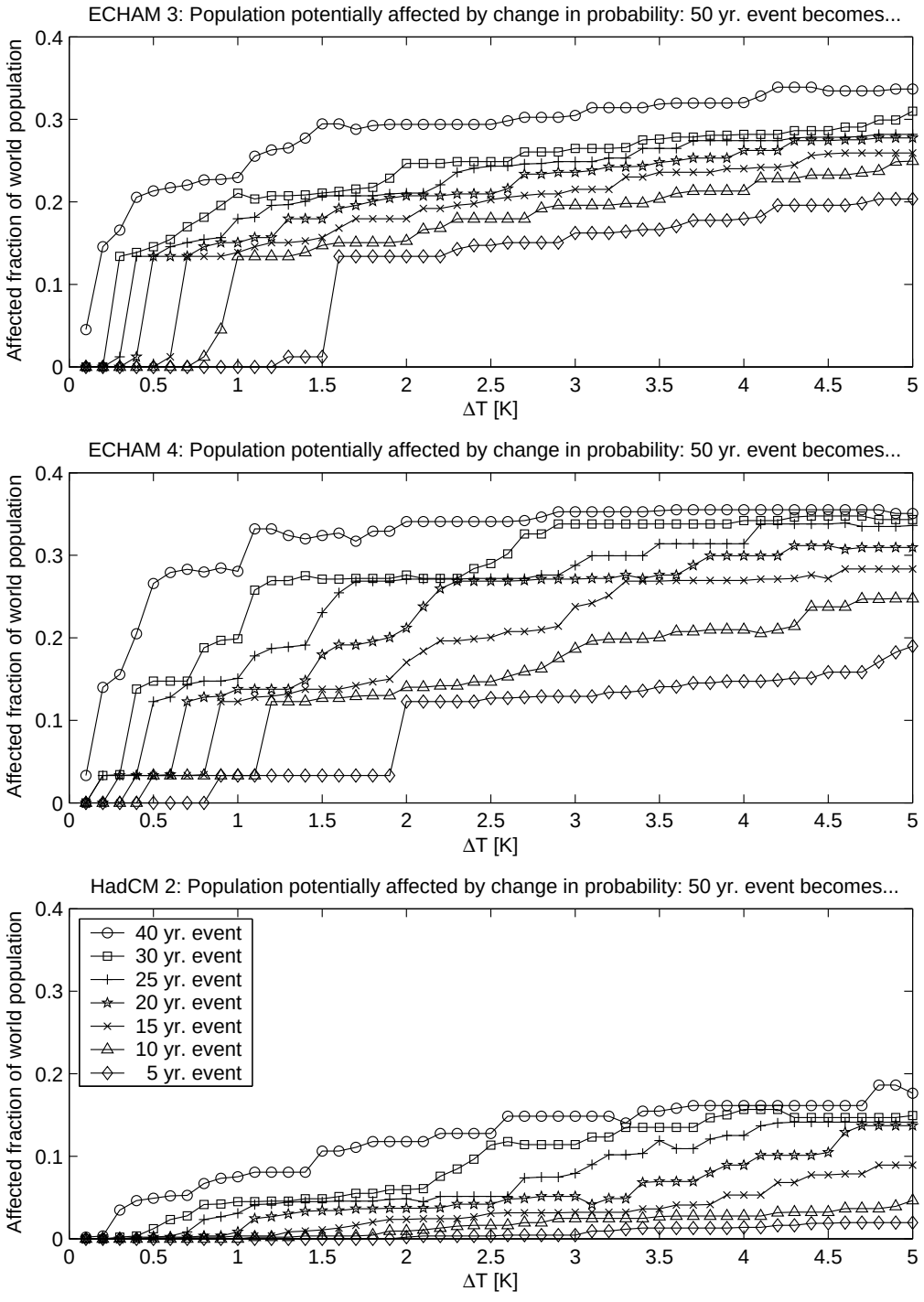

Figure 4.5: Fraction of world population in 2100 affected by changed probability of 50-year maximum runoff event, dependent on change in global mean temperature ΔT. Climate change patterns were taken from ECHAM 3 (upper panel), ECHAM 4 (middle) and HadCM 2 (bottom). The legend for all plots is shown in the bottom panel.

but since the population affected is time-dependent due to the change in population, time is an additional dimension to the CIRF. Therefore projections of the CIRF have to be presented.

Results for this analysis, derived using the climate change patterns from the three GCMs, are shown in Fig. 4.5 for the population in 2100. Using the climate change patterns obtained from ECHAM 3, shown in Fig. 4.5, upper panel, one can see that the population affected by a change in probability of the former 50-year event to a 25-year event (marked by plus signs) rises steeply for a global warming $\Delta T \geq 0.3$K. The rise in fraction of world population affected then slows at a global warming $\Delta T = 0.5$K, where about 13% of world population are affected. The fraction of world population affected finally reaches about 28% at $\Delta T = 5$K. The non-smooth nature of these curves is due to to the fact that once a basin crosses the threshold, it's population is added to the total at once. The large initial increase in the plots for ECHAM 3 and ECHAM 4 is mainly due to the Ganges basin with it's projected population of 762 million in 2100.

This series of figures also highlights the uncertainty in these estimates. If one considers the fraction of population obtained using the climate change patterns derived from ECHAM 4, shown in Fig. 4.5, middle, the overall shape of the curves is similar to the the ones obtained using ECHAM 3, while the threshold temperatures may be somewhat shifted. Using HadCM 2, shown in Fig. 4.5, bottom, the overall picture is quite different. The fractions of world population affected are significantly lower, and the increases are less steep than in the cases using the ECHAM models. This difference between the projections by the different models is largely due to the different estimates of future monsoon rainfall. While the ECHAM models project increases in monsoon precipitation, HadCM 2 projects a decrease, and due to the large population in the Ganges basin, this has a large effect on the projected population affected.

A different projection of the CIRF is shown in the upper panel of Fig. 4.6. Here, the time dependence of the population affected by a change of the 50-year event to a 25-year event is shown, based on climate change patterns from ECHAM 3. Overall, the time dependence is not very large, but the maximum fraction of population is affected, if the population of 2075 is considered, whereas the consideration of the population of 2000 yields the lowest estimate of population affected.

Taking up the results from the sensitivity analysis in section 4.4.3, the sensitivity of the CIRF to the most influential configurations in the sensitivity experiments is also determined. Apart from the CIRF generated with standard model parameters, CIRFs are also generated for the model configurations "B" and "D", which showed the highest (B) and lowest (D) mean absolute Δ_{50yr} in section 4.4.3. Results of this analysis, again conducted using climate change patterns generated by ECHAM 3, are shown in the lower

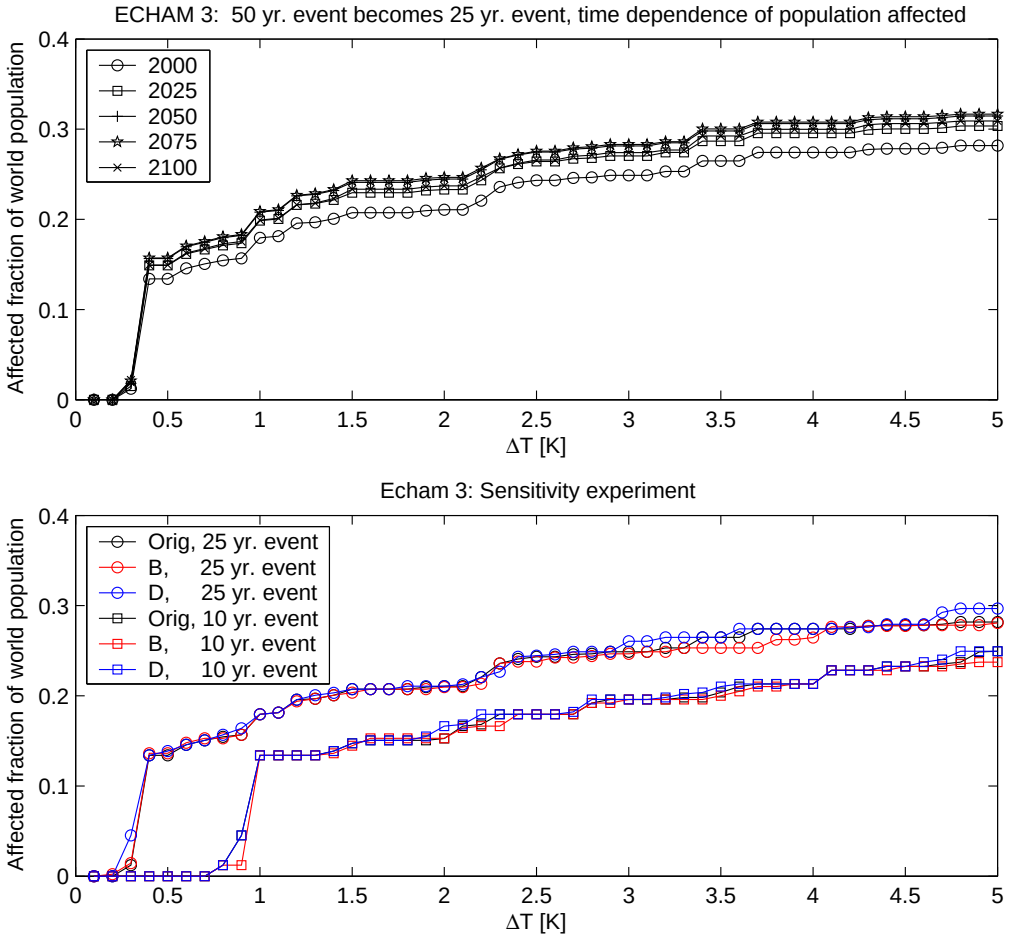

Figure 4.6: Fraction of world population affected by changed probability of 50-year maximum runoff event, dependent on change in global mean temperature ΔT. Climate change patterns were taken from ECHAM 3. Upper panel: Time dependence of population affected by change of 50-year maximum runoff event to 25-year maximum runoff event. Lower panel: Sensitivity of population in 2100 affected to parameter variations as in sensitivity experiments B and D.

panel of Fig. 4.6. Here, the population in 2100 affected by a change of the 50-year to a 25-year and a 10-year event is shown for the original configuration, as well as configurations B and D. Obviously the configurations in the sensitivity experiments have only a small influence on the CIRF. While some differences between the different configurations can be determined, these differences are very small and only occur in isolated river systems. Therefore the CIRF is robust with respect to the uncertain parameterizations investigated in section 4.4.3

In the fi nal section, the CIRF shown in Fig. 4.5 is used within the TWA to calculate emission corridors, where the fraction of world population affected by changes in fboding probability is limited.

4.6 Emission corridors limiting the change in flooding probability

The CIRF developed in the previous section can be used to determine emission corridors that show the emissions that are still possible, if the number of people affected by a change in $P(Q_{50yr})$ is to be limited.

In order to obtain the emission corridors, the ICLIPS climate model is used. It was already presented in chapter 3, Eq. 3.9-3.11. The model parameters are kept as described in chapter 3, with the exception of two changes. First of all, the reference period of the climatology used is 1961-1990. Therefore, this timeframe also defi nes the initial conditions the model uses to calculate future climate states. Second, as the model contains just a primitive carbon cycle and no other greenhouse gases, a CO_2-equivalent formulation is used. In this formulation, the radiative forcing by all forcing agents is converted to the CO_2 concentration that would generate the same radiative forcing. Climate sensitivity is set to 3K.

As a guardrail various settings are possible. This analysis focuses on the change in probability of the 50-year maximum runoff event, as calculated by the model when forced with 20th century observed climate, yet other events can easily be used. The guardrails are defi ned as limits to the percentage of world population that are affected by a change in $P(Q_{50yr})$ to a specifi ed new probability.

In addition to these guardrail settings, the same constraints on the change in emissions are imposed as in chapter 3. The change in emissions is parameterized as $\dot{E} = gE$, and the maximal emission reduction is limited to 4% p.a.. The rate of change in emission reduction is also bounded as $0 \leq \dot{g} \leq -(g_0 + g_{max})/t_{trans}$, with $t_{trans} = 20$ yrs and $g_{max} = -0.04$. The initial growth in emissions g_0 is determined by the optimization, but limited to be between 1% p.a. and 3% p.a..

The corridor boundaries are then calculated by performing a constrained optimization, where the maximum (minimum) in emissions allowed by the constraints is determined for successive points in time in order to determine the upper (lower) boundary of the emission corridor (Leimbach and Bruckner, 2001, Bruckner et al., 2003b).

Fig. 4.7 shows emission corridors of the CO_2-equivalent emissions that are possible, if not more than 20% of the world population in 2100 are to be affected by a change in probability of the 50-year max. runoff event, based on the climate change patterns

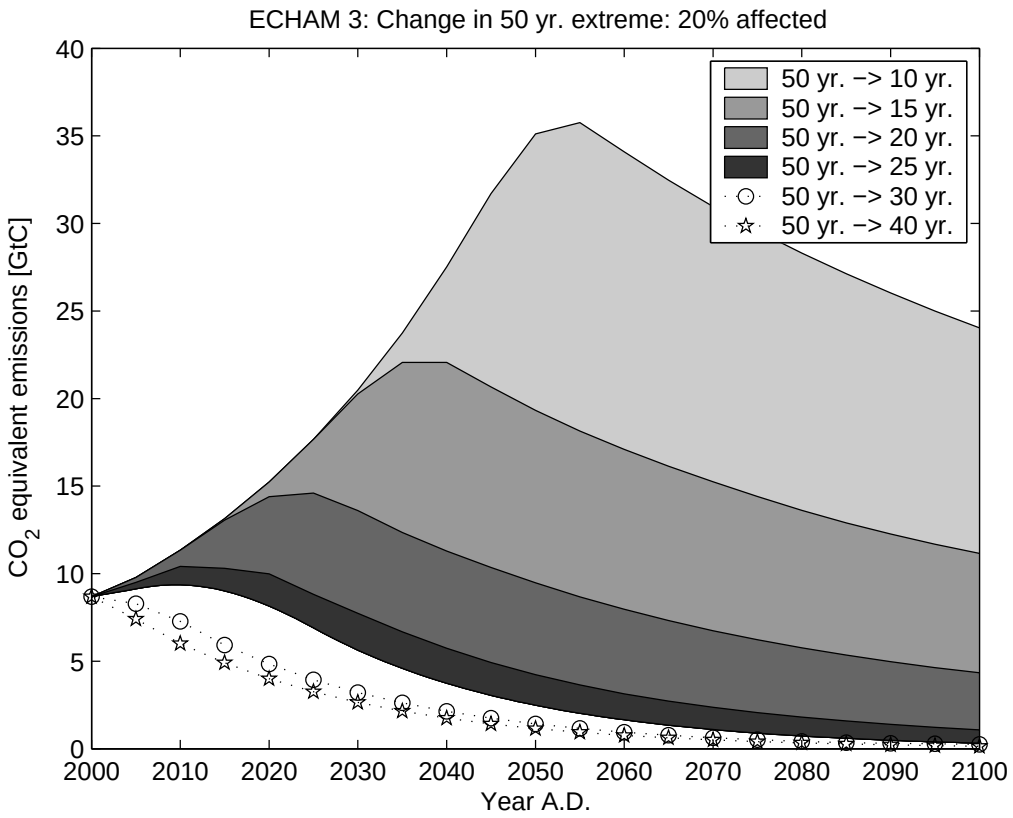

Figure 4.7: Emission corridor limiting the change in fboding probability. CO_2 equivalent emissions allowable, if less than 20% of world population are to be affected by a change in probability of the 50-year max. runoff event to the new probability shown in the legend. Based on the climate model ECHAM 3.

generated by ECHAM 3. The plot shows the emission corridors for a change of the 50-year event to the new probabilities shown in the legend. The actual emission corridor is the total shaded area between the upper boundary of the respective shaded area and the lower boundary of all the shaded areas. Please note that the upper boundaries of the 40-year, shown as a dotted line with stars, and the 30-year emission corridors, shown as a dotted line with circles, are actually located *below* the lower boundary. The emission corridors therefore are empty sets: only emission reduction strategies that involve emission reductions larger than 4% p.a. would produce a valid solution, and as emission reductions are limited to 4% p.a. for socio-economic reasons, these guardrails cannot be observed.

As detailed in section 3.3.3, the corridors derived this way are *necessary* corridors. All emission strategies that lie outside the corridor, or leave the corridor at some point in

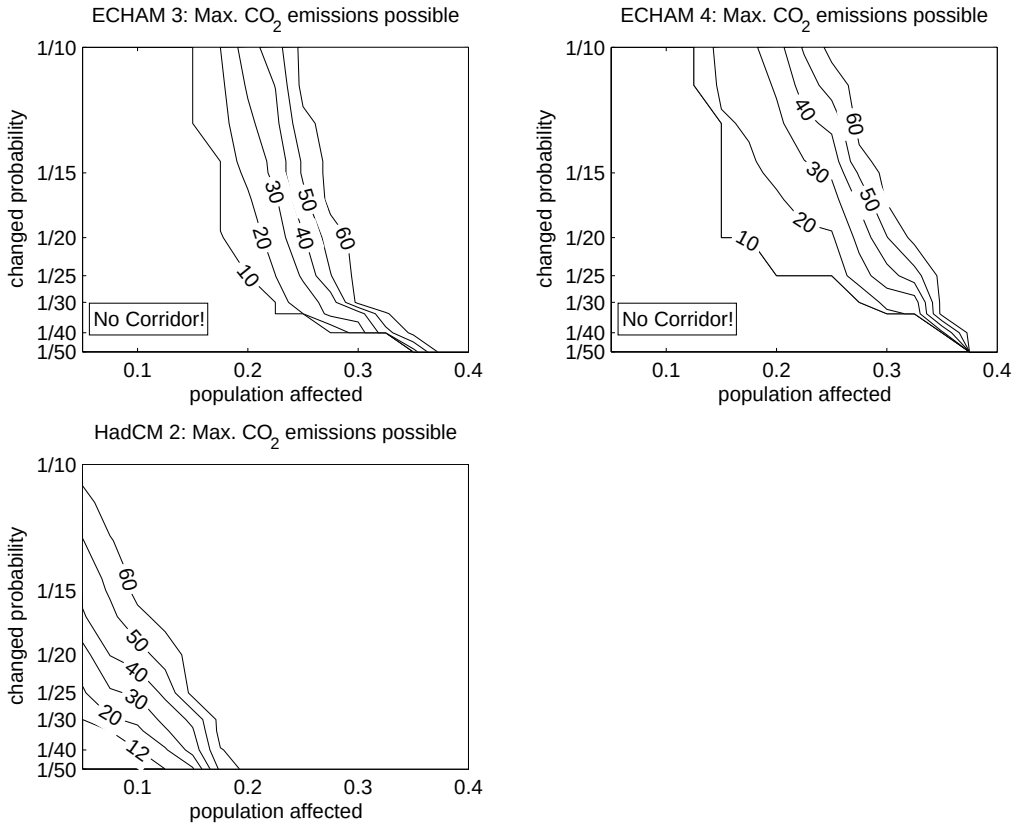

Figure 4.8: Maximum of the emission corridors for the climate change patterns generated by all three GCMs. Shown are the maximal CO_2 equivalent emissions allowed, if the population affected by the change in flooding probability is to be limited. In the lower left-hand corner of the three plots, no viable emission corridors exist.

time, definitely violate the guardrail. For emission strategies that lie completely within the corridor, one has to check, whether they violate the guardrails or not. Especially emission strategies that stay close to the upper boundary of the emission corridor for most of the time are not acceptable. For further information on the interpretation of emission corridors see Kriegler and Bruckner (2004).

Fig. 4.8 presents a different perspective to the emission corridors. In Fig. 4.8 isolines are presented that mark the maximum of the emission corridors for varying changes in probability and population affected. This figure also highlights the considerable uncertainty that is still inherent in this analysis, due to the different climate change patterns generated by the different GCMs. Shown are isoline diagrams for the GCM patterns considered, with ECHAM 3 shown on the upper left, ECHAM 4 on the upper right, and HadCM 2 on the lower left. On the lower left-hand side of the figures, no emission cor-

ridor exists that could limit the population affected by the changed flooding probability to these numbers. This is due to the fact that the maximum in emissions of the allowable minimum emissions trajectory is 9.4 GtC, due to the transition time scale and the maximum emission reductions imposed, which still implies a temperature change of about 1.3°C relative to the 1961-1990 average global mean temperature. Emissions above a maximum of 60 GtC were not evaluated, since these imply temperature changes larger than 5°C – a temperature change, where the simple climate model used is not applicable any more.

If the ECHAM models should prove to be correct, it will be impossible to prevent 20% of the world population from being affected by the 50-year maximum runoff event becoming a 25-year event, and more than 10% will be affected by even larger changes in probability. This is mainly due to the large increases in precipitation that the ECHAM models project for the Ganges basin. If, on the other hand, HadCM 2 should prove to be correct, the population affected will be less dramatic, but it will still be impossible to prevent 10% of world population from being affected by a change of the 50-year to a 40-year event.

4.7 Discussion and Conclusions

The modeling results presented in the previous sections suggest, that changes in the probability of large scale flooding due to changes in precipitation in the course of future climate change might have a severe impact on a significant portion of world's population. Not only does the simulation with a single climate change scenario suggest an increase in probabilities for large scale floods, but even more significant are the results obtained within the application of the tolerable windows approach (TWA).

Within this application of the TWA, the portion of the world population experiencing an increase of the probability of what is today a 50-year event has been implemented as a constraint for future climate change. Within this first step, a probabilistic climate impact impact response function (CIRF) is implemented, which is based on the model presented before. This CIRF gives the portion of world population which experiences a specified shift in flooding probabilities as a function of the global mean temperature. In a second step, the corridors of admissible emissions were calculated, which comply with this constraint and which do not exceed a reduction rate of more than 4% p.a. Both, the climate impact response function and the resulting corridors suggest that:

- There is a significant risk that even a small increase in global mean temperature by less than 0.5°C brings about a significant increase in flooding probabilities, which can affect up to 20% of the world population. Here, results differ with different

spatial patterns of climate change obtained from three GCMs. More specific, the risk does depends on the fate of the Indian Monsoon, as the two ECHAM GCMs implemented both show its strengthening. Therefore, the pertaining uncertainties on the monsoon are not only of relevance for agriculture, but also for floods.

- Within the "wet" worlds of the ECHAM models, there is no reasonable emission scenario to insure that only small fractions of world population are affected by increases in the probabilities of major floods. If, for example, we want to avoid that more than 20% of the world population are affected, we have to reckon with shifts in probabilities where what has been a 50-year event in the 20th century becomes at least a 25-year event over the next 100 years.

- The danger of such "TINAs" (there is no alternative) imply, that adaptation to increasing flooding probabilities are inevitable. Given the possibility that these shifts might happen with rather small increases in global mean temperature, adaptation measures need to be taken soon, which calls for an increasing effort to study and understand the processes of adaptation.

With respect to the probabilistic tolerable windows approach, this chapter has demonstrated how a probabilistic climate impact response function can be determined and employed in the TWA. Using stochastic techniques, the change in probability of flood events was determined, depending on the change in climate. Therefore, stochastic information was shown to be a valuable tool in a policy advice application.

One aspect that is missing in this assessment are the other kinds of floods that could not be included here. Flash floods and floods caused by very intense, short-duration precipitation events cannot be modeled on scales as coarse as the ones used here. Since the probability of such events may also change in a changed climate, the population affected by such changes might be even larger than shown here, but not smaller.

Of course the results are subject to a large range of uncertainties. Some of them have been taken into account, e. g. by using climate change patterns from different GCMs, or by assessing the model uncertainty through a sensitivity analysis. Nevertheless, some other uncertainties pertain. Here, particularly the question how climate variability might change in the course of global warming or the limited reproducibility of historical streamflows by models in general have to be mentioned. In addition, the uncertainty in climate sensitivity, which was in chapter 3 shown to be a very important factor, was not considered in the determination of emission corridors.

The main uncertainty with respect to changes in flooding probability could unfortunately not be addressed in a satisfying manner. While the climate change patterns from different GCMs gave different possibilities of the spatio-temporal characteristics

of changes in climate, it was not possible to determine a single change in probability for a certain river basin, as opposed to the three different estimates given by the three patterns. Therefore the uncertainty could be addressed, but not resolved.

The main potential improvement would therefore be a better estimate of the spatio-temporal changes in climate. While we used the pattern-scaling approach with patterns derived from single GCMs here, the different simulations by different GCMs contain a large uncertainty. If combined patterns from multiple GCMs and a probability distribution over these were available, it would be possible to derive a single probabilistic CIRF, not a CIRF for each of the GCMs the climate change patterns were derived from. This would therefore improve the representation of the uncertainty contained in the assessment, which would facilitate its consideration.

The second development this approach could profi t from are improved estimates of the future variability of climatic variables. Our current approach rests on the assumption that future variability patterns will be similar to todays, but it appears likely that this will not be the case.

Nevertheless, we consider the model as good enough to conclude that an increase in fboding probabilities should be a major reason for concern about climate change. Increased modeling efforts need to be undertaken to localize the critical regions for increased fboding, in order to get improved information for adaptation priorities.

Chapter 5

Summary and Outlook

5.1 Summary

In this thesis we have shown that stochastic information can yield valuable insights into the climate system. Stochastic information can be used for the reduction of uncertainty in assessments of the current state of the climate system, as well as for the comprehensive consideration of uncertainty in assessments of future climate change. The uncertainty that is ever-present in assessments of climate change makes the information gained by the use of stochastic methods even more valuable, since the information gained this way can not in all cases be gained by deterministic means.

Three general classes of uncertainty with respect to the assessment of changes in climate were assumed. These classes are:

1. uncertainty that is caused by natural variability
2. uncertainty caused by insuffi cient knowledge, and
3. uncertainty that arises as a result of the freedom of human choice.

We have demonstrated that stochastic information can be a valuable tool for considering, communicating, and even reducing two of these uncertainties.

Uncertainty caused by the unpredictability of human decisions is the one class of uncertainty, where stochastic information as presented in this thesis does not aid the consideration and reduction of uncertainty. Since the TWA doesn't predict human decisions, it avoids this uncertainty, but this class of uncertainty is not considered explicitly in this thesis. It could be addressed using scenarios, but not using the techniques employed in this thesis. What stochastic information may do with respect to this uncertainty is that it may *influence* human decisions, if the communication of uncertainty inherent

in the assessment of climate change is improved by the use of stochastic information, resulting in a better informed policy-making process.

Uncertainty caused by insufficient knowledge is a different matter in this respect. Here, stochastic information may greatly improve the assessment of changes in climate, and two aspects to this matter were developed in this thesis. In chapter 2, an indicator was developed that may reduce the uncertainty about the distance of the climate system to a nonlinear threshold. It was shown that properties of fluctuations can be used to obtain information not accessible by deterministic means. Here, stochastic information is able to reduce uncertainty by giving an independent estimate of the distance to the bifurcation point. In chapter 3, on the other hand, it was shown how stochastic information can be utilized to consider uncertainty in the integrated assessment of climate change. The probabilistic TWA developed there is able to incorporate uncertainty caused by insufficient knowledge, if the uncertainty can be expressed as uncertainty in model parameters, for which a probability distribution is known. This also aids the communication of the uncertainty inherent in climate change assessments, since uncertainty that is considered explicitly can be communicated more easily.

Finally, there is uncertainty caused by natural variability. Here, stochastic information may also aid the assessment of changes in climate. With the use of stochastic techniques, natural variability can be incorporated in assessments of climate change. With respect to natural variability, chapter 2 has shown that the consideration of natural variability may actually reduce other uncertainties, since it can be utilized to obtain additional information. The consideration of natural variability in a policy guidance model for the integrated assessment of climate change was demonstrated in chapter 3. Within the framework of the TWA, natural variability leads to a certain probability that guardrails set in order to limit the consequences of climate change are violated, if the guardrails are set appropriately, i. e. if the guardrail is not just defined by the mean climate. The probabilistic TWA developed in chapter 3 can consider this probability, and it allows to set guardrails that limit the probability of an event happening. This cause of uncertainty was also considered in chapter 4, where a probabilistic climate impact response function was developed that allows the limitation of changes in floboding probability within the TWA. Here, stochastic techniques were used to determine the natural variability of temperature and precipitation under changes climate conditions, allowing an assessment of changes in floboding probability due to climate change.

This thesis therefore has shown that stochastic information potentially is a very valuable tool in the assessment of changes in climate.

With respect to the uncertainty inherent in the assessment of changes in future climate, the results of the analyses in chapters 3 and 4 show that a very large uncertainty,

if not the most important uncertainty, is the uncertainty about the reaction of the climate system itself to changes in radiative forcing. The large uncertainty in climate sensitivity considered in chapter 3 leads to very little maneuvering space for humanity, if a change in global mean temperature larger than 2°C is to be avoided with high probability, and if the uncertainty is fully taken into account, i. e. the probability of large climate sensitivities is non-zero. The uncertainty caused by natural variability, on the other hand, has a much smaller effect on emission corridors. Similarly, the probabilistic climate impact response function for changes in flooding probability developed in chapter 4 shows little sensitivity to the variation of parameters in the hydrological model, but a very large sensitivity to the climate change patterns derived from different GCMs. Here, the spatial pattern of climate change was therefore the most important uncertain factor in the assessment, and this large uncertainty prevented the derivation of a *single* change in flooding probability for a given change in mean climate, as opposed to the three distinct changes in probability derived using the patterns derived from three different GCMs. The uncertainty in regional climate change implied also touches upon the thermohaline circulation investigated in chapter 2, since the stability of the THC depends on the freshwater balance in the North Atlantic region.

5.2 Outlook

This thesis partly has the character of a conceptual "playground", where new concepts are explored and implemented for the first time. Applications of the concepts will have to follow in order to make the development of these new concepts worthwhile for climate policy-making.

The indicator for the proximity to a saddle-node bifurcation in the THC developed in chapter 2 will have to be investigated further. A first step in this direction has already been made, since we have shown in a separate publication (Held and Kleinen, 2004) that the approach can also be used in models of intermediate complexity. The next step therefore is the application to a full three dimensional GCM in order to show that the indicator can also be successfully employed there. In addition, there are other systems it could be applied to. Here, transitions in ecosystems come to mind, as well as the Indian monsoon, which may contain a saddle-node bifurcation (Zickfeld, 2003).

The probabilistic TWA developed in chapter 3 is an improvement over the deterministic TWA, since some of the uncertainty in climate change assessment can now be considered explicitly. This is important in the policy advice application the TWA is intended for, since the consideration and communication of uncertainty is an urgent task

that could so far not be tackled in a satisfying manner within the deterministic TWA. Since the groundwork has now been laid, future applications will be sure to follow.

A similar outlook can be seen for the probabilistic climate impact response functions developed in chapter 4. The conceptual framework developed in this thesis will allow the application of the concept to other impacts of climate change, where climate change leads to e. g. changes in probabilities of extreme events, or impacts where the uncertainty is so large that a probabilistic framework has to be employed. The full potential of a probabilistic climate impact response function has, however, not yet been demonstrated. A probabilistic CIRF could also include a measure of the uncertainty, whether a certain impact level will be reached, as outlined in section 3.3.2. This aspect was not demonstrated here, since the focus was on impacts of climate change, where probabilities of extreme events change, but future applications could include it.

Appendix A

List of river basins considered

No.	Name	Pop. 2100 [10^6]	Area [10^5km^2]	No.	Name	Pop. 2100 [10^6]	Area [10^5km^2]
1	Ganges	762	16.33	43	Sao Francisco	23	6.17
2	Indus	284	11.46	44	Ob	22	25.77
3	Niger	180	22.46	45	Chao Phraya	21	1.42
4	Zaire	157	37.09	46	Galana	21	1.18
5	Huang He	128	8.96	47	Elbe	20	1.49
6	Parana	128	26.69	48	Brahmani	19	0.58
7	Huai	125	2.45	49	Cross	19	0.52
8	Krishna	108	2.52	50	Rabarmati	19	0.28
9	Mississippi	104	32.12	51	Dnepr	19	5.10
10	Godavari	100	3.12	52	Panuco	18	0.92
11	Hai Ho	93	2.46	53	Po	18	1.02
12	Shatt el Arab	87	9.70	54	Mahi	17	0.29
13	Zhujiang	80	4.10	55	Sacramento	17	1.93
14	Zambezi	79	19.94	56	Tana (Ken)	16	0.99
15	St. Lawrence	71	12.70	57	Kizil Irmak	15	1.10
16	Damodar	61	0.60	58	Penner	15	0.54
17	Amur	61	29.11	59	Wisla	15	1.81
18	Mekong	60	7.76	60	Seine	13	0.74
19	Danube	54	7.90	61	Dongjiang	13	0.34
20	Amazon	50	58.70	62	Senegal	13	8.50
21	Balsas	48	1.23	63	Paraiba do Sul	13	0.63
22	Brahmani	46	1.42	64	Don	12	4.24
23	Syr-Darya	44	10.73	65	Menjiang	12	0.66
24	Volta	44	3.99	66	Meuse	11	0.43
25	Amu-Darya	43	6.14	67	Jacui	11	0.81
26	Limpopo	43	4.21	68	Kura	11	2.20
27	Magdalena	42	2.52	69	Hudson	11	0.43
28	Rhine	41	1.66	70	Rufi ji	11	1.87
29	Irrawaddy	40	4.07	71	Trinity	11	0.48
30	Volga	35	14.67	72	Urugay	10	3.56
31	Cauweri	35	0.79	73	Farah	10	3.86
32	Liao	34	2.75	74	Bandama	10	1.04
33	Jubba	34	8.18	75	Columbia	10	7.26
34	Narmada	32	1.14	76	Cuanza	10	1.64
35	Grande de Santiago	31	1.92	77	Cheliff	9	0.58
36	Tapti	28	0.67	78	Sebou	9	0.39
37	Chari	27	15.76	79	Motagua	9	0.27
38	Jordan	27	2.70	80	Asi	9	0.28
39	Orange	24	9.46	81	Comoe	9	0.83
40	Orinoco	24	10.42	82	Odra	9	1.20
41	Fuchun Jiang	23	0.67	83	Sassandra	9	0.77
42	Hong	23	1.71				

Bibliography

J. C. Adam and D. P. Lettenmaier. Adjustment of global gridded precipitation for systematic bias. *Journal of Geophysical Research*, 108(D9):4257, 2003.

J. Alcamo, M. B. Endejan, F. Kaspar, and T. Rösch. The GLASS model: a strategy for quantifying global environmental security. *Environmental Science & Policy*, 4(1): 1–12, 2001.

J. Alcamo, E. Kreileman, M. Krol, R. Leemans, J. Bollen, J. van Minnen, M. Schaefer, S. Toet, and B. de Vries. Global modelling of environmental change: an overview of IMAGE 2.1. In J. Alcamo, R. Leemans, and E. Kreileman, editors, *Global Change Scenarios of the 21st Century. Results from the IMAGE 2.1 Model*, pages 3–96. Elsevier, Oxford, U.K., 1998.

N. G. Andronova and M. E. Schlesinger. Objective estimation of the probability density function for climate sensitivity. *Journal of Geophysical Research*, 106(D19):22605–22611, 2001.

N. W. Arnell. Climate change and global water resources. *Global Environmental Change*, 9(S1):S31–S49, 1999a.

N. W. Arnell. A simple water balance model for the simulation of streamflow over a large geographic domain. *Journal of Hydrology*, 217(3-4):314–335, 1999b.

V. K. Arora and G. J. Boer. Effects of simulated climate change on the hydrology of major river basins. *Journal of Geophysical Research*, 106(D4):3335–3348, 2001.

J.-P. Aubin and A. Cellina. *Differential Inclusions. Set-Valued Maps and Viability Theory.* Springer Verlag, Berlin, 1984.

J.-P. Aubin, G. da Prato, and H. Frankowska. Stochastic invariance for differential inclusions. *Journal of Set-Valued Analysis*, 8:181–201, 2000.

J.-P. Aubin and H. Frankowska. *Set-Valued Analysis.* Birkhäuser, Boston, 1990.

A. Becker and U. Grünewald. Flood risk in central europe. *Science*, 300:1099, 2003.

G. Berz. Catastrophes and climate change: Concerns and possible countermeasures of the insurance industry. *Mitigation and Adaptation Strategies for Global Change*, 4 (3-4):283–293, 1999.

B. A. Bodo. Monthly discharge data for world rivers (excluding former Soviet Union). Version 1.3, available online at http://dss.ucar.edu/datasets/ds552.1, 2001a.

B. A. Bodo. Monthly discharges for 2400 rivers and streams of the former Soviet Union. Version 1.1, available online at http://dss.ucar.edu/datasets/ds553.2, 2001b.

G. Bond, W. Showers, M. Cheseby, R. Lotti, P. Almasi, P. deMenocal, P. Priore, H. Cullen, I. Hajdas, and G. Bonani. A pervasive millennial-scale cycle in north atlantic holocene and glacial climates. *Science*, Volume 278(5341):1257–1266, 1997.

M. J. Booij. Extreme daily precipitation in western europe with climate change at appropriate spatial scales. *International Journal of Climatology*, 22(1):69–85, 2002.

A. Bronstert, D. Niehoff, and G. Bürger. Effects of climate and land-use change on storm runoff generation: present knowledge and modelling capabilities. *Hydrological Processes*, 16(2):509 – 529, 2002.

T. Bruckner, G. Hooss, H.-M. Füssel, and K. Hasselmann. Climate system modeling in the framework of the tolerable windows approach: The ICLIPS climate model. *Climatic Change*, 56(1-2):119–137, 2003a.

T. Bruckner, G. Petschel-Held, M. Leimbach, and F. L. Toth. Methodological aspects of the tolerable windows approach. *Climatic Change*, 56(1-2):73–89, 2003b.

T. Bruckner, G. Petschel-Held, F. Tóth, H.-M. Füssel, C. Helm, M. Leimbach, and H.-J. Schellnhuber. Climate change decision-support and the tolerable windows approach. *Environmental Modeling and Assessment*, 4(4):217–234, 1999.

K. Bryan and F. C. Hansen. A stochastic model of north atlantic climate variability on decade-to-century time scales. In D. G. Martinson, K. Bryan, M. Ghil, M. M. Hall, T. R. Karl, E. S. Sarachik, S. Sorooshian, and L. D. Talley, editors, *Natural Climate Variability on Decade-to-Century Time Scales*. National Academy Press, 1995.

D. Cameron, K. Beven, and J. Tawn. An evaluation of three stochastic rainfall models. *Journal of Hydrology*, 228(1-2):130–149, 2000.

P. Cessi. A simple box model of stochastically thermohaline flow. *Journal of Physical Oceanography*, 24(8):1911–1920, 1994.

CIESIN. Gridded population of the world (gpw), version 2. Center for International Earth Science Information Network (CIESIN), Columbia University; International Food Policy Research Institute (IFPRI); and World Resources Institute (WRI). CIESIN, Columbia University, Palisades, NY, 2000. Available at http://sedac.ciesin.columbia.edu/plue/gpw.

P. U. Clark, N. G. Pisias, T. F. Stocker, and A. J. Weaver. The role of the thermohaline circulation in abrupt climate change. *Nature*, 415:863–869, 2002.

M. Collins, S. F. B. Tett, and C. Cooper. The internal climate variability of HadCM3, a version of the hadley centre coupled model without flux adjustments. *Climate Dynamics*, 17(1):61–81, 2001.

U. Cubasch, G. A. Meehl, G. J. Boer, R. J. Stouffer, M. Dix, A. Noda, C. A. Senior, S. Raper, and K. S. Yap. Projections of future climate change. In J. T. Houghton, Y. Ding, D. J. Griggs, M. Noguer, P. J. van der Linden, X. Dai, K. Maskell, and C. A. Johnson, editors, *Climate Change 2001: The Scientific Basis. Contribution of Working Group I to the Third Assessment Report of the Intergovernmental Panel on Climate Change*, chapter 9, pages 525–582. Cambridge University Press, 2001.

K. Deimling. *Multivalued Differential Equations*. De Gruyter, Berlin, Germany, 1992.

C. Deser, M. Holland, G. Reverdin, and M. Timlin. Decadal variations in labrador sea ice cover and north atlantic sea surface temperatures. *Journal of Geophysical Research*, 107(C5):10.1029/2000JC000683, 2002.

H. Dowlatabadi. Bumping against a gas ceiling. *Climatic Change*, 46(3):391–407, 2000.

P. Döll, F. Kaspar, and B. Lehner. A global hydrological model for deriving water availability indicators: model tuning and validation. *Journal of Hydrology*, 270(1-2):105–134, 2003.

J. Edmonds, M. W. H. Pitcher, R. Richels, T. M. L. Wigley, and C. MacCracken. An integrated assessment of climate change and the accelerated introduction of advanced energy technologies: An application of minicam 1.0. *Mitigation Adaptation Strategies*, 1:311–339, 1996.

C. A. Federer, C. Vörösmarty, and B. Fekete. Intercomparison of methods for calculating potential evaporation in regional and global water balance models. *Water Resources Research*, 32(7):2315–2321, 1996.

B. M. Fekete and C. J. Vörösmarty. Uncertainties in precipitation and their impacts on runoff estimates. *Journal of Climate*, 17(2):294–304, 2004.

B. M. Fekete, C. J. Vörösmarty, and W. Grabs. Global composite runoff fi elds on observed river discharge and simulated water balances. Report 22, Global Runoff Data Center, 1999.

B. M. Fekete, C. J. Vörösmarty, and W. Grabs. High-resolution fi elds of global runoff combining observed river discharge and simulated water balances. *Global Biogeochemical Cycles*, 16(3):10.1029/1999GB001254, 2002.

C. E. Forest, P. H. Stone, A. P. Sokolov, M. R. Allen, and M. D. Webster. Quantifying uncertainties in climate system properties with the use of recent climate observations. *Science*, 295:113–117, 2002.

S. Funtowicz and J. R. Ravetz. Science for the post-normal age. *Futures*, 25:739–755, 1993.

H.-M. Füssel. *Impacts analysis for inverse integrated assessment of climate change*. PhD thesis, Universität Potsdam, 2003.

H.-M. Füssel, F. L. Toth, J. G. van Minnen, and F. Kaspar. Climate impact response functions as impact tools in the tolerable windows approach. *Climatic Change*, 56 (1-2):91–117, 2003.

A. Ganopolski, V. Petoukhov, S. Rahmstorf, V. Brovkin, M. Claussen, A. Eliseev, and C. Kubatzki. CLIMBER-2: a climate system model of intermediate complexity. part II: Model sensitivity. *Climate Dynamics*, 17(10):735–751, 2001.

C. W. Gardiner. *Handbook of Stochastic Methods*. Springer, 2nd edition, 1994.

D. Gerten, S. Schaphoff, U. Haberlandt, W. Lucht, and S. Sitch. Terrestrial vegetation and water balance – hydrological evaluation of a dynamic global vegetation model. *Journal of Hydrology*, 286(1-4):249–270, 2004.

J. M. Gregory, R. J. Stouffer, S. C. B. Raper, P. A. Stott, and N. A. Rayner. An observationally constrained estimate of the climate sensitivity. *Journal of Climate*, 15: 3117–3121, 2002.

H. Haken. *Synergetics*. Springer, 2nd edition, 1980.

W. R. Hamon. Computation of direct runoff amounts from storm rainfall. *Int. Assoc. Sci. Hydrol. Publ.*, 63:52–62, 1963.

K. Hasselmann. Stochastic climate models. Part I. Theory. *Tellus*, 28:473–485, 1976.

K. Hasselmann, S. Hasselmann, R. Giering, V. Ocana, and H. v. Storch. Sensitivity study of optimal CO_2 emission paths using a simplified structural integrated assessment model (SIAM). *Climatic Change*, 37(2):345–386, 1997.

H. Held and T. Kleinen. Detection of climate system bifurcations by degenerate fingerprinting. *Geophysical Research Letters*, 31:L23207, 2004.

K. J. Hennessy, J. M. Gregory, and J. F. B. Mitchell. Changes in daily precipitation under enhanced greenhouse conditions. *Climate Dynamics*, 13(9):667–680, 1997.

J. T. Houghton, Y. Ding, D. J. Griggs, M. Noguer, P. J. van der Linden, X. Dai, K. Maskell, and C. A. Johnson, editors. *Climate Change 2001: The Scientific Basis. Contribution of Working Group I to the Third Assessment Report of the Intergovernmental Panel on Climate Change*, 2001. Cambridge University Press, Cambridge, United Kingdom and New York, NY, USA.

R. W. Houghton and M. H. Visbeck. Quasi-decadal salinity fluctuations in the labrador sea. *Journal of Physical Oceanography*, 32(2):687–701, 2002.

M. F. Hutchinson. Stochastic space-time weather models from ground-based data. *Agricultural and Forest Meteorology*, 73(3-4):237–264, 1995.

T. C. Johns, R. E. Carnell, J. F. Crossley, J. M. Gregory, J. F. B. Mitchell, C. A. Senior, S. F. B. Tett, and R. A. Wood. The second hadley centre coupled ocean-atmosphere GCM: model description, spinup and validation. *Climate Dynamics*, 13:103 – 134, 1997.

R. Joseph, M. Ting, and P. Kumar. Multiple-scale spatio-temporal variability of precipitation over the coterminous united states. *Journal of Hydrometeorology*, 1:373–392, 2000.

T. Kleinen. Zeitverhalten der Thermohalinen Zirkulation unter Einfluß des anthropogenen Treibhauseffektes. Master's thesis, Universität Potsdam, 2000.

T. Kleinen, H. Held, and G. Petschel-Held. The potential role of spectral properties in detecting thresholds in the earth system: application to the thermohaline circulation. *Ocean Dynamics*, 53(2):53–63, 2003.

T. Kleinen and G. Petschel-Held. Integrated assessment of changes in flooding probabilities due to climate change. submitted to Climatic Change, 2004.

P. E. Kloeden and E. Platen. *Numerical Solution of Stochastic Differential Equations*. Springer, 3rd edition, 1999.

R. Knutti and T. F. Stocker. Limited predictability of the future thermohaline circulation close to an instability threshold. *Journal of Climate*, 15(2):179–186, 2002.

E. Kriegler. *Imprecise Probability Analysis for Integrated Assessment of climate change*. PhD thesis, Univerität Potsdam, 2005.

E. Kriegler and T. Bruckner. Sensitivity analysis of emissions corridors for the 21st century. *Climatic Change*, 66(3):345–387, 2004.

Z. W. Kundzewicz, D. Graczyk, T. Maurer, I. Przymusińska, M. Radziejewski, C. Svensson, and M. Szwed. Detection of change in world-wide hydrological time series of maximum annual fbw. To be published as WMO report, 2003.

Z. W. Kundzewicz and H.-J. Schellnhuber. Floods in the IPCC TAR perspective. *Natural Hazards*, 31:111–128, 2004.

R. Leemans and W. Cramer. The IIASA database for mean monthly values of temperature, precipitation and cloudiness of a global terrestrial grid. Rr-91-18, International Institute for Applied Systems Analysis (IIASA), 1991.

M. Leimbach and T. Bruckner. Influence of economic constraints on the shape of emission corridors. *Computational Economics*, 18:173–191, 2001.

R. J. Lempert, M. E. Schlesinger, S. C. Bankes, and N. G. Andronova. The impacts of climate variability on near-term policy choices and the value of information. *Climatic Change*, 45(1):129–161, 2000.

Y. Li, K. M. L. Saxena, and S. Cong. Estimation of the extreme fbw distributions by stochastic models. *Extremes*, 1(4):423–448, 1999.

X. Liang, D. P. Lettenmaier, E. F. Wood, and S. J. Burges. A simple hydrologically based model of land surface water and energy fluxes for general circulation models. *Journal of Geophysical Research*, 99:14415–14428, 1994.

J. G. Lockwood. Is potential evapotranspiration and its relationship with actual evapotranspiration sensitive to elevated atmospheric CO_2 levels? *Climatic Change*, 41(2): 193–212, 1999.

W. Lutz, W. C. Sanderson, and S. Scherbov, editors. *The End of World Population Growth in the 21st Century: New Challenges for Human Capital Formation and Sustainable Development*. Earthscan, London, 2004.

H. Madsen, P. F. Rasmussen, and D. Rosbjerg. Comparison of annual maximum series and partial duration series methods for modeling extreme hydrologic events. 1. At-site modeling. *Water Resources Research*, 33:747–757, 1997.

E. Maier-Reimer and K. Hasselmann. Transport and storage of CO_2 in the ocean – an inorganic ocean-circulation carbon cycle model. *Climate Dynamics*, 2:63–90, 1987.

S. Manabe and R. J. Stouffer. Two stable equilibria of a coupled ocean-atmosphere model. *Journal of Climate*, 1:841–866, 1988.

A. S. Manne, R. Mendelsohn, and R. G. Richels. MERGE – a model for evaluating regional and global effects of ghg reduction policies. *Energy Policy*, 23:17–34, 1995.

B. D. Marchi and J. R. Ravetz. Risk management and governance: a post-normal science approach. *Futures*, 31:647–653, 1999.

J. J. McCarthy, O. F. Canziani, N. A. Leary, D. J. Dokken, and K. S. White, editors. *Climate Change 2001: Impacts, Adaptation, and Vulnerability. Contribution of Working Group II to the Third Assessment Report of the Intergovernmental Panel on Climate Change*, 2001. Cambridge University Press, Cambridge, United Kingdom and New York, NY, USA.

L. O. Mearns, C. Rosenzweig, and R. Goldberg. Mean and variance change in climate scenarios: Methods, agricultural applications, and measures of uncertainty. *Climatic Change*, 35(4):367–396, 1997.

J. R. Meigh, A. A. McKenzie, and K. J. Sene. A grid-based approach to water scarcity estimates for eastern and southern africa. *Water Resources Management*, 13:85–115, 1999.

B. Metz, O. Davidson, R. Swart, and J. Pan, editors. *Climate Change 2001: Mitigation. Contribution of Working Group III to the Third Assessment Report of the Intergovernmental Panel on Climate Change*, 2001. Cambridge University Press, Cambridge, United Kingdom and New York, NY, USA.

P. C. D. Milly, R. T. Wetherald, K. A. Dunne, and T. L. Delworth. Increasing risk of great fbods in a changing climate. *Nature*, 415:514 – 517, 2002.

M. M. Q. Mirza. Global warming and changes in the probability of occurrence of fbods in bangladesh and implications. *Global Environmental Change*, 12(2):127–138, 2002.

J. F. B. Mitchell, T. C. Johns, M. Eagles, W. J. Ingram, and R. A. Davis. Towards the construction of climate change scenarios. *Climatic Change*, 41(3-4):547–581, 1999.

T. D. Mitchell. Pattern scaling: An examination of the accuracy of the technique for describing future climates. *Climatic Change*, 60(3):217–242, 2003.

A. H. Monahan. Stabilization of climate regimes by noise in a simple model of the thermohaline circulation. *Journal of Physical Oceanography*, 32(7):2072–2085, 2002.

A. H. Monahan, A. Timmermann, and G. Lohmann. Comments on "noise-induced transitions in a simplifi ed model of the thermohaline circulation". *Journal of Physical Oceanography*, 32(3):1112–1116, 2002.

M. G. Morgan and D. W. Keith. Subjective judgements by climate experts. *Environmental Policy Analysis*, 29:468–476, 1995.

Munich Re. Forum disasters: Flooding in europe 2002. Internet document http://www.munichre.com/6/04/fboding_in_europe_e.asp, 2004. Downloaded on Dec 20, 2004.

M. New, M. Hulme, and P. Jones. Representing twentieth-century space-time climate variability. part II: Development of 1901-96 monthly grids of terrestrial surface climate. *Journal of Climate*, 13(13):2217–2238, 2000.

B. Nijssen, G. O'Donnell, D. P. Lettenmaier, D. Lohmann, and E. F. Wood. Predicting the discharge of global rivers. *Journal of Climate*, 14:3307–3323, 2001.

W. D. Nordhaus. *Managing the Global Commons. The Economics of Climate Change*. MIT Press, Cambridge, 1994.

W. D. Nordhaus and Z. Yang. A regional dynamic equilibrium model of alternative climate change strategies. *American Economic Review*, 86:741–765, 1996.

T. Oki, T. Nishimura, and P. Dirmeyer. Assessment of annual runoff from land surface models using total runoff integrating pathways (TRIP). *Journal of the Meteorological Society of Japan*, 77:235–255, 1999.

H. Österle, F.-W. Gerstengarbe, and P.-C. Werner. Homogenisierung und Aktualisierung des Klimadatensatzes der Climate Research Unit of East Anglia, Norwich. In *Proc. 6. Deutsche Klimatagung, Klimavariabilität*, pages 326–329, 2003.

T. N. Palmer. Predicting uncertainty in forecasts of weather and climate. *Reports on Progress in Physics*, 63(2):71–116, 2000.

M. E. Paté-Cornell. Uncertainties in risk analysis: Six levels of treatment. *Reliability Engineering & System Safety*, 54:95–111, 1996.

J. Peixoto and A. H. Oort. *Physics of Climate*. Springer, 1991.

V. Petoukhov, A. Ganopolski, V. Brovkin, M. Claussen, A. Eliseev, C. Kubatzki, and S. Rahmstorf. CLIMBER-2: A climate system model of intermediate complexity. part I: model description and performance for present climate. *Climate Dynamics*, 16: 1–17, 2000.

G. Petschel-Held, H.-J. Schellnhuber, T. Bruckner, F. L. Tóth, and K. Hasselmann. The tolerable windows approach: Theoretical and methodological foundations. *Climatic Change*, 41(3/4):303–331, 1999.

E. L. Plambeck, C. Hope, and J. Anderson. The Page95 model: Integrating the science and economics of global warming. *Energy Economics*, 19:77–101, 1997.

W. H. Press, S. A. Teukolsky, W. T. Vetterling, and B. P. Flannery. *Numerical Recipes in Fortran 77. The Art of Scientific Computing*. Cambridge University Press, Cambridge, second edition, 1997.

S. Rahmstorf. Bifurcations of the atlantic thermohaline circulation in response to changes in the hydrological cycle. *Nature*, 378:145–149, 1995.

S. Rahmstorf. On the freshwater forcing and transport of the atlantic thermohaline circulation. *Climate Dynamics*, 12:799–811, 1996.

S. Rahmstorf and A. Ganopolski. Long-term global warming scenarios computed with an effi cient coupled climate model. *Climatic Change*, 43:353–367, 1999a.

S. Rahmstorf and A. Ganopolski. Simple theoretical model may explain apparent climate instability. *Journal of Climate*, 12:1349–1352, 1999b.

S. Rahmstorf, J. Marotzke, and J. Willebrand. Stability of the thermohaline circulation. In W. Krauss, editor, *The warm water sphere of the North Atlantic ocean*, pages 129–158. Borntraeger, Stuttgart, 1996.

J. R. Ravetz. Integrated environmental assessment forum: developing guidelines for "good practice". ULYSSES Working Paper WP-97-1, Darmstadt University of Technology, Darmstadt, Germany, 1997.

J. R. Ravetz. What is post-normal science. *Futures*, 31:647–653, 1999.

H. Risken. *The Fokker-Planck Equation*. Springer, 3rd. edition, 1996.

E. Roeckner, K. Arpe, L. Bengtsson, M. Christoph, M. Claussen, L. Dümenil, M. Esch, M. Giorgetta, U. Schlese, and U. Schulzweida. The atmospheric general circulation model ECHAM-4: Model description and simulation of present-day climate. Report 218, Max Planck Institute for Meteorology, 1996.

C. Rooth. Hydrology and ocean circulation. *Progress in Oceanography*, 11:131–149, 1982.

J. Rotmans, H. de Boois, and R. J. Swart. Image: an integrated model to assess the greenhouse effect. Technical Report 758471009, RIVM, Bilthoven, The Netherlands, 1989.

J. Rotmans and M. B. A. van Asselt. Uncertainty in integrated assessment modelling: A labyrinthic path. *Integrated Assessment*, 2(2):43–55, 2001.

G. L. Russell and J. R. Miller. Global river runoff calculated from a global atmospheric general circulation model. *Journal of Hydrology*, 117:241–254, 1990.

T. M. Saloranta. Post-normal science and the global climate change issue. *Climatic Change*, 50:395–404, 2001.

M. Scheffer, S. Carpenter, J. A. Foley, C. Folke, and B. Walker. Catastrophic shifts in ecosystems. *Nature*, 413:591–596, 2001.

M. Scheffer and S. R. Carpenter. Catastrophic regime shifts in ecosystems: linking theory to observation. *TRENDS in Ecology and Evolution*, 18:648–656, 2003.

A. Schiller, U. Mikolajevicz, and R. Voss. The stability of the north atlantic thermohaline circulation in a coupled ocean-atmosphere general circulation model. *Climate Dynamics*, 13(5):325–347, 1997.

A. Schmittner and A. J. Weaver. Dependence of multiple climate states on ocean mixing parameters. *Geophysical Research Letters*, 28(6):1027–1030, 2001.

J. R. Scott, J. Marotzke, and P. H. Stone. Interhemispheric thermohaline circulation in a coupled box model. *Journal of Physical Oceanography*, 29:351–365, 1999.

M. V. Shabalova, W. P. A. van Deursen, and T. A. Buishand. Assessing future discharge of the river rhine using regional climate model integrations and a hydrological model. *Climate Research*, 23(3):233–246, 2003.

J. B. Smith, H. Schellnhuber, and M. Q. Mirza. Lines of evidence for vulnerability to climate change: A synthesis. In O. Canziani and J. M. Carthy, editors, *Climate*

Change 2001: Impacts, Adaption and Vulnerability - Contribution of Working Group II to the Third Assessment Report of the IPCC, chapter 19, pages 914–967. Cambridge University Press, 2001.

D. Sornette. *Critical Phenomena in Natural Sciences*. Springer, 2000.

D. A. Stainforth, T. Aina, C. Christensen, M. Collins, N. Faull, D. J. Frame, J. A. Kettleborough, S. Knight, A. Martin, J. M. Murphy, C. Piani, D. Sexton, L. A. Smith, R. A. Spicer, A. J. Thorpe, and M. R. Allen. Uncertainty in predictions of the climate response to rising levels of greenhouse gases. *Nature*, 433:403–406, 2005.

T. F. Stocker and A. Schmittner. Influence of CO_2 emission rates on the stability of the thermohaline circulation. *Nature*, 388:862–865, 1997.

H. Stommel. Thermohaline convection with two stable regimes of flow. *Tellus*, 13: 224–241, 1961.

H. M. Stommel and W. R. Young. The average T-S relation of a stochastically forced box model. *Journal of Physical Oceanography*, 23:151–158, 1993.

R. Swart, M. Berk, M. Janssen, E. Kreileman, and R. Leemans. the safe landing approach: risks and trade-offs in climate change. In J. Alcamo, R. Leemans, and E. Kreileman, editors, *Global Change Scenarios of the 21st Century. Results from the IMAGE 2.1 Model*, pages 193–218. Elsevier, Oxford, U.K., 1998.

C. W. Thornthwaite. An approach toward a rational classification of climate. *Geographical Review*, 38, 1948.

A. Timmermann and G. Lohmann. Noise-induced transitions in a simplified model of the thermohaline circulation. *Journal of Physical Oceanography*, 30(8):1891–1900, 2000.

S. Titz, T. Kuhlbrodt, S. Rahmstorf, and U. Feudel. On freshwater-dependent bifurcations in box models of the interhemispheric thermohaline circulation. *Tellus*, 54(1): 89–98, 2002.

R. S. J. Tol. Safe policies in an uncertain climate: an application of FUND. *Global Environmental Change*, 9:221–232, 1999.

R. S. J. Tol. Estimates of the damage costs of climate change. part i: Benchmark estimates. *Environmental and Resource Economics*, 21:47–73, 2002.

F. L. Toth. Climate policy in light of climate science: The ICLIPS project. *Climatic Change*, 56(1-2):7–36, 2003.

F. L. Toth, T. Bruckner, H.-M. Füssel, M. Leimbach, and G. Petschel-Held. Integrated assessment of long-term climate policies: Part 1 - model presentation. *Climatic Change*, 56(1-2):37–56, 2003a.

F. L. Toth, T. Bruckner, H.-M. Füssel, M. Leimbach, and G. Petschel-Held. Integrated assessment of long-term climate policies: Part 2 - model results and uncertainty analysis. *Climatic Change*, 56(1-2):57–72, 2003b.

K. E. Trenberth, A. Dai, R. M. Rasmussen, and D. B. Parsons. The changing character of precipitation. *Bulletin of the American Meteorological Society*, 84(9):1205–1217, 2003.

E. Tziperman. Proximity of the present-day thermohaline circulation to an instability threshold. *Journal of Physical Oceanography*, 30:90–104, 2000.

UNESCO. *Discharge of selected rivers of the world; a contribution to the International Hydrological Decade*, volume 5. Unesco Press, Paris, 1974.

United Nations. *Framework Convention on Climate Change*. United Nations, 1995.

M. B. A. van Asselt and J. Rotmans. Uncertainty in perspective. *Global Environmental Change*, 6(2):121–157, 1996.

E. van Daalen, W. Thissen, and M. Berk. The delft process: experiences with a dialogue between policy makers and global modellers. In J. Alcamo, R. Leemans, and E. Kreileman, editors, *Global Change Scenarios of the 21st Century. Results from the IMAGE 2.1 Model*, pages 267–286. Elsevier, Oxford, U.K., 1998.

T. S. von Deimling, H. Held, A. Ganopolski, and S. Rahmstorf. Climate sensitivity range derived from large ensemble simulations of glacial climate constrained by proxy data. In *Workshop report of the IPCC WG1 Workshop on Climate sensitivity, 26-29 July 2004, Paris*. IPCC, 2004.

H. von Storch and F. W. Zwiers. *Statistical Analysis in Climate Research*. Cambridge University Press, 1999.

J.-S. von Storch, P. Müller, R. J. Stouffer, R. Voss, and S. F. B. Tett. Variability of deep-ocean mass transport: Spectral shapes and spatial scales. *Journal of Climate*, 13(11): 1916–1935, 2000.

R. Voss, W. May, and E. Roeckner. Enhanced resolution modelling study on anthropogenic climate change: changes in extremes of the hydrological cycle. *International Journal of Climatology*, 22(7):755–777, 2002.

R. Voss, R. Sausen, and U. Cubasch. Periodically synchronously coupled integrations with the atmosphere-ocean general circulation model ECHAM3/LSG. *Climate Dynamics*, 14:249–266, 1998.

C. J. Vörösmarty, C. A. Federer, and A. L. Schloss. Potential evaporation functions compared on US watersheds: Possible implications for global-scale water balance and terrestrial ecosystem modeling. *Journal of Hydrology*, 207(3-4):147–169, 1998.

C. J. Vörösmarty, B. M. Fekete, M. Meybeck, and R. B. Lammers. Global system of rivers: Its role in organizing continental land mass and defi ning land-to-ocean linkages. *Global Biogeochemical Cycles*, 14(2):599–621, 2000.

C. J. Vörösmarty, C. J. Willmott, B. J. Choudhury, A. L. Schloss, T. K. Stearns, S. M. Robeson, and T. J. Dorman. Analyzing the discharge regime of a large tropical river through remote sensing, ground-based climatic data, and modeling. *Water Resources Research*, 32(10):3137–3150, 1996.

J. E. Walsh and D. H. Portis. Variations of precipitation and evaporation over the north atlantic ocean, 1958-1997. *Journal of Geophysical Research*, 104(D14):16613–16631, 1999.

B. A. Warren. Deep circulation of the world ocean. In *Evolution of Physical Oceanography*, pages 6–40. MIT Press, 1981.

WBGU. Szenario zur Ableitung globaler CO_2-Reduktionsziele und Umsetzungsstrategien. Stellungnahme aus Anlaß der 1. Vertragsstaatenkonferenz zum Rahmenübereinkommen über Klimaänderungen in Berlin, Wissenschaftlicher Beirat der Bundesregierung für Globale Umweltveränderungen, Bremerhaven, 1995.

M. D. Webster and A. P. Sokolov. A methodology for quantifying uncertainty in climate projections. *Climatic Change*, 46:417–446, 2000.

J. Weyant, O. Davidson, H. Dowlatabadi, J. Edmonds, M. Grubb, E. Parson, R. Richels, J. Rotmans, P. Shukla, R. Tol, W. Cline, and S. Fankhauser. Integrated assessment of climate change: An overview and comparison of approaches and results. In J. Bruce, H. Lee, and E. Haites., editors, *Climate Change 1995: Economic and Social Dimensions of Climate Change. Contribution of WG III to the Second Assessment Report of the Intergovernmental Panel on Climate Change*. Cambridge University Press, Cambridge, 1996.

S. Wiggins. *Introduction to applied nonlinear dynamical systems and chaos*. Springer, New York, 1990.

R. L. Wilby and T. M. L. Wigley. Downscaling general circulation model output: a review of methods and limitations. *Progress in Physical Geography*, 21(4):530–548, 1997.

R. L. Wilby, T. M. L. Wigley, D. Conway, P. D. Jones, B. C. Hewitson, J. Main, and D. S. Wilks. Statistical downscaling of general circulation model output: A comparison of methods. *Water Resources Research*, 34(11):2995–3008, 1998.

D. S. Wilks and R. L. Wilby. The weather generation game: a review of stochastic weather models. *Progress in Physical Geography*, 23(3):329–357, 1999.

C. J. Willmott. Some comments on the evaluation of model performance. *Bulletin of the American Meteorological Society*, 63:1309–1313, 1982.

C. J. Willmott and K. Matsuura. Terrestrial air temperature and precipitation: Monthly and annual time series (1950 - 1999). Available online at http://climate.geog.udel.edu/˜climate/html_pages/archive.html, 2001.

R. A. Wood, A. B. Keen, J. F. B. Mitchell, and J. M. Gregory. Changing spatial structure of the thermohaline circulation in response to atmospheric CO_2 forcing in a climate model. *Nature*, 399:572–575, 1999.

C.-Y. Xu. From GCMs to river flow: a review of downscaling methods and hydrologic modelling approaches. *Progress in Physical Geography*, 23(2):229–249, 1999.

K. Zickfeld. *Modeling Large-Scale Singular Climate Events for Integrated Assessment*. PhD thesis, Universität Potsdam, 2003.

K. Zickfeld and T. Bruckner. Reducing the risk of abrupt climate change: Emissions corridors preserving the atlantic thermohaline circulation. *Integrated Assessment*, 4: 106–115, 2003.

Acknowledgements

Many people gave me support and advice during the preparation of this thesis, and I am very grateful to every one of them. Without their help the completion of this dissertation would not have been possible.

I especially want to express my gratitude to John Schellnhuber, Gerhard Petschel-Held and Hermann Held for the guidance, support and inspiration they gave me. I am deeply indebted to you.

Numerous others have supported me as well, and I cannot even attempt to name every single one. Every rule has it’s exceptions, though, and these are:

Nico Bauer
Thomas Bruckner
Klaus Eisenack
Anja Heigl
Günter Kleinen
Katharina Kleinen-von Königslöw
Brigitte Knopf
Ulrike von Königslöw
Elmar Kriegler
Till Kuhlbrodt
Anja Reischke
Danny Rogler